

# A $Z_4$ Scotogenic Model with Higgs Portal

Noel Jonathan Jobu\*, Kenji Nishiwaki†

*Shiv Nadar University,  
Tehsil Dadri, Gautam Buddha Nagar, Uttar Pradesh, 201314, India*

August 27, 2025

## Abstract

We propose a new Scotogenic type model based on a global  $Z_4$  symmetry involving dark matter candidates. After the symmetry breaking as  $Z_4$  to  $Z_2$  via the singlet scalar vacuum expectation value (VEV), the lightest Majorana fermion works as a viable thermal freeze-out dark matter (DM) candidate, and the mass terms for active neutrinos are generated as a finite quantum correction at the 1-loop level. A key point of realising our Scotogenic structure is to introduce two types of Majorana fermions (heavy right-handed neutrinos) and inert Higgs doublets with opposite  $Z_4$  parities. Since a large VEV for the singlet scalar is not so harmful in an appropriate realisation of the Higgs mechanism for the SM gauge symmetry, we can naturally realise a TeV-scale fermionic DM candidate, where constraints via direct detection experiments are less than those for sub-TeV DM. Our scenario involves the Higgs-portal DM interactions, which help the realisation of the correct DM relic abundance. Relying on the structure of the model, it is possible to find a natural partner for coannihilation. Our scenario can be investigated via the measurement of the Higgs trilinear self-coupling at the Large Hadron Collider. The simplest way to evade the domain-wall problem by adding a tiny soft  $Z_2$  breaking term works, keeping a sufficient longevity of the decaying DM lifetime.

---

\*E-mail: nj702@snu.edu.in

†E-mail: kenji.nishiwaki@snu.edu.in

# 1 Introduction

It is well known that the original form of the Standard Model (SM) should be upgraded, at least in the sector associated with neutrinos, due to the observations of neutrino oscillations, which originate from minuscule but nonzero masses of the neutrinos in the SM. Over the last two decades or more after the confirmation of the neutrino oscillations [1, 2] (refer to Review [3]), the experimental developments in neutrino oscillation have been significant, and now provide relevant constraints on the CP-violating phase of the Pontecorvo-Maki-Nakagawa-Sakata (PMNS) matrix [4–6]. The measurements of the three mixing angles and the CP phase will be significantly upgraded in the coming next-generation experiments, e.g., DUNE [7] and Hyper-Kamiokande [8]. Given this situation, it is becoming increasingly important to consider the structure of the neutrino sector in depth. Furthermore, it should be noted that the neutrino sector significantly impacts the possible scenarios in the early stages of the universe in conjunction with dark matter and other matters.

A key question is: What is the origin of the tiny masses of the neutrinos? The simplest scenario relies on the Yukawa terms with the Higgs doublet, the doublet lepton fields and the newly added right-handed singlet neutrinos, where the Dirac mass terms for the neutrinos are successfully generated via the Higgs mechanism, but we should swallow to introduce tiny Yukawa couplings, at least  $\mathcal{O}(10^{-12})$  or smaller. A relaxation in the tuning of Yukawa couplings is realised by adopting the see-saw mechanism, where the Yukawa structure of the sub-eV neutrino masses (and also mixings) involves connections with other heavy particles (see Review [9]). Depending on how the left-handed active neutrinos couple with heavy particles, see-saw scenarios are classified as Canonical/Type-I [10–15], Type-II [16–20], Type-III [21], Inverse [22, 23], Linear [23–25], and others. Note that a seminal application of the right-handed neutrinos, which can appear in the see-saw texture, is the Baryogenesis via Leptogenesis [26].

There are interesting variations of the see-saw scenario, suggested by the quantum nature of neutrinos. The above scenarios considered the case where neutrino mass terms exist at the lowest order of perturbation, but it is also possible that these are produced quantumly via loops of heavy new particles. As suggested by the results of the operator analysis [27, 28], if active neutrino mass terms are represented as higher-dimensional operators of the SM fields in a gauge-invariant way (before the electroweak symmetry breaking), no divergences emerge in such loop-induced neutrino mass terms. We list early-stage concrete models based on this idea [29–34] (see also Review on this kind of models [35]). A branch of such scenarios called the *Scotogenic* model is a fascinating arena in particle physics, where additional symmetry/symmetries (imposed on such a model) ensure the loop origin of the active neutrino mass terms but also the stability of a new particle, which behaves as a dark matter (DM) [36]. In this type of scenario, neutrino physics is mutually connected with dark matter physics, and the model predictability will be enhanced. Lots of studies have been done on such ideas in many contexts based on various kinds of symmetries; based on global  $Z_2$  symmetry [37–99], based on other kinds of global discrete symmetries [100–120], and other embedding varieties, including those based on continuous-symmetry cases [121–176].<sup>1</sup>

However, it should be noted here that the ordinary Weakly Interacting Massive Particle (WIMP) DM paradigm based on the thermal freeze-out scenario has recently reached a crossroads due to significant progress with null observations in the LUX-ZEPLIN (LZ) direct observation experiment [182, 183]. Several ideas to evade the tight bounds in the freeze-out DM scenario, e.g., fermionic DM with pseudoscalar mediator [184–189], and pseudo-Nambu-Goldstone boson (pNGB) DM [190–194] (see also [195–197] for embeddings to grand-unified scenarios).

Another simple scenario is to rely on the enhancement of the DM pair annihilation near a resonance of

---

<sup>1</sup>Scenarios with bound-state dark matter are discussed in [177, 178]. Another fascinating class (without DM candidates) is loop-induced neutrino masses under extra coloured scalars; see e.g., [179–181] as early works.

New Particle	$SU(3)_C$	$SU(2)_L$	$U(1)_Y$	$Z_4$	Spin
$S$	1	1	0	-1	0 (Real)
$\eta_A$	1	2	1	$+i$	0 (Complex)
$\eta_B$	1	2	1	$-i$	0 (Complex)
$N_{A_iR}$ ( $i = 1, 2, 3$ )	1	1	0	$+i$	1/2 (Right-handed)
$N_{B_iR}$ ( $i = 1, 2, 3$ )	1	1	0	$-i$	1/2 (Right-handed)

Table 1: Matter contents added to this model are summarised.  $SU(3)_C$ ,  $SU(2)_L$  and  $U(1)_Y$  represent the degrees of freedom of the colour, weak-isospin and hypercharge, respectively. All Standard Model fields take +1 of the  $Z_4$  parity. The index  $i$  takes one to three and discriminates three generations.

a mediator in an  $s$ -channel, where we can keep the coupling between DM and its mediator sizably small, and thereby, it is not difficult to suppress the (spin-independent) cross section in DM direct detections. A favoured region of the DM-mass range would be a TeV region since more severe bounds have been imposed in the sub-TeV domain [182, 183]. We propose a new Scotogenic scenario based on the global  $Z_4$  symmetry, where the vacuum expectation value (VEV) of an additional singlet scalar breaks it to  $Z_2$ . The residual  $Z_2$  symmetry ensures the stability of DM, and a large VEV of the singlet scalar naturally realises a TeV-scale Majorana fermionic DM.

This paper is organised as follows. In Section 2, we introduce our Scotogenic model based on a  $Z_4$  global symmetry and derive the form of the one-loop induced neutrino mass terms. In Section 3, we provide constraints on our scenario, namely, the lepton flavour violation, the oblique correction and the stability of the scalar potential. In Section 4, we summarise our formulas for calculating the dark matter relic abundance and direct detection. In Section 5, we provide our results of numerical calculations and show that we can reproduce the observed neutrino texture at one-loop level and the observed dark matter relic abundance consistently. In Section 6, we discuss the current constraint and future prospects of the constraint on our scenario via the measurement of the Higgs trilinear self-coupling at the Large Hadron Collider (LHC). In Section 7, we comment on possible prescriptions to evade the domain-wall problem in our scenario. In Section 8, we summarise our results and provide some comments. In Appendix A, the decay width of the  $SU(2)_L$ -singlet scalar is provided. In Appendix B, the results of the numerical scans without the coannihilation effect are shown.

## 2 A $Z_4$ -based Scotogenic Model

### 2.1 Model Setup

Here, we introduce our model, which is a Scotogenic-type model based on a discrete  $Z_4$  symmetry, where no extension of the gauge groups from those of the Standard Model. Table 1 shows a summary of the matter contents we introduced, where we introduce one real  $SU(2)_L$ -singlet scalar  $S$ , two complex  $SU(2)_L$ -doublet scalars  $\eta_A$  and  $\eta_B$ , and six (two kinds of three-generation)  $SU(2)_L$ -singlet right-handed neutrinos  $N_{A_iR}$  and  $N_{B_iR}$  ( $i = 1, 2, 3$ ). Note that for the scalar doublets and right-handed fermions, type- $A$  and type- $B$  particles take opposite  $Z_4$  parities as  $+i$  and  $-i$ , respectively. The trivial  $Z_4$  parity (+1) is assigned for all of the SM particles.

In our scenario, the possible leptonic Yukawa terms are as follows,

$$-\mathcal{L}_{\text{Yukawa}} = Y_A^{i\alpha} \overline{N'_{A_iR}} \eta_A^T (i\sigma_2) L_{\alpha L} + Y_B^{i\alpha} \overline{N'_{B_iR}} \eta_B^T (i\sigma_2) L_{\alpha L}$$

$$+ \frac{m_{N_{ij}}}{2} \overline{(N'_{A_i R})^c} N'_{B_j R} + \frac{m_{N_{ij}}}{2} \overline{(N'_{B_i R})^c} N'_{A_j R} + \frac{y_{A_{ij}}}{2} S \overline{(N'_{A_i R})^c} N'_{A_j R} + \frac{y_{B_{ij}}}{2} S \overline{(N'_{B_i R})^c} N'_{B_j R} + \text{h.c.}, \quad (2.1)$$

and the possible scalar potential terms are written down as

$$\begin{aligned} \mathcal{V} = & +m_H^2 (H^\dagger H) + m_{\eta_A}^2 (\eta_A^\dagger \eta_A) + m_{\eta_B}^2 (\eta_B^\dagger \eta_B) + \frac{m_S^2}{2} S^2 + \frac{\lambda_{HS}}{2} S^2 (H^\dagger H) \\ & + \frac{\lambda_H}{2} (H^\dagger H)^2 + \frac{\lambda_S}{4} S^4 + \frac{\lambda_{2a}}{2} (\eta_A^\dagger \eta_A)^2 + \frac{\lambda_{2b}}{2} (\eta_B^\dagger \eta_B)^2 + \frac{\lambda_{2c}}{2} (\eta_A^\dagger \eta_A) (\eta_B^\dagger \eta_B) \\ & + \frac{\lambda_{2d}}{2} (\eta_A^\dagger \eta_B) (\eta_B^\dagger \eta_A) + \lambda_{3A} (H^\dagger H) (\eta_A^\dagger \eta_A) + \lambda_{3B} (H^\dagger H) (\eta_B^\dagger \eta_B) \\ & + \lambda_{4A} (H^\dagger \eta_A) (\eta_A^\dagger H) + \lambda_{4B} (H^\dagger \eta_B) (\eta_B^\dagger H) + \frac{1}{2} \left[ \lambda_5 (H^\dagger \eta_A) (H^\dagger \eta_B) + \lambda_6 (\eta_A^\dagger \eta_B)^2 + \text{h.c.} \right] \\ & + \mu_S S (\eta_A^\dagger \eta_B) + \mu_S^* S (\eta_B^\dagger \eta_A) + \frac{\lambda_{S\eta_A}}{2} S^2 (\eta_A^\dagger \eta_A) + \frac{\lambda_{S\eta_B}}{2} S^2 (\eta_B^\dagger \eta_B), \end{aligned} \quad (2.2)$$

where  $H$  denotes the  $SU(2)_L$  Higgs doublet to trigger the spontaneous electroweak symmetry breaking;  $i$  and  $\alpha$  run from one to three, representing the three generations of the right-handed neutrinos and left-handed Lepton doublets  $L_{\alpha L}$ , respectively.  $\sigma_2$  is the 2nd Pauli matrix.

In the following analysis, we will assume that  $\mu_S$  is a real parameter and  $m_{N_{ij}}$ ,  $y_{A_{ij}}$  and  $y_{B_{ij}}$  are real and diagonal for simplicity. Also, we will take  $\lambda_6 = 0$ . The fermion with the superscript  $(N_R)^c$  denotes the charge conjugation of  $N_R$ .

The  $SU(2)_L$  doublets are parametrised as follows,<sup>2</sup>

$$L_{\alpha L} = \begin{pmatrix} \nu'_\alpha \\ l'_\alpha \end{pmatrix}_L, \quad H = \begin{pmatrix} 0 \\ \frac{1}{\sqrt{2}} (v_H + h') \end{pmatrix}, \quad \eta_{A,B} = \begin{pmatrix} \eta'_{A,B}^+ \\ \eta'_{A,B}^0 \end{pmatrix} = \begin{pmatrix} \eta'_{A,B}^+ \\ \frac{1}{\sqrt{2}} (\eta'_{R_{A,B}} + i\eta'_{I_{A,B}}) \end{pmatrix}, \quad (2.3)$$

and the singlet scalar,

$$S = (v_S + s'), \quad (2.4)$$

where we took the unitary gauge and the prime symbol for components, representing that they are gauge eigenstates. We focus on the following configuration of the VEVs of the scalars,

$$\langle H \rangle = \begin{pmatrix} 0 \\ v_H/\sqrt{2} \end{pmatrix}, \quad \langle S \rangle = v_S, \quad \langle \eta_A \rangle = \begin{pmatrix} 0 \\ 0 \end{pmatrix}, \quad \langle \eta_B \rangle = \begin{pmatrix} 0 \\ 0 \end{pmatrix}, \quad (2.5)$$

where the  $Z_4$  symmetry is spontaneously broken down to  $Z_2$ , and therefore, the lightest particle with  $+i$  or  $-i$   $Z_4$  parity is protected by a residual symmetry and becomes a dark matter candidate. The inert condition for  $\eta_A$  and  $\eta_B$  is necessary to keep the residual  $Z_2$  symmetry.

The tadpole conditions,

$$\frac{\partial \mathcal{V}}{\partial h} \Big|_{h=s=0} = 0 = \frac{\partial \mathcal{V}}{\partial s} \Big|_{h=s=0}, \quad (2.6)$$

---

<sup>2</sup>Note that

$$\begin{aligned} \overline{(N'_{A_i R})^c} N'_{B_j R} &= \overline{(N'_{B_j R})^c} N'_{A_i R}. \\ Y_A^{i\alpha} \overline{N'_{A_i R}} \eta_A^T (i\sigma_2) L_{\alpha L} + \text{h.c.} &= Y_A^{i\alpha} \overline{N'_{A_i R}} \left[ \nu'_{\alpha L} \eta'^0_A - l'^-_{\alpha L} \eta'^+_A \right] + (Y_A^{i\alpha})^* \left[ \overline{\nu'_{\alpha L}} \left( \eta'^0_A \right)^* - \overline{l'^-_{\alpha L}} \eta'^-_A \right] N'_{A_i R}. \end{aligned}$$

lead to the forms

$$\frac{\lambda_H}{2}v_H^2 + \frac{\lambda_{HS}}{2}v_S^2 = -m_H^2, \quad \frac{\lambda_{HS}}{2}v_H^2 + \lambda_S v_S^2 = -m_S^2, \quad (2.7)$$

which are solved as

$$v_H^2 = \frac{2[2(-m_H^2)\lambda_S - (-m_S^2)\lambda_{HS}]}{2\lambda_H\lambda_S - \lambda_{HS}^2}, \quad v_S^2 = \frac{2[(-m_S^2)\lambda_H - (-m_H^2)\lambda_{HS}]}{2\lambda_H\lambda_S - \lambda_{HS}^2}, \quad (2.8)$$

where the Higgs VEV  $v_H$  should take  $\simeq 246$  GeV. After the application of the tadpole conditions in Eq. (2.7), the mass matrix squared for  $h'$  and  $s'$  in this order reads

$$\mathcal{M}^2[h', s'] = \begin{bmatrix} \lambda_H v_H^2 & \lambda_{HS} v_H v_S \\ \lambda_{HS} v_H v_S & 2\lambda_S v_S^2 \end{bmatrix} = \begin{bmatrix} c_\alpha & -s_\alpha \\ s_\alpha & c_\alpha \end{bmatrix} \begin{bmatrix} M_h^2 & 0 \\ 0 & M_s^2 \end{bmatrix} \begin{bmatrix} c_\alpha & s_\alpha \\ -s_\alpha & c_\alpha \end{bmatrix}, \quad (2.9)$$

where  $h$  is the SM-like Higgs boson with  $M_h = 125$  GeV and  $s$  an additional CP-even scalar boson. The mixing angle  $\alpha$  is determined as

$$\sin(2\alpha) = -\frac{2\lambda_{HS} v_H v_S}{M_h^2 - M_s^2}, \quad (2.10)$$

where the gauge eigenstates and the mass eigenstates (denoted without the prime symbol) are related as

$$\begin{bmatrix} h' \\ s' \end{bmatrix} = \begin{bmatrix} c_\alpha & -s_\alpha \\ s_\alpha & c_\alpha \end{bmatrix} \begin{bmatrix} h \\ s \end{bmatrix}. \quad (2.11)$$

Next, we see the mass structure of the other scalars. Under our assumption that  $\mu_S$  is real, the mass matrices squared for  $\eta'_{R_A}$  and  $\eta'_{R_B}$ , and  $\eta'_{I_A}$  and  $\eta'_{I_B}$  yield

$$\mathcal{M}^2[\eta'_{R_A}, \eta'_{R_B}] = \begin{bmatrix} m_{R_{AA}}^2 & m_{R_{AB}}^2 \\ m_{R_{AB}}^2 & m_{R_{BB}}^2 \end{bmatrix} = U_R \begin{bmatrix} M_{R_2}^2 & 0 \\ 0 & M_{R_2}^2 \end{bmatrix} U_R^\dagger, \quad (2.12)$$

$$\mathcal{M}^2[\eta'_{I_A}, \eta'_{I_B}] = \begin{bmatrix} m_{I_{AA}}^2 & m_{I_{AB}}^2 \\ m_{I_{AB}}^2 & m_{I_{BB}}^2 \end{bmatrix} = U_I \begin{bmatrix} M_{I_1}^2 & 0 \\ 0 & M_{I_2}^2 \end{bmatrix} U_I^\dagger, \quad (2.13)$$

where the components are defined as

$$m_{R_{AA}}^2 = m_{I_{AA}}^2 = m_{\eta_A}^2 + \frac{\lambda_{3A}}{2}v_H^2 + \frac{\lambda_{4A}}{2}v_H^2 + \frac{\lambda_{S\eta_A}}{2}v_S^2, \quad (2.14)$$

$$m_{R_{BB}}^2 = m_{I_{BB}}^2 = m_{\eta_B}^2 + \frac{\lambda_{3B}}{2}v_H^2 + \frac{\lambda_{4B}}{2}v_H^2 + \frac{\lambda_{S\eta_B}}{2}v_S^2, \quad (2.15)$$

$$m_{R_{AB}}^2 = \mu_S v_S + \frac{\lambda_5}{2}v_H^2, \quad (2.16)$$

$$m_{I_{AB}}^2 = \mu_S v_S - \frac{\lambda_5}{2}v_H^2. \quad (2.17)$$

The matrices diagonalise the mass matrices,

$$U_R = \begin{bmatrix} c_{\theta_R} & -s_{\theta_R} \\ s_{\theta_R} & c_{\theta_R} \end{bmatrix}, \quad U_I = \begin{bmatrix} c_{\theta_I} & -s_{\theta_I} \\ s_{\theta_I} & c_{\theta_I} \end{bmatrix}; \quad \begin{bmatrix} \eta'_{R_A} \\ \eta'_{R_B} \end{bmatrix} = U_R \begin{bmatrix} \eta_{R_1} \\ \eta_{R_2} \end{bmatrix}, \quad \begin{bmatrix} \eta'_{I_A} \\ \eta'_{I_B} \end{bmatrix} = U_I \begin{bmatrix} \eta_{I_1} \\ \eta_{I_2} \end{bmatrix}, \quad (2.18)$$

$$\tan(2\theta_R) = \frac{2m_{R_{AB}}^2}{m_{R_{AA}}^2 - m_{R_{BB}}^2}, \quad \tan(2\theta_I) = \frac{2m_{I_{AB}}^2}{m_{I_{AA}}^2 - m_{I_{BB}}^2}, \quad (2.19)$$

where their mass eigenvalues are given as

$$M_{R_1}^2 = \frac{1}{2} \left[ m_{R_{AA}}^2 + m_{R_{BB}}^2 + \sqrt{4m_{R_{AB}}^4 + (m_{R_{AA}}^2 - m_{R_{BB}}^2)^2} \right], \quad (2.20)$$

$$M_{R_2}^2 = \frac{1}{2} \left[ m_{R_{AA}}^2 + m_{R_{BB}}^2 - \sqrt{4m_{R_{AB}}^4 + (m_{R_{AA}}^2 - m_{R_{BB}}^2)^2} \right], \quad (2.21)$$

$$M_{I_1}^2 = \frac{1}{2} \left[ m_{I_{AA}}^2 + m_{I_{BB}}^2 + \sqrt{4m_{I_{AB}}^4 + (m_{I_{AA}}^2 - m_{I_{BB}}^2)^2} \right], \quad (2.22)$$

$$M_{I_2}^2 = \frac{1}{2} \left[ m_{I_{AA}}^2 + m_{I_{BB}}^2 - \sqrt{4m_{I_{AB}}^4 + (m_{I_{AA}}^2 - m_{I_{BB}}^2)^2} \right]. \quad (2.23)$$

Similarly, the mass matrix for the charged scalars yields

$$\mathcal{M}^2 [\eta_A'^+, \eta_B'^+] = \begin{bmatrix} m_{\eta_A^+}^2 & m_{\eta_{AB}^+}^2 \\ m_{\eta_{AB}^+}^2 & m_{\eta_B^+}^2 \end{bmatrix}, \quad (2.24)$$

with

$$m_{\eta_A^+}^2 = m_{\eta_A}^2 + \frac{\lambda_{3A}}{2} v_H^2 + \frac{\lambda_{S\eta_A}}{2} v_S^2, \quad (2.25)$$

$$m_{\eta_B^+}^2 = m_{\eta_B}^2 + \frac{\lambda_{3B}}{2} v_H^2 + \frac{\lambda_{S\eta_B}}{2} v_S^2, \quad (2.26)$$

$$m_{\eta_{AB}^+}^2 = \mu_S v_S, \quad (2.27)$$

$$\mathcal{M}^2 [\eta_A'^+, \eta_B'^+] = U_{\text{cs}} \begin{bmatrix} M_{\eta_1^+}^2 & 0 \\ 0 & M_{\eta_2^+}^2 \end{bmatrix} U_{\text{cs}}^\dagger, \quad \begin{bmatrix} \eta_A'^+ \\ \eta_B'^+ \end{bmatrix} = U_{\text{cs}} \begin{bmatrix} \eta_1^+ \\ \eta_2^+ \end{bmatrix}, \quad U_{\text{cs}} = \begin{bmatrix} c_{\theta_{\text{cs}}} & -s_{\theta_{\text{cs}}} \\ s_{\theta_{\text{cs}}} & c_{\theta_{\text{cs}}} \end{bmatrix}. \quad (2.28)$$

Deriving the formulas for mass eigenvalues and  $\tan(2\theta_{\text{cs}})$  is straightforward as

$$M_{\eta_1^+}^2 = \frac{1}{2} \left[ m_{\eta_A^+}^2 + m_{\eta_B^+}^2 + \sqrt{4m_{\eta_{AB}^+}^2 + (m_{\eta_A^+}^2 - m_{\eta_B^+}^2)^2} \right], \quad (2.29)$$

$$M_{\eta_2^+}^2 = \frac{1}{2} \left[ m_{\eta_A^+}^2 + m_{\eta_B^+}^2 - \sqrt{4m_{\eta_{AB}^+}^2 + (m_{\eta_A^+}^2 - m_{\eta_B^+}^2)^2} \right], \quad (2.30)$$

$$\tan(2\theta_{\text{cs}}) = \frac{2 m_{\eta_{AB}^+}^2}{m_{\eta_A^+}^2 - m_{\eta_B^+}^2}. \quad (2.31)$$

Finally, under our assumption that all of  $m_{N_{ij}}$ ,  $y_{A_{ij}}$  and  $y_{B_{ij}}$  ( $i, j = 1, 2, 3$ ) are assumed to be real and diagonal, the mass terms of the right-handed neutrinos decomposed into each generation as follows,

$$-\frac{1}{2} \sum_{i=1}^3 \left[ \overline{(N'_{A_i R})^c}, \overline{(N'_{B_i R})^c} \right] \mathcal{M}_{N_{ii}} \begin{bmatrix} N'_{A_i R} \\ N'_{B_i R} \end{bmatrix} + \text{h.c.}, \quad (2.32)$$

where a (complex) orthogonal matrix diagonalises the symmetric Majorana mass terms as

$$\mathcal{M}_{N_{ii}} = \begin{bmatrix} y_{A_{ii}} v_S & m_{N_{ii}} \\ m_{N_{ii}} & y_{B_{ii}} v_S \end{bmatrix} = U_{N_i} \begin{bmatrix} M_{N_{A_i}} & 0 \\ 0 & M_{N_{B_i}} \end{bmatrix} (U_{N_i})^\text{T}, \quad U_{N_i} = \begin{bmatrix} c_{\theta_{N_i}} & -s_{\theta_{N_i}} \\ s_{\theta_{N_i}} & c_{\theta_{N_i}} \end{bmatrix}, \quad (2.33)$$

with

$$M_{N_{A_i}} = \frac{1}{2} \left[ y_{A_{ii}} v_S + y_{B_{ii}} v_S + \sqrt{4m_{N_{ii}}^2 + (y_{A_{ii}} v_S - y_{B_{ii}} v_S)^2} \right], \quad (2.34)$$

$$M_{N_{B_i}} = \frac{1}{2} \left[ y_{A_{ii}} v_S + y_{B_{ii}} v_S - \sqrt{4m_{N_{ii}}^2 + (y_{A_{ii}} v_S - y_{B_{ii}} v_S)^2} \right]. \quad (2.35)$$

The diagonalised basis (without the prime symbol) of the Majorana mass terms is defined as

$$\begin{bmatrix} N'_{A_i R} \\ N'_{B_i R} \end{bmatrix} = U_{N_i} \begin{bmatrix} N_{A_i R} \\ N_{B_i R} \end{bmatrix}. \quad (2.36)$$

We introduce the following compact notation for clarity in the mass eigenbases:

$$\begin{aligned} \mathcal{L}_{\text{Yukawa}} \supset & - \sum_{s^0=\eta_{R_1}, \eta_{R_2}, \eta_{I_1}, \eta_{I_2}} \left[ \mathcal{Y}_{A_i \alpha}^{(s^0)} \overline{N_{A_i R}} \nu_{\alpha L} s^0 + \mathcal{Y}_{B_i \alpha}^{(s^0)} \overline{N_{B_i R}} \nu_{\alpha L} s^0 \right] \\ & + \sum_{s^+ = \eta_1^+, \eta_2^+} \left[ \mathcal{Y}_{A_i \alpha}^{(s^+)} \overline{N_{A_i R}} \ell_{\alpha L}^- s^+ + \mathcal{Y}_{B_i \alpha}^{(s^+)} \overline{N_{B_i R}} \ell_{\alpha L}^- s^+ \right] + \text{h.c.}, \end{aligned} \quad (2.37)$$

with

$$\begin{aligned} \mathcal{Y}_{A_i \alpha}^{(\eta_{R_1})} &= + \frac{Y_A^{i\alpha}}{\sqrt{2}} c_{N_i} c_{\theta_R} + \frac{Y_B^{i\alpha}}{\sqrt{2}} s_{N_i} s_{\theta_R}, & \mathcal{Y}_{B_i \alpha}^{(\eta_{R_1})} &= - \frac{Y_A^{i\alpha}}{\sqrt{2}} s_{N_i} c_{\theta_R} + \frac{Y_B^{i\alpha}}{\sqrt{2}} c_{N_i} s_{\theta_R}, \\ \mathcal{Y}_{A_i \alpha}^{(\eta_{R_2})} &= - \frac{Y_A^{i\alpha}}{\sqrt{2}} c_{N_i} s_{\theta_R} + \frac{Y_B^{i\alpha}}{\sqrt{2}} s_{N_i} c_{\theta_R}, & \mathcal{Y}_{B_i \alpha}^{(\eta_{R_2})} &= + \frac{Y_A^{i\alpha}}{\sqrt{2}} s_{N_i} s_{\theta_R} + \frac{Y_B^{i\alpha}}{\sqrt{2}} c_{N_i} c_{\theta_R}, \\ \mathcal{Y}_{A_i \alpha}^{(\eta_{I_1})} &= + i \frac{Y_A^{i\alpha}}{\sqrt{2}} c_{N_i} c_{\theta_I} + i \frac{Y_B^{i\alpha}}{\sqrt{2}} s_{N_i} s_{\theta_I}, & \mathcal{Y}_{B_i \alpha}^{(\eta_{I_1})} &= - i \frac{Y_A^{i\alpha}}{\sqrt{2}} s_{N_i} c_{\theta_I} + i \frac{Y_B^{i\alpha}}{\sqrt{2}} c_{N_i} s_{\theta_I}, \\ \mathcal{Y}_{A_i \alpha}^{(\eta_{I_2})} &= - i \frac{Y_A^{i\alpha}}{\sqrt{2}} c_{N_i} s_{\theta_I} + i \frac{Y_B^{i\alpha}}{\sqrt{2}} s_{N_i} c_{\theta_I}, & \mathcal{Y}_{B_i \alpha}^{(\eta_{I_2})} &= + i \frac{Y_A^{i\alpha}}{\sqrt{2}} s_{N_i} s_{\theta_I} + i \frac{Y_B^{i\alpha}}{\sqrt{2}} c_{N_i} c_{\theta_I}, \\ \mathcal{Y}_{A_i \alpha}^{(\eta_1^+)} &= + Y_A^{i\alpha} c_{N_i} c_{\theta_{\text{cs}}} + Y_B^{i\alpha} s_{N_i} s_{\theta_{\text{cs}}}, & \mathcal{Y}_{B_i \alpha}^{(\eta_1^+)} &= - Y_A^{i\alpha} s_{N_i} c_{\theta_{\text{cs}}} + Y_B^{i\alpha} c_{N_i} s_{\theta_{\text{cs}}}, \\ \mathcal{Y}_{A_i \alpha}^{(\eta_2^+)} &= - Y_A^{i\alpha} c_{N_i} s_{\theta_{\text{cs}}} + Y_B^{i\alpha} s_{N_i} c_{\theta_{\text{cs}}}, & \mathcal{Y}_{B_i \alpha}^{(\eta_2^+)} &= + Y_A^{i\alpha} s_{N_i} s_{\theta_{\text{cs}}} + Y_B^{i\alpha} c_{N_i} c_{\theta_{\text{cs}}}, \end{aligned} \quad (2.38)$$

where the relative sign originates from the  $i\sigma_2$  matrix in Eq. (2.1).

## 2.2 Loop-Induced Neutrino Mass Terms

In our scenario, as in the original Scotogenic model, the left-handed active neutrino mass terms are radiatively generated at a one-loop level, where we adopt the parametrisation

$$\mathcal{L}_{\text{this model}} \supset - \frac{1}{2} \mathcal{M}_{\alpha \beta}^\nu \overline{(\nu'_{\alpha L})^c} \nu'_{\beta L} + \text{h.c..} \quad (2.39)$$

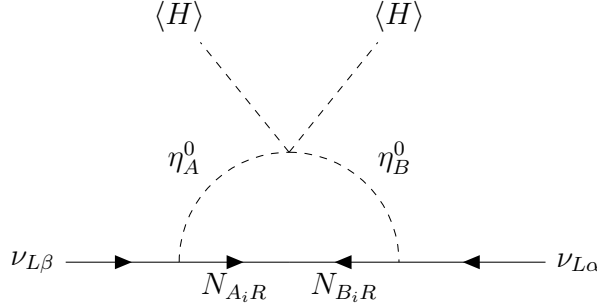


Figure 1: The topology of loop-induced mass generation is depicted in gauge eigenstates.

The calculation of the one-loop diagrams in Fig. 1 with the dimensional regularisation brings us the result,

$$\begin{aligned}
\mathcal{M}_{\alpha\beta}^\nu = & - \sum_{s^0=\eta_{R_1}, \eta_{R_2}, \eta_{I_1}, \eta_{I_2}} \sum_{i=1}^3 \frac{M_{N_{A_i}} \mathcal{Y}_{A_i\alpha}^{(s^0)} \mathcal{Y}_{A_i\beta}^{(s^0)}}{(4\pi)^2} \left\{ \frac{1}{\varepsilon} - \gamma + \log(4\pi) - \int_0^1 dx \log [x M_{s^0}^2 + (1-x) M_{N_{A_i}}^2 - i\epsilon] \right\} \\
& - \sum_{s^0=\eta_{R_1}, \eta_{R_2}, \eta_{I_1}, \eta_{I_2}} \sum_{i=1}^3 \frac{M_{N_{B_i}} \mathcal{Y}_{B_i\alpha}^{(s^0)} \mathcal{Y}_{B_i\beta}^{(s^0)}}{(4\pi)^2} \left\{ \frac{1}{\varepsilon} - \gamma + \log(4\pi) - \int_0^1 dx \log [x M_{s^0}^2 + (1-x) M_{N_{B_i}}^2 - i\epsilon] \right\} \\
= & - \sum_{s^0=\eta_{R_1}, \eta_{R_2}, \eta_{I_1}, \eta_{I_2}} \sum_{i=1}^3 \frac{M_{N_{A_i}} \mathcal{Y}_{A_i\alpha}^{(s^0)} \mathcal{Y}_{A_i\beta}^{(s^0)}}{(4\pi)^2} \left\{ - \int_0^1 dx \log [x M_{s^0}^2 + (1-x) M_{N_{A_i}}^2 - i\epsilon] \right\} \\
& - \sum_{s^0=\eta_{R_1}, \eta_{R_2}, \eta_{I_1}, \eta_{I_2}} \sum_{i=1}^3 \frac{M_{N_{B_i}} \mathcal{Y}_{B_i\alpha}^{(s^0)} \mathcal{Y}_{B_i\beta}^{(s^0)}}{(4\pi)^2} \left\{ - \int_0^1 dx \log [x M_{s^0}^2 + (1-x) M_{N_{B_i}}^2 - i\epsilon] \right\},
\end{aligned} \tag{2.40}$$

where  $1/\varepsilon$  and  $\gamma$  represent a divergent pole and the Euler-Mascheroni constant. As expected from the nature of higher-dimensional operators, the divergences in the active-neutrino mass terms are cancelled out in each of the  $A$  and  $B$  parts by use of Eq. (2.38). Note that this matrix is non-diagonal due to the degrees of freedom of  $\alpha$  and  $\beta$  ( $\alpha, \beta = 1, 2, 3$ ). Ignoring the  $i\epsilon$  term in the loop integral of heavy particles Eq. (2.40) we get,

$$\int_0^1 dx \log [x M_{s^0}^2 + (1-x) M_{N_{A_i}}^2] = -1 + \frac{M_{N_{A_i}}^2 \log(M_{N_{A_i}}^2) - M_{s^0}^2 \log(M_{s^0}^2)}{M_{N_{A_i}}^2 - M_{s^0}^2}. \tag{2.41}$$

As is apparent from the summation of the neutral scalars in Eq. (2.40),  $\mathcal{M}_{\alpha\beta}^\nu$  is dependent on the mass difference between the real and imaginary scalars, since their contributions are opposite to each other. If  $M_{R_1} = M_{I_1}$  and  $M_{R_2} = M_{I_2}$  all mass contribution to  $\mathcal{M}_{\alpha\beta}^\nu$  vanishes. The difference in their masses is parameterised by the coupling  $\lambda_5$  as seen in Eqs. (2.16) and (2.17).  $v_S$  must also be nonzero for a finite mass contribution.

Hereafter, we restrict the Yukawa parameter under the condition for further simplicity,

$$Y_A^{i\alpha} \longrightarrow Y^{i\alpha} \longleftarrow Y_B^{i\alpha}, \tag{2.42}$$

where so  $\mathcal{M}_{\alpha\beta}^\nu$  becomes

$$\mathcal{M}_{\alpha\beta}^\nu \rightarrow \sum_{i=1}^3 Y^{i\alpha} \mathcal{X}_i Y^{i\beta}, \quad (2.43)$$

where the derivation of  $\mathcal{X}_i$  is straightforward as

$$\begin{aligned} \mathcal{X}_i := & + \sum_{s^0=\eta_{R_1}, \eta_{R_2}, \eta_{I_1}, \eta_{I_2}} \frac{M_{N_{A_i}} \left( \mathcal{Y}_{A_i\alpha}^{(s^0)} / Y^{i\alpha} \right) \left( \mathcal{Y}_{A_i\beta}^{(s^0)} / Y^{i\beta} \right)}{(4\pi)^2} \int_0^1 dx \log \left[ x M_{s^0}^2 + (1-x) M_{N_{A_i}}^2 \right] \\ & + \sum_{s^0=\eta_{R_1}, \eta_{R_2}, \eta_{I_1}, \eta_{I_2}} \frac{M_{N_{B_i}} \left( \mathcal{Y}_{B_i\alpha}^{(s^0)} / Y^{i\alpha} \right) \left( \mathcal{Y}_{B_i\beta}^{(s^0)} / Y^{i\beta} \right)}{(4\pi)^2} \int_0^1 dx \log \left[ x M_{s^0}^2 + (1-x) M_{N_{B_i}}^2 \right], \end{aligned} \quad (2.44)$$

and this form follows the Casas-Ibarra parametrisation [198],<sup>3</sup>

$$Y^{i\alpha} = \sqrt{\mathcal{X}^{-1}} R_\nu \sqrt{M_{\hat{m}_\nu}} U_{\text{PMNS}}^\dagger, \quad (2.45)$$

where the following three-by-three matrices are introduced

$$\mathcal{X} := \begin{bmatrix} \mathcal{X}_1 & 0 & 0 \\ 0 & \mathcal{X}_2 & 0 \\ 0 & 0 & \mathcal{X}_3 \end{bmatrix}, \quad \sqrt{\mathcal{X}^{-1}} = \begin{bmatrix} (\mathcal{X}_1)^{-1/2} & 0 & 0 \\ 0 & (\mathcal{X}_2)^{-1/2} & 0 \\ 0 & 0 & (\mathcal{X}_3)^{-1/2} \end{bmatrix}, \quad \sqrt{M_{\hat{m}_\nu}} = \begin{bmatrix} \sqrt{\hat{m}_{\nu_1}} & 0 & 0 \\ 0 & \sqrt{\hat{m}_{\nu_2}} & 0 \\ 0 & 0 & \sqrt{\hat{m}_{\nu_3}} \end{bmatrix}. \quad (2.46)$$

$\hat{m}_{\nu_i}$  ( $i = 1, 2, 3$ ) are the mass eigenvalues of the three active neutrinos. Also,  $R_\nu$  and  $U_{\text{PMNS}}^\dagger$  are an arbitrary three-by-three orthogonal matrix and the PMNS matrix, respectively. As the only condition on  $R_\nu$  is that it is orthogonal, it provides the physical degrees of freedom in the Yukawa couplings after realising the observed masses and mixings of the active neutrinos.

While any orthogonal matrix  $R_\nu$  may be used in the Casas-Ibarra parameterisation, we scanned for an instance that produced a favourable Yukawa texture, i.e., high Yukawa for the 3rd generation Majorana neutrinos (DM and co-annihilating candidate). In the following analysis, we focus on the choice of  $R_\nu$ ,

$$R_\nu = \begin{bmatrix} 0.11641348 & 0.78579266 & 0.60743542 \\ -0.74517440 & -0.33523731 & 0.57648163 \\ 0.65663005 & -0.51975555 & 0.54652643 \end{bmatrix}. \quad (2.47)$$

Also, we assume the normal ordering of the three neutrino masses. Based on the data [200], we determine  $\hat{m}_{\nu_1} = 0.01 \text{ eV}$ ,  $\hat{m}_{\nu_2} = \hat{m}_{\nu_1} + \sqrt{\Delta m_{21}^2} = \hat{m}_{\nu_1} + 8.6 \times 10^{-3} \text{ eV} = 0.0186 \text{ eV}$ , and  $\hat{m}_{\nu_3} = \hat{m}_{\nu_1} + \sqrt{\Delta m_{32}^2 + \Delta m_{21}^2} = \hat{m}_{\nu_1} + 0.05 \text{ eV} = 0.060 \text{ eV}$ . For the mixing angles, we follow the parametrisation,

$$U_{\text{PMNS}} = \begin{pmatrix} c_{12}c_{13} & s_{12}c_{13} & s_{13}e^{-i\delta_{\text{CP}}} \\ -s_{12}c_{23} - c_{12}s_{13}s_{23}e^{i\delta_{\text{CP}}} & c_{12}c_{23} - s_{12}s_{13}s_{23}e^{i\delta_{\text{CP}}} & c_{13}s_{23} \\ s_{12}s_{23} - c_{12}s_{13}c_{23}e^{i\delta_{\text{CP}}} & -c_{12}s_{23} - s_{12}s_{13}c_{23}e^{i\delta_{\text{CP}}} & c_{13}c_{23} \end{pmatrix},$$

where  $c_{ij} = \cos \theta_{ij}$ ,  $s_{ij} = \sin \theta_{ij}$ , and  $\delta_{\text{CP}}$  the CP-violating phase, and we will adopt the best-fit result for the normal mass ordering in Table 1 of [201];  $\theta_{12} = 33.68^\circ$ ,  $\theta_{23} = 43.3^\circ$ ,  $\theta_{13} = 8.56^\circ$ , and  $\delta_{\text{CP}} = 212^\circ$ .

---

<sup>3</sup>A systematic generalisation of this parametrisation is found in [199].

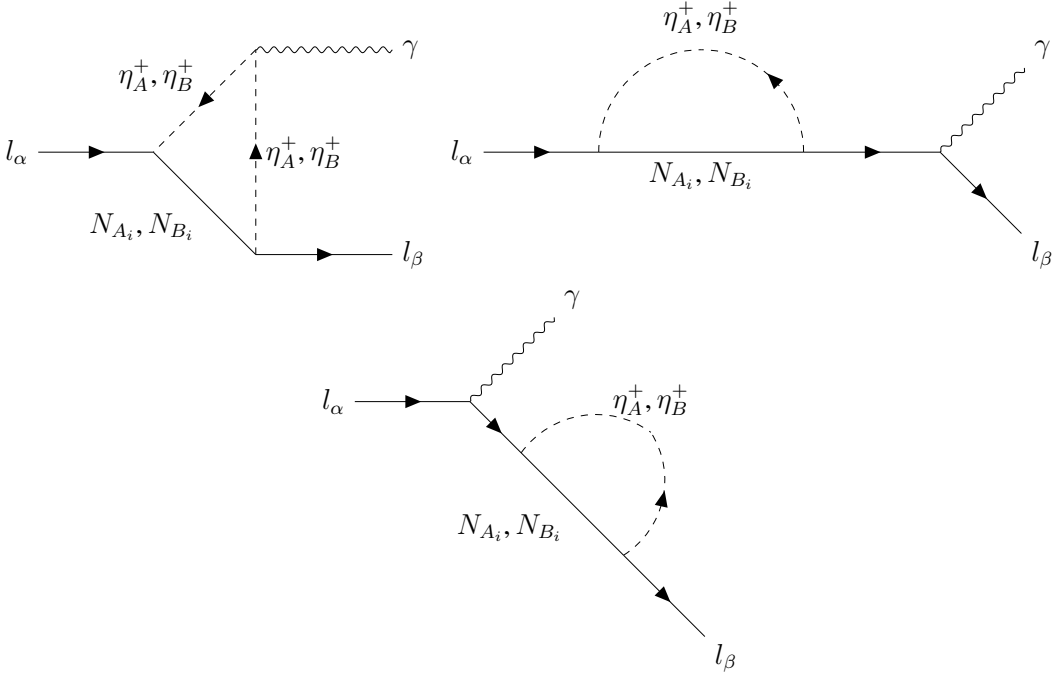


Figure 2: The Feynman diagrams contributing to  $l_\alpha \rightarrow l_\beta + \gamma$  are shown in mass eigenstates.

### 3 Non-DM Constraints on the Model

This section will discuss constraints other than DM physics on our  $Z_4$ -based Scotogenic scenario.

#### 3.1 Lepton Flavour Violation

We present the formulae involved in calculating the branching ratios of  $l_\alpha \rightarrow l_\beta + \gamma$  ( $l_1 = e$ ,  $l_2 = \mu$ ,  $l_3 = \tau$ ), as shown in Fig. 2. The general form of the decay amplitudes squared is given by

$$|\mathcal{M}_{\alpha\beta}|^2 = \frac{e^2 m_{l_\alpha}^6}{4(4\pi)^4} \left| \sum_{i=1}^3 \sum_{s^+ = \eta_1^+, \eta_2^+} \left[ \frac{\left(\mathcal{Y}_{A_i\beta}^{(s^+)}\right)^* \mathcal{Y}_{A_i\alpha}^{(s^+)} }{M_{s^+}^2} F_2\left(\frac{M_{N_{A_i}}^2}{M_{s^+}^2}\right) + \frac{\left(\mathcal{Y}_{B_i\beta}^{(s^+)}\right)^* \mathcal{Y}_{B_i\alpha}^{(s^+)} }{M_{s^+}^2} F_2\left(\frac{M_{N_{B_i}}^2}{M_{s^+}^2}\right) \right] \right|^2, \quad (3.1)$$

where  $\alpha$  and  $\beta$  represent the initial and final lepton external states, assuming  $m_{l_\alpha} > m_{l_\beta}$  and the function  $F_2(x)$  is defined as

$$F_2(x) = \frac{1 - 6x + 3x^2 + 2x^3 - 6x^2 \ln x}{6(1 - x^4)}. \quad (3.2)$$

The decay width can be calculated using [202],

$$\Gamma_{l_\alpha \rightarrow l_\beta + \gamma} = \frac{p^*}{8\pi m_{l_\alpha}^2} |\mathcal{M}_{\alpha\beta}|^2, \quad p^* = \frac{1}{2m_{l_\alpha}} (m_{l_\alpha}^2 - m_{l_\beta}^2). \quad (3.3)$$

Using the total decay width  $\Gamma_\mu$ , the branching ratio of  $l_\alpha \rightarrow l_\beta + \gamma$  is estimated as

$$\text{Br}(l_\alpha \rightarrow l_\beta + \gamma) = \frac{\Gamma_{l_\alpha \rightarrow l_\beta + \gamma}}{\Gamma_\alpha}. \quad (3.4)$$

Channel	Observational upper limits
$\text{Br}(\mu^- \rightarrow e^- + \gamma)$	$< 3.1 \times 10^{-13}$ [203]
$\text{Br}(\tau^- \rightarrow \mu^- + \gamma)$	$< 4.4 \times 10^{-8}$ [204]
$\text{Br}(\tau^- \rightarrow e^- + \gamma)$	$< 3.3 \times 10^{-8}$ [204]

Table 2: Lepton flavour violation observational bounds at 90% confidence level (CL).

We will use the lifetimes  $\tau_\mu = 2.1969811 \times 10^{-6}$  s and  $\tau_\tau = 2.903 \times 10^{-13}$  s [200] and the experimental constraints on the three processes, summarised in Table 2.

### 3.2 Oblique Constraint

Following the prescription in [205], we define two matrices  $U$  and  $V$  having dimensions  $n_d \times n$  and  $n_d \times m$ . Here,  $n_d (= 3)$  is the number of  $SU(2)_L$  doublet scalars. In terms of the numbers of  $n_c (= 0)$  and  $n_n (= 1)$ , which are the numbers of complex  $SU(2)_L$ -singlet and real  $SU(2)_L$ -singlet scalars with zero hypercharge,  $n$  and  $m$  are defined as  $n := n_d + n_c (= 3)$  and  $m := n_n + 2n_d (= 7)$ , which represent the singly charged and neutral components' numbers (including the would-be Nambu-Goldstone (NG) degrees of freedom), respectively.  $U$  and  $V$  must satisfy,

$$\begin{bmatrix} G^+ \\ \eta'_A^+ \\ \eta'_B^+ \end{bmatrix} = U \begin{bmatrix} G^+ \\ \eta_1^+ \\ \eta_2^+ \end{bmatrix}, \quad \begin{bmatrix} h' + iG^0 \\ \eta'_{R_A} + i\eta'_{I_A} \\ \eta'_{R_B} + i\eta'_{I_B} \end{bmatrix} = V \begin{bmatrix} G^0 \\ h \\ \eta_{R_1} \\ \eta_{I_1} \\ \eta_{R_2} \\ \eta_{I_2} \\ s \end{bmatrix}, \quad (3.5)$$

where  $G^+$  and  $G^0$  are the would-be NG bosons of the SM Higgs doublet, corresponding to the longitudinal degrees of freedom, respectively. The structures of  $U$  and  $V$  are identified as

$$U = \begin{pmatrix} 1 & 0 & 0 \\ 0 & c_{\theta_{\text{cs}}} & -s_{\theta_{\text{cs}}} \\ 0 & s_{\theta_{\text{cs}}} & c_{\theta_{\text{cs}}} \end{pmatrix}, \quad (3.6)$$

$$V = \begin{pmatrix} i & c_\alpha & 0 & 0 & 0 & 0 & -s_\alpha \\ 0 & 0 & c_{\theta_R} & ic_{\theta_I} & -s_{\theta_R} & -is_{\theta_I} & 0 \\ 0 & 0 & s_{\theta_R} & is_{\theta_I} & c_{\theta_R} & ic_{\theta_I} & 0 \end{pmatrix}. \quad (3.7)$$

From this setup, we can calculate the deviation of the  $\rho$  parameter  $\Delta\rho$  using the general formula in [205],

$$\begin{aligned} \Delta\rho = & \frac{g^2}{64\pi^2 M_W^2} \left[ \sum_{a=2}^n \sum_{b=2}^m |(U^\dagger V)_{ab}|^2 F(m_a^2, m_b^2) \right. \\ & - \sum_{b=2}^{m-1} \sum_{b'=b+1}^m [\text{Im}(V^\dagger V)_{bb'}]^2 F(m_b^2, m_{b'}^2) \\ & \left. - 2 \sum_{a=2}^{n-1} \sum_{a'=a+1}^n [(U^\dagger U)_{aa'}]^2 F(m_a^2, m_{a'}^2) \right] \end{aligned}$$

$$\begin{aligned}
& + 3 \sum_{b=2}^m \left[ \text{Im} (V^\dagger V)_{1b} \right]^2 \left[ F(M_Z^2, m_b^2) - F(M_W^2, m_b^2) \right] \\
& - 3 \left[ F(M_Z^2, M_h^2) - F(M_W^2, M_h^2) \right] \Bigg], \tag{3.8}
\end{aligned}$$

where  $g$  is the  $SU(2)_L$  gauge coupling, and  $M_W$  and  $M_Z$  are the  $W$ -boson and  $Z$ -boson masses.  $m_a$  (also  $m_{a'}$ ) and  $m_b$  (also  $m_{b'}$ ) denote the masses of the charged scalars and neutral scalars in the mass eigenstates, respectively. The two states identified by  $a = 1$  or  $b = 1$  are unphysical; therefore, they are not considered in Eq. (3.8). Equation (3.8) is simplified in the models with no  $SU(2)_L$ -singlet charged scalars, as in our model, where the third term proportional to  $U^\dagger U$  vanishes as  $U^\dagger U$  in unity, and since the summation is over off-diagonal elements, the term has no contributions. The function  $F(x, y)$  in Eq. (3.8) is defined as

$$F(x, y) = \begin{cases} 0 & \text{if } x = y, \\ \frac{x+y}{2} - \frac{xy \ln(x/y)}{x-y} & \text{otherwise.} \end{cases} \tag{3.9}$$

To compare with observational results [206], we use the parameter  $T$ ,

$$T = \frac{\Delta\rho}{\alpha(M_Z)}. \tag{3.10}$$

We consider the case when  $U = 0$ , and we use the central value of  $\alpha(M_Z) = (127.951 \pm 0.009)^{-1}$ , which is the quantum-electrodynamical fine structure constant defined in the  $\overline{\text{MS}}$  scheme with 5 quark flavours [206]. We will target the following value via statistical analysis [200]:

$$T = 0.01 \pm 0.12. \tag{3.11}$$

### 3.3 Vacuum Stability

#### 3.3.1 Boundness from below

For the constraints via bounded from below, we need to look at the quartic part of the potential  $\mathcal{V}^{(4)}$  defined as

$$\begin{aligned}
\mathcal{V}^{(4)}(H, \eta_A, \eta_B, S) = & \frac{\lambda_{HS}}{2} S^2 (H^\dagger H) + \frac{\lambda_{S\eta_A}}{2} S^2 (\eta_A^\dagger \eta_A) + \frac{\lambda_{S\eta_B}}{2} S^2 (\eta_B^\dagger \eta_B) \\
& + \frac{\lambda_H}{2} (H^\dagger H)^2 + \frac{\lambda_S}{4} S^4 + \frac{\lambda_{2a}}{2} (\eta_A^\dagger \eta_A)^2 + \frac{\lambda_{2b}}{2} (\eta_B^\dagger \eta_B)^2 + \frac{\lambda_{2c}}{2} (\eta_A^\dagger \eta_A) (\eta_B^\dagger \eta_B) \\
& + \frac{\lambda_{2d}}{2} (\eta_A^\dagger \eta_B) (\eta_B^\dagger \eta_A) + \lambda_{3A} (H^\dagger H) (\eta_A^\dagger \eta_A) + \lambda_{3B} (H^\dagger H) (\eta_B^\dagger \eta_B) \\
& + \lambda_{4A} (H^\dagger \eta_A) (\eta_A^\dagger H) + \lambda_{4B} (H^\dagger \eta_B) (\eta_B^\dagger H) + \frac{1}{2} [\lambda_5 (H^\dagger \eta_A) (H^\dagger \eta_B) + \text{h.c.}], \tag{3.12}
\end{aligned}$$

where we took  $\lambda_6 = 0$  (refer to Eq. (2.2)). Assuming fields are real, we can rewrite the potential  $\mathcal{V}^{(4)}$  as described in [207],

$$\mathcal{V}^{(4)} = x^T \Lambda x, \tag{3.13}$$

with

$$x = \begin{pmatrix} H^2 \\ \eta_A^2 \\ \eta_A \eta_B \\ \eta_B^2 \\ S^2 \end{pmatrix}, \quad (3.14)$$

and

$$\Lambda = \begin{pmatrix} \frac{\lambda_H}{2} & \frac{\lambda_{3A} + \lambda_{4A}}{2} & \frac{\lambda_5}{2} & \frac{\lambda_{3B} + \lambda_{4B}}{2} & \frac{\lambda_{HS}}{4} \\ \frac{\lambda_{3A} + \lambda_{4A}}{2} & \frac{\lambda_{2a}}{2} & 0 & \frac{(1-c)}{2} \left( \frac{\lambda_{2c}}{2} + \frac{\lambda_{2d}}{2} \right) & \frac{\lambda_{S\eta A}}{4} \\ \frac{\lambda_5}{2} & 0 & c \left( \frac{\lambda_{2c}}{2} + \frac{\lambda_{2d}}{2} \right) & 0 & 0 \\ \frac{\lambda_{3B} + \lambda_{4B}}{2} & \frac{(1-c)}{2} \left( \frac{\lambda_{2c}}{2} + \frac{\lambda_{2d}}{2} \right) & 0 & \frac{\lambda_{2b}}{2} & \frac{\lambda_{S\eta B}}{4} \\ \frac{\lambda_{HS}}{4} & \frac{\lambda_{S\eta A}}{4} & 0 & \frac{\lambda_{S\eta B}}{4} & \frac{\lambda_S}{4} \end{pmatrix}. \quad (3.15)$$

$c$  is an arbitrary constant due to the ambiguity in  $(\eta_A \eta_B)^2$  terms.

The requirement of stability means demanding that the quartic part of the potential  $\mathcal{V}^{(4)} > 0$  as the fields  $\phi_i \rightarrow \infty$ . To find the conditions for  $\mathcal{V}^{(4)} > 0$  we can impose positivity condition on  $\Lambda$  [207]. We use the Sylvester criterion for the positivity of  $\Lambda$ , assuming  $\phi_i \phi_j \in \mathcal{R}$ . We must apply the Sylvester criterion to all permutations of the basis vector  $x$ . Sylvester's criterion states that a  $n \times n$  Hermitian matrix  $\Lambda$  is positive-definite if and only if all the following matrices have a positive determinant: the upper left 1-by-1 corner of  $\Lambda$ , the upper left 2-by-2 corner of  $\Lambda$ , and go on. This sequence continues till  $\Lambda$  itself.

We can then write down the general conditions,

$$\lambda_{ii} > 0, \quad (3.16)$$

$$\lambda_{ii} \lambda_{jj} - \lambda_{ij}^2 > 0 \quad \text{for } i \neq j, \quad (3.17)$$

$$\begin{vmatrix} \lambda_{ii} & \lambda_{ij} & \lambda_{ik} \\ \lambda_{ji} & \lambda_{jj} & \lambda_{jk} \\ \lambda_{ki} & \lambda_{kj} & \lambda_{kk} \end{vmatrix} > 0 \quad \text{for } i \neq j \neq k, \quad \begin{vmatrix} \lambda_{ii} & \lambda_{ij} & \lambda_{ik} & \lambda_{il} \\ \lambda_{ji} & \lambda_{jj} & \lambda_{jk} & \lambda_{jl} \\ \lambda_{ki} & \lambda_{kj} & \lambda_{kk} & \lambda_{kl} \\ \lambda_{li} & \lambda_{lj} & \lambda_{lk} & \lambda_{ll} \end{vmatrix} > 0 \quad \text{for } i \neq j \neq k \neq l, \quad (3.18)$$

$$\text{Det}[\Lambda] > 0. \quad (3.19)$$

$\lambda_{ij}$ 's are the elements of matrix  $\Lambda$  where  $i, j, k = 1, 2, 3, 4, 5$  are the represent the element position of the matrix.

We get 5 constraints from the  $1 \times 1$  matrix,

$$\lambda_H > 0, \quad \lambda_{2a} > 0, \quad \lambda_{2b} > 0, \quad c(\lambda_{2c} + \lambda_{2d}) > 0, \quad \lambda_S > 0, \quad (3.20)$$

We get the following independent constraints from the  $2 \times 2$  matrices,

$$\lambda_H \lambda_{2a} - (\lambda_{3A} + \lambda_{4A})^2 > 0, \quad \lambda_H \lambda_{2b} - (\lambda_{3B} + \lambda_{4B})^2 > 0, \quad (3.21)$$

$$2\lambda_{2a}\lambda_S - \lambda_{S\eta A}^2 > 0, \quad 2\lambda_{2b}\lambda_S - \lambda_{S\eta B}^2 > 0, \quad (3.22)$$

$$2\lambda_H\lambda_S - \lambda_{HS}^2 > 0, \quad c\lambda_H(\lambda_{2c} + \lambda_{2d}) - \lambda_5^2 > 0, \quad (3.23)$$

$$4\lambda_{2a}\lambda_{2b} - (1-c)^2(\lambda_{2c} + \lambda_{2d})^2 > 0, \quad (3.24)$$

where 10 constraints appear from them if we do not remove redundancies. We get the following independent constraints from the  $3 \times 3$  matrices,

$$\begin{vmatrix} \frac{\lambda_H}{2} & \frac{\lambda_{3A}+\lambda_{4A}}{2} & \frac{\lambda_5}{2} \\ \frac{\lambda_{3A}+\lambda_{4A}}{2} & \frac{\lambda_{2a}}{2} & 0 \\ \frac{\lambda_5}{2} & 0 & c\left(\frac{\lambda_{2c}}{2} + \frac{\lambda_{2d}}{2}\right) \end{vmatrix} > 0, \quad \begin{vmatrix} \frac{\lambda_H}{2} & \frac{\lambda_{3B}+\lambda_{4B}}{2} & \frac{\lambda_5}{2} \\ \frac{\lambda_{3B}+\lambda_{4B}}{2} & \frac{\lambda_{2b}}{2} & 0 \\ \frac{\lambda_5}{2} & 0 & c\left(\frac{\lambda_{2c}}{2} + \frac{\lambda_{2d}}{2}\right) \end{vmatrix} > 0, \quad (3.25)$$

$$\begin{vmatrix} \frac{\lambda_H}{2} & \frac{\lambda_{HS}}{4} & \frac{\lambda_{3A}+\lambda_{4A}}{2} \\ \frac{\lambda_{HS}}{4} & \frac{\lambda_S}{4} & \frac{\lambda_{S\eta A}}{4} \\ \frac{\lambda_{3A}+\lambda_{4A}}{2} & \frac{\lambda_{S\eta A}}{4} & \frac{\lambda_{2a}}{2} \end{vmatrix} > 0, \quad \begin{vmatrix} \frac{\lambda_H}{2} & \frac{\lambda_{HS}}{4} & \frac{\lambda_{3B}+\lambda_{4B}}{2} \\ \frac{\lambda_{HS}}{4} & \frac{\lambda_S}{4} & \frac{\lambda_{S\eta B}}{4} \\ \frac{\lambda_{3B}+\lambda_{4B}}{2} & \frac{\lambda_{S\eta B}}{4} & \frac{\lambda_{2b}}{2} \end{vmatrix} > 0, \quad (3.26)$$

$$\begin{vmatrix} \frac{\lambda_H}{2} & \frac{\lambda_{3A}+\lambda_{4A}}{2} & \frac{\lambda_{3B}+\lambda_{4B}}{2} \\ \frac{\lambda_{3A}+\lambda_{4A}}{2} & \frac{\lambda_{2a}}{2} & \frac{(1-c)}{2}\left(\frac{\lambda_{2c}}{2} + \frac{\lambda_{2d}}{2}\right) \\ \frac{\lambda_{3B}+\lambda_{4B}}{2} & \frac{(1-c)}{2}\left(\frac{\lambda_{2c}}{2} + \frac{\lambda_{2d}}{2}\right) & \frac{\lambda_{2b}}{2} \end{vmatrix} > 0, \quad \begin{vmatrix} \frac{\lambda_S}{4} & \frac{\lambda_{S\eta A}}{4} & \frac{\lambda_{S\eta B}}{4} \\ \frac{\lambda_{S\eta A}}{4} & \frac{\lambda_{2a}}{2} & \frac{(1-c)}{2}\left(\frac{\lambda_{2c}}{2} + \frac{\lambda_{2d}}{2}\right) \\ \frac{\lambda_{S\eta B}}{4} & \frac{(1-c)}{2}\left(\frac{\lambda_{2c}}{2} + \frac{\lambda_{2d}}{2}\right) & \frac{\lambda_{2b}}{2} \end{vmatrix} > 0, \quad (3.27)$$

$$\begin{vmatrix} \frac{\lambda_H}{2} & \frac{\lambda_{HS}}{4} & \frac{\lambda_5}{2} \\ \frac{\lambda_{HS}}{4} & \frac{\lambda_S}{4} & 0 \\ \frac{\lambda_5}{2} & 0 & \frac{\lambda_{2b}}{2} \end{vmatrix} > 0, \quad (3.28)$$

where 10 constraints appear from them if we do not remove redundancies. We get the following independent constraints from the  $4 \times 4$  matrices,

$$\begin{vmatrix} \frac{\lambda_H}{2} & \frac{\lambda_{3A}+\lambda_{4A}}{2} & \frac{\lambda_5}{2} & \frac{\lambda_{3B}+\lambda_{4B}}{2} \\ \frac{\lambda_{3A}+\lambda_{4A}}{2} & \frac{\lambda_{2a}}{2} & 0 & \frac{(1-c)}{2}\left(\frac{\lambda_{2c}}{2} + \frac{\lambda_{2d}}{2}\right) \\ \frac{\lambda_5}{2} & 0 & c\left(\frac{\lambda_{2c}}{2} + \frac{\lambda_{2d}}{2}\right) & 0 \\ \frac{\lambda_{3B}+\lambda_{4B}}{2} & \frac{(1-c)}{2}\left(\frac{\lambda_{2c}}{2} + \frac{\lambda_{2d}}{2}\right) & 0 & \frac{\lambda_{2b}}{2} \end{vmatrix} > 0, \quad (3.29)$$

$$\begin{vmatrix} \frac{\lambda_H}{2} & \frac{\lambda_{3A}+\lambda_{4A}}{2} & \frac{\lambda_5}{2} & \frac{\lambda_{HS}}{4} \\ \frac{\lambda_{3A}+\lambda_{4A}}{2} & \frac{\lambda_{2a}}{2} & 0 & \frac{\lambda_{S\eta A}}{4} \\ \frac{\lambda_5}{2} & 0 & c\left(\frac{\lambda_{2c}}{2} + \frac{\lambda_{2d}}{2}\right) & 0 \\ \frac{\lambda_{HS}}{4} & \frac{\lambda_{S\eta A}}{4} & 0 & \frac{\lambda_S}{4} \end{vmatrix} > 0, \quad (3.30)$$

$$\begin{vmatrix} \frac{\lambda_H}{2} & \frac{\lambda_{3B}+\lambda_{4B}}{2} & \frac{\lambda_5}{2} & \frac{\lambda_{HS}}{4} \\ \frac{\lambda_{3B}+\lambda_{4B}}{2} & \frac{\lambda_{2b}}{2} & 0 & \frac{\lambda_{S\eta B}}{4} \\ \frac{\lambda_5}{2} & 0 & c\left(\frac{\lambda_{2c}}{2} + \frac{\lambda_{2d}}{2}\right) & 0 \\ \frac{\lambda_{HS}}{4} & \frac{\lambda_{S\eta B}}{4} & 0 & \frac{\lambda_S}{4} \end{vmatrix} > 0, \quad (3.31)$$

$$\begin{vmatrix} \frac{\lambda_H}{2} & \frac{\lambda_{3A}+\lambda_{4A}}{2} & \frac{\lambda_{3B}+\lambda_{4B}}{2} & \frac{\lambda_{HS}}{4} \\ \frac{\lambda_{3A}+\lambda_{4A}}{2} & \frac{\lambda_{2a}}{2} & \frac{(1-c)}{2}\left(\frac{\lambda_{2c}}{2} + \frac{\lambda_{2d}}{2}\right) & \frac{\lambda_{S\eta A}}{4} \\ \frac{\lambda_{3B}+\lambda_{4B}}{2} & \frac{(1-c)}{2}\left(\frac{\lambda_{2c}}{2} + \frac{\lambda_{2d}}{2}\right) & \frac{\lambda_{2b}}{2} & \frac{\lambda_{S\eta B}}{4} \\ \frac{\lambda_{HS}}{4} & \frac{\lambda_{S\eta A}}{4} & \frac{\lambda_{S\eta B}}{4} & \frac{\lambda_S}{4} \end{vmatrix} > 0, \quad (3.32)$$

where 5 constraints appear from them if we do not remove redundancies.

We must also constrain the value of  $c$  as described in [207], from second constraint of Eq. (3.23) requires  $|c| \geq |c_0|$ ,

$$c_0 = \frac{1}{(\lambda_{2c} + \lambda_{2d})} \left( \frac{\lambda_5^2}{\lambda_H} \right) \quad (3.33)$$

The extrema solutions of the left-hand side of the inequality Eq. (3.29) with respect to  $c$  are  $c_+$ ,  $c_-$ . We check which solution gives the maximum value for the inequality of Eq. (3.29) by substituting for  $c$  in its second derivative.

Finally, we have constraints,

$$c = \begin{cases} \max(c_0, c_+) & \text{if } (\lambda_{2c} + \lambda_{2d}) > 0, \\ \max(c_0, c_-) & \text{if } (\lambda_{2c} + \lambda_{2d}) < 0, \\ 0 & \text{if } (\lambda_{2c} + \lambda_{2d}) = 0. \end{cases} \quad (3.34)$$

We can compare and check our results with [208] for the  $Z_4$  three doublet model if we turn off coupling with the  $S$  field and take its mass to zero. Our result is a match.

### 3.3.2 Inert condition via Hessian

The potential in Eq. (2.2) should not develop a VEV in the inert direction. We find these constraints by constructing the hessian matrix  $H$  described in [208].

$$(H)_{ij} = \frac{\partial^2 \mathcal{V}}{\partial \phi_i \partial \phi_j} \Big|_{\phi_i = \langle \phi_i \rangle, \phi_j = \langle \phi_j \rangle}, \quad (3.35)$$

where  $\phi_i, \phi_j = \{H, \eta_A, \eta_B, S\}$  assuming  $\phi_i \in \mathcal{R}$ . We consider the minimum case  $\{v_H, 0, 0, v_S\}$ .

$$H = \begin{pmatrix} 2m_H^2 + 3v_H^2 \lambda_H + v_S^2 \lambda_{HS} & 0 & 0 & \sqrt{2}v_H v_S \lambda_{HS} \\ 0 & 2m_{\eta_A}^2 + v_H^2 (\lambda_{3A} + \lambda_{4A}) + v_S^2 \lambda_{S\eta_A} & \frac{\lambda_5 v_h^2}{4} & 0 \\ 0 & \frac{\lambda_5 v_h^2}{4} & m_{\eta_B}^2 + v_H^2 (\lambda_{3B} + \lambda_{4B}) + v_S^2 \lambda_{S\eta_B} & 0 \\ \sqrt{2}v_H v_S \lambda_{HS} & 0 & 0 & m_S^2 + \frac{v_H^2}{2} \lambda_{HS} + 3v_S^2 \lambda_S \end{pmatrix} \quad (3.36)$$

The Hessian must be positive, therefore we impose the Sylvester criterion to get the following constraints,

$$\begin{aligned} 2m_H^2 + 3v_H^2 \lambda_H + v_S^2 \lambda_{HS} &> 0, & 2m_{\eta_A}^2 + v_H^2 (\lambda_{3A} + \lambda_{4A}) + v_S^2 \lambda_{S\eta_A} &> 0 \\ 2m_{\eta_B}^2 + v_H^2 (\lambda_{3B} + \lambda_{4B}) + v_S^2 \lambda_{S\eta_B} &> 0, & m_S^2 + \frac{v_H^2}{2} \lambda_{HS} + 3v_S^2 \lambda_S &> 0. \end{aligned} \quad (3.37)$$

$$\begin{aligned} (2m_{\eta_A}^2 + v_H^2 (\lambda_{3A} + \lambda_{4A}) + v_S^2 \lambda_{S\eta_A}) (m_{\eta_B}^2 + v_H^2 (\lambda_{3B} + \lambda_{4B}) + v_S^2 \lambda_{S\eta_B}) - \left( \frac{\lambda_5 v_h^2}{4} \right)^2 &> 0, \\ (2m_H^2 + 3v_H^2 \lambda_H + \lambda_{HS} v_S^2) \left( m_S^2 + \frac{v_H^2}{2} \lambda_{HS} + 3v_S^2 \lambda_S \right) - 2(v_H v_S \lambda_{HS})^2 &> 0. \end{aligned} \quad (3.38)$$

Here, we have simplified and removed redundant constraints of the criteria.

## 4 Dark Matter Phenomenology

As we discussed in Section 2.1, the lightest fermion that possesses the  $Z_4$  parity  $+i$  or  $-i$  is stabilised by the residual  $Z_2$  parity, and it can be a dark matter candidate  $\chi$ . In this paper, we focus on the scenario that one of the heavy Majorana neutrinos  $N_{A_i}$  or  $N_{B_i}$  ( $i = 1, 2, 3$ ) is a dark matter candidate. Which one is appropriate will be debated later.

We will consider the ordinary thermal freeze-out scenario in our Scotogenic model. First, we will briefly summarise the scenario of dark matter. We follow the procedure in [209] in our implementation.

### 4.1 Relic Density through Thermal Freeze-out

#### 4.1.1 Thermal averaging

We first calculate the unpolarized annihilation rate,

$$W_{ij \rightarrow kl} = \frac{p_{kl}}{16\pi^2 g_i g_j S_{kl} \sqrt{s}} \int \overline{|\mathcal{M}_{ij \rightarrow kl}|^2} d\Omega, \quad \overline{|\mathcal{M}_{ij \rightarrow kl}|^2} := \sum_{\text{internal d.o.f.}} |\mathcal{M}_{ij \rightarrow kl}|^2, \quad (4.1)$$

where  $\sqrt{s}$  is the total energy of the centre-of-the-mass system and  $d\Omega$  is the solid angle for the final state.  $\sum_{\text{internal d.o.f.}} |\mathcal{M}_{ij \rightarrow kl}|^2$  is the square amplitude of the process  $ij \rightarrow kl$  averaged over initial internal degrees of freedoms (d.o.f.) and summing over final d.o.f. [210]. The subscripts  $i, j$  in Eq. (4.1) represent different species of initial dark matter particles and  $k, l$  are final SM particle species. The indices  $k$  and  $l$  discriminate particles in final states, and  $p_{kl}$  is the final centre of mass momentum, which is defined as,

$$p_{kl} = \frac{\sqrt{s - (m_k + m_l)^2} \sqrt{s - (m_k - m_l)^2}}{2\sqrt{s}}, \quad (4.2)$$

where  $g_i$  is the degrees of freedom for the dark matter particles ( $g_1 = 2$  for Majorana-fermion dark matter), and  $S_{kl}$  is the symmetry factor  $S_{kl} = 2$  for identical final particles and  $S_{kl} = 1$  otherwise. If we focus on a single DM candidate with no co-annihilation,  $i$  and  $j$  take only one, the effective unpolarized annihilation rate is,

$$W_{\text{eff}} = \sum_{k,l} W_{11 \rightarrow kl}. \quad (4.3)$$

$W_{\text{eff}}$  is the annihilation rate summed over all final state SM particles ( $k, l$ ).

At equilibrium, we approximate the momentum distribution of the dark matter candidate to follow the Maxwell-Boltzmann distribution. We now integrate the annihilation rate over the momentum distribution of the dark matter population,

$$\mathcal{A} = \frac{g^2 T}{4\pi^4} \int_0^\infty dp_{\text{eff}} p_{\text{eff}}^2 W_{\text{eff}} K_1 \left( \frac{\sqrt{s}}{T} \right), \quad (4.4)$$

$$p_{\text{eff}} = p_{11} = \frac{1}{2} \sqrt{s - 4M_\chi^2}, \quad (4.5)$$

where  $T$  describes the temperature,  $p_{\text{eff}}$  is the incoming momentum of the DM particle (in the centre of mass frame) and  $K_1(x)$  is a modified Bessel function of the second kind of order one. Equilibrium number density of the dark matter  $n_{\text{eq}}$  is

$$n_{\text{eq}} = \frac{T}{2\pi^2} g_\chi M_\chi^2 K_2 \left( \frac{M_\chi}{T} \right), \quad (4.6)$$

where  $K_2(x)$  is a modified Bessel function of the second kind of order two. The thermalised cross-section can then be put together,

$$\langle \sigma_{\text{eff}} v \rangle = \frac{\mathcal{A}}{n_{\text{eq}}^2}. \quad (4.7)$$

In the case of co-annihilating dark matter, there is an additional normalisation for the case of co-annihilation. We calculate the effective unpolarised annihilation rate,

$$W_{\text{eff}} = \sum_{i,j} \sum_{k,l} \frac{p_{ij}}{p_{11}} \frac{g_i g_j}{g_1^2} W_{ij \rightarrow kl}, \quad (4.8)$$

$p_{11}$  is the initial centre of mass momentum when the two initial-state particles are the dark matter ( $i = j = 1$ ), while  $p_{ij}$  is that when the initial-state particles are the  $i$ -th and  $j$ -th dark matter candidates, defined as

$$p_{ij} = \frac{\sqrt{s - (M_{\chi_i} + M_{\chi_j})^2} \sqrt{s - (M_{\chi_i} - M_{\chi_j})^2}}{2\sqrt{s}}. \quad (4.9)$$

Also, the equilibrium number density in Eq. (4.6) is modified as

$$n_{\text{eq}} = \frac{T}{2\pi^2} \sum_i g_i M_{\chi_i}^2 K_2 \left( \frac{M_{\chi_i}}{T} \right), \quad (4.10)$$

where the summations over  $i$  in Eq. (4.10) is taken over the dark-matter candidates relevant in the co-annihilation.<sup>4</sup>

To calculate the thermal cross section in Eq. (4.7), we approximate  $T = T_{f_i}$  and  $x = x_f$  in the equilibrium number density as the different particles decouple at different temperatures.

$$T_{f_i} = \frac{M_{\chi_i}}{x_f}. \quad (4.11)$$

In the momentum integration of Eq. (4.4), we replace  $T$  with  $T_{f_1}$  as it is integrated over dark matter temperature.

#### 4.1.2 Boltzmann equation

Let us consider the quantity  $Y$ ; it is the ratio of dark matter number density  $n$  to entropy density of the universe  $s$ ,

$$Y = \frac{n}{s}. \quad (4.12)$$

---

<sup>4</sup>Furthermore, we should modify the variable  $Y$  [defined in Eq. (4.12)] in the thermal equilibrium, appearing in the Boltzmann equation to describe the thermal Freeze-out DM scenario in Eq. (4.13) for the coannihilation case as [209]

$$Y_{\text{eq}} = \frac{45x^2}{4\pi^4 h_{\text{eff}}} \sum_i g_i \left( \frac{M_{\chi_i}}{M_{\chi_1}} \right)^2 K_2 \left( x \frac{M_{\chi_i}}{M_{\chi_1}} \right).$$

We make the same scaling modification to the rescaled variable [defined in Eq. (4.16)] as described earlier, the new yield at equilibrium is

$$y_{\text{eq}} = \frac{M_{\text{PL}} \sqrt{g^*} x^2}{\sqrt{90} h_{\text{eff}} \pi^3} \sum_i g_i \left( \frac{M_{\chi_i}}{M_{\chi_1}} \right)^2 K_2 \left( x \frac{M_{\chi_i}}{M_{\chi_1}} \right).$$

$Y$  is the measure of dark matter number density; solving the following Boltzmann equation allows us to compare  $Y_\infty$  after the freeze-out mechanism as measured by Planck [211]  $\Omega h^2 = 0.120 \pm 0.001$ ,

$$\frac{dY}{dx} = -\sqrt{\frac{\pi}{45G}} \frac{\sqrt{g^*} M_\chi}{x^2} \langle \sigma_{\text{eff}} v \rangle (Y^2 - Y_{\text{eq}}^2), \quad (4.13)$$

and the distribution of  $Y$  in the thermal equilibrium is represented as

$$Y_{\text{eq}} = \frac{n_{\text{eq}}}{s} = \frac{45x^2}{4\pi^4 h_{\text{eff}}} g_1 K_2(x), \quad (4.14)$$

where we introduced the dimensionless inverse temperature  $x$  as

$$x := \frac{m_1}{T}. \quad (4.15)$$

$g^*$  is the energy density degrees of freedom,  $h_{\text{eff}}$  is the entropy density degrees of freedom of the universe,  $G$  is the gravitational constant. We use the scaling trick suggested by [212] to rescale the Boltzmann equation Eq. (4.13) by multiplying it with a constant  $(M_{\text{PL}}(\frac{8\pi^2 g^*}{45})^{1/2})$ , we make the required changes to the Boltzmann equation.

$$\frac{dy}{dx} = -\langle \sigma_{\text{eff}} v \rangle M_\chi \frac{(y^2 - y_{\text{eq}}^2)}{x^2}, \quad y_{(\text{eq})} := M_{\text{PL}} \left( \frac{8\pi^2 g^*}{45} \right)^{1/2} Y_{(\text{eq})}, \quad (4.16)$$

$$y_{\text{eq}} = \frac{M_{\text{PL}} \sqrt{g^*} x^2}{\sqrt{90} h_{\text{eff}} \pi^3} g_1 K_2(x), \quad (4.17)$$

where  $y_{(\text{eq})}$  is the new rescaled abundance and  $M_{\text{PL}}$  is reduced Planck mass defined by  $M_{\text{PL}} = (8\pi G)^{-1/2}$ . This modification prevents numerical instabilities, which are common while solving the Boltzmann equation.

To solve Eq. (4.16), we approximate  $T = T_f$  and  $x = x_f$  when we calculate Eq. (4.7) which makes  $\langle \sigma v \rangle_{\text{eff}}$  a constant within the region of integration, where  $T_f$  and  $x_f$  represent the temperature at which dark matter decouples or freezes out of the thermal bath ( $x_f = M_\chi/T_f$ ).  $x_f$  typically ranges from 20 to 25, so we use  $x_f = 20$  for our numerical analysis. Above 100 GeV, the degrees of freedom  $g^* \simeq h_{\text{eff}} \approx 100$  and significantly decreases only at QCD phase transition (150 – 214 MeV) [213]. Since we are considering TeV-scale dark matter mass, we can use the typical value of  $g^* \simeq h_{\text{eff}} \approx 100$  as a constant throughout the integration range of the Boltzmann equation because decoupling will occur before a significant change in  $g^*$  and  $h_{\text{eff}}$ .

To obtain relic density analytically, we need to integrate the Boltzmann equation from  $x = 0$  to  $x_\infty := M_\chi/T_0$  where  $T_0$  is the present photon temperature of the universe ( $T_0 \sim 10^{-4}$  eV). We also have a boundary condition that is imposed  $Y_{\text{eq}} = Y(x = 0)$ , but practically, this is outside of the range of validity of the non-relativistic expressions used. In our analysis we take  $Y_{\text{eq}} = Y(x = 1)$  and integrate from  $x = 1$  to  $x = 10^3$ . We have verified there is no strong dependence on  $x$  for small  $x$  for the lower limit of the integration. We also check that  $x = 10^3$  is sufficiently large, beyond which the changes in relic density is insignificant.

At  $x = 10^3$ , we obtain the final abundance of dark matter, which can be plugged into the following formula to get the present dark matter relic density [209],

$$\Omega h^2 = 2.755 \times 10^8 \times \frac{M_\chi}{\text{GeV}} \times Y_\infty, \quad (4.18)$$

where  $Y_\infty$  is defined as  $Y(x = 10^3)$ .

### 4.1.3 Lepton-portal contributions

In our scenario, where one of the heavy Majorana neutrinos is a thermal dark matter particle  $\chi$ , through the Yukawa interaction in Eq. (2.37), the pair-annihilation channels  $\chi\chi \rightarrow l_\alpha \bar{l}_\beta$  and  $\chi\chi \rightarrow \nu_\alpha \bar{\nu}_\beta$  ( $\alpha, \beta = 1, 2, 3$ ) contribute. We get the following scattering amplitudes contributing to the relic abundance in the freeze-out scenario;  $\mathcal{M}_t$  and  $\mathcal{M}_u$  are the total  $t$ -channel and  $u$ -channel amplitudes, respectively.

$$4\overline{\left|\mathcal{M}_t^{(L)}\right|^2} = \sum_{\alpha, \beta = e, \mu, \tau} \left[ (t - M_\chi^2 - m_{l_\alpha}^2) (t - M_\chi^2 - m_{l_\beta}^2) \right] \left| \sum_{s^+ = \eta_1^+, \eta_2^+} \frac{\left(\mathcal{Y}_{\chi\alpha}^{(s^+)}\right)^* \mathcal{Y}_{\chi\beta}^{(s^+)} }{t - M_{s^+}^2} \right|^2 \\ + \sum_{\alpha, \beta = e, \mu, \tau} \left[ (t - M_\chi^2 - m_{\nu_\alpha}^2) (t - M_\chi^2 - m_{\nu_\beta}^2) \right] \left| \sum_{s^0 = \eta_{R1}, \eta_{R2}, \eta_{I1}, \eta_{I2}} \frac{\left(\mathcal{Y}_{\chi\alpha}^{(s^0)}\right)^* \mathcal{Y}_{\chi\beta}^{(s^0)} }{t - M_{s^0}^2} \right|^2, \quad (4.19)$$

$$4\overline{\left|\mathcal{M}_u^{(L)}\right|^2} = \sum_{\alpha, \beta = e, \mu, \tau} \left[ (u - M_\chi^2 - m_{l_\alpha}^2) (u - M_\chi^2 - m_{l_\beta}^2) \right] \left| \sum_{s^+ = \eta_1^+, \eta_2^+} \frac{\left(\mathcal{Y}_{\chi\alpha}^{(s^+)}\right)^* \mathcal{Y}_{\chi\beta}^{(s^+)} }{u - M_{s^+}^2} \right|^2 \\ + \sum_{\alpha, \beta = e, \mu, \tau} \left[ (u - M_\chi^2 - m_{\nu_\alpha}^2) (u - M_\chi^2 - m_{\nu_\beta}^2) \right] \left| \sum_{s^0 = \eta_{R1}, \eta_{R2}, \eta_{I1}, \eta_{I2}} \frac{\left(\mathcal{Y}_{\chi\alpha}^{(s^0)}\right)^* \mathcal{Y}_{\chi\beta}^{(s^0)} }{u - M_{s^0}^2} \right|^2, \quad (4.20)$$

$$4 \left( \overline{\mathcal{M}_t^{(L)\dagger} \mathcal{M}_u^{(L)}} + \overline{\mathcal{M}_u^{(L)\dagger} \mathcal{M}_t^{(L)}} \right) = \\ - \sum_{\alpha, \beta = e, \mu, \tau} 2 \left( s - m_{l_\alpha}^2 - m_{l_\beta}^2 \right) M_\chi^2 \text{Re} \left[ \sum_{s_1^+ = \eta_1^+, \eta_2^+} \left( \frac{\mathcal{Y}_{\chi\alpha}^{(s_1^+)} \left(\mathcal{Y}_{\chi\beta}^{(s_1^+)}\right)^*}{t - M_{s_1^+}^2} \right) \sum_{s_2^+ = \eta_1^+, \eta_2^+} \left( \frac{\left(\mathcal{Y}_{\chi\alpha}^{(s_2^+)}\right)^* \mathcal{Y}_{\chi\beta}^{(s_2^+)} }{u - M_{s_2^+}^2} \right) \right] \\ - \sum_{\alpha, \beta = e, \mu, \tau} 2 \left( s - m_{\nu_\alpha}^2 - m_{\nu_\beta}^2 \right) M_\chi^2 \text{Re} \left[ \sum_{\substack{s_1^0 = \eta_{R1}, \eta_{R2}, \\ \eta_{I1}, \eta_{I2}}} \left( \frac{\mathcal{Y}_{\chi\alpha}^{(s_1^0)} \left(\mathcal{Y}_{\chi\beta}^{(s_1^0)}\right)^*}{t - M_{s_1^0}^2} \right) \sum_{\substack{s_2^0 = \eta_{R1}, \eta_{R2}, \\ \eta_{I1}, \eta_{I2}}} \left( \frac{\left(\mathcal{Y}_{\chi\alpha}^{(s_2^0)}\right)^* \mathcal{Y}_{\chi\beta}^{(s_2^0)} }{u - M_{s_2^0}^2} \right) \right], \quad (4.21)$$

where  $\text{Re}[X]$  represents the real part of  $X$ , and we introduced the notation about the suffix for the Yukawa couplings in Eq. (2.37),

$$\mathcal{Y}_{\chi\alpha}^{(s)} := \text{the corresponding one from } \mathcal{Y}_{A_1\alpha}^{(s)}, \mathcal{Y}_{A_2\alpha}^{(s)}, \mathcal{Y}_{A_3\alpha}^{(s)}, \mathcal{Y}_{B_1\alpha}^{(s)}, \mathcal{Y}_{B_2\alpha}^{(s)}, \mathcal{Y}_{B_3\alpha}^{(s)}. \quad (4.22)$$

In the case of coannihilation, there are additional diagrams associated with the co-annihilating particle; we use the convention  $\chi_1$  for the DM candidate and  $\chi_2$  for the co-annihilating particle. In addition to

the  $t$ -channel diagrams for  $\chi_2\chi_2 \rightarrow l_\alpha\overline{l}_\beta$  that is added to dark matter annihilation, we will also have  $\chi_1\chi_2 \rightarrow l_\alpha\overline{l}_\beta$  as described above. The  $u$ -channel and mixed interaction only contribute to  $\chi_i\chi_i \rightarrow l_\alpha\overline{l}_\beta$  since  $\chi_1$  and  $\chi_2$  are not identical particles. The corresponding amplitudes squared for the coannihilation are written down as

$$4 \left( \left| \mathcal{M}_t^{(\text{L,co})} \right|^2 \right)_{ij} = \sum_{\alpha,\beta=e,\mu,\tau} \left[ (t - M_{\chi_i}^2 - m_{l_\alpha}^2) (t - M_{\chi_j}^2 - m_{l_\beta}^2) \right] \left| \sum_{s^+ = \eta_1^+, \eta_2^+} \frac{\left( \mathcal{Y}_{\chi_i \alpha}^{(s^+)} \right)^* \mathcal{Y}_{\chi_j \beta}^{(s^+)} }{t - M_{s^+}^2} \right|^2 + \sum_{\alpha,\beta=e,\mu,\tau} \left[ (t - M_{\chi_i}^2 - m_{\nu_\alpha}^2) (t - M_{\chi_j}^2 - m_{\nu_\beta}^2) \right] \left| \sum_{s^0 = \eta_{R_1}, \eta_{R_2}, \eta_{I_1}, \eta_{I_2}} \frac{\left( \mathcal{Y}_{\chi_i \alpha}^{(s^0)} \right)^* \mathcal{Y}_{\chi_j \beta}^{(s^0)} }{t - M_{s^0}^2} \right|^2, \quad (4.23)$$

$$4 \left( \left| \mathcal{M}_u^{(\text{L,co})} \right|^2 \right)_{ii} = \sum_{\alpha,\beta=e,\mu,\tau} \left[ (u - M_{\chi_i}^2 - m_{l_\alpha}^2) (u - M_{\chi_i}^2 - m_{l_\beta}^2) \right] \left| \sum_{s^+ = \eta_1^+, \eta_2^+} \frac{\left( \mathcal{Y}_{\chi_i \alpha}^{(s^+)} \right)^* \mathcal{Y}_{\chi_i \beta}^{(s^+)} }{u - M_{s^+}^2} \right|^2 + \sum_{\alpha,\beta=e,\mu,\tau} \left[ (u - M_{\chi_i}^2 - m_{\nu_\alpha}^2) (u - M_{\chi_i}^2 - m_{\nu_\beta}^2) \right] \left| \sum_{s^0 = \eta_{R_1}, \eta_{R_2}, \eta_{I_1}, \eta_{I_2}} \frac{\left( \mathcal{Y}_{\chi_i \alpha}^{(s^0)} \right)^* \mathcal{Y}_{\chi_i \beta}^{(s^0)} }{u - M_{s^0}^2} \right|^2, \quad (4.24)$$

$$4 \left( \mathcal{M}_t^{(\text{L,co})\dagger} \mathcal{M}_u^{(\text{L,co})} + \mathcal{M}_u^{(\text{L,co})\dagger} \mathcal{M}_t^{(\text{L,co})} \right)_{ii} = - \sum_{\alpha,\beta=e,\mu,\tau} 2 \left( s - m_{l_\alpha}^2 - m_{l_\beta}^2 \right) M_{\chi_i}^2 \text{Re} \left[ \sum_{s_1^+ = \eta_1^+, \eta_2^+} \left( \frac{\mathcal{Y}_{\chi_i \alpha}^{(s_1^+)} \left( \mathcal{Y}_{\chi_i \beta}^{(s_1^+)} \right)^*}{t - M_{s_1^+}^2} \right) \sum_{s_2^+ = \eta_1^+, \eta_2^+} \left( \frac{\left( \mathcal{Y}_{\chi_i \alpha}^{(s_2^+)} \right)^* \mathcal{Y}_{\chi_i \beta}^{(s_2^+)} }{u - M_{s_2^+}^2} \right) \right] - \sum_{\alpha,\beta=e,\mu,\tau} 2 \left( s - m_{\nu_\alpha}^2 - m_{\nu_\beta}^2 \right) M_{\chi_i}^2 \text{Re} \left[ \sum_{\substack{s_1^0 = \eta_{R_1}, \eta_{R_2}, \\ \eta_{I_1}, \eta_{I_2}}} \left( \frac{\mathcal{Y}_{\chi_i \alpha}^{(s_1^0)} \left( \mathcal{Y}_{\chi_i \beta}^{(s_1^0)} \right)^*}{t - M_{s_1^0}^2} \right) \sum_{\substack{s_2^0 = \eta_{R_1}, \eta_{R_2}, \\ \eta_{I_1}, \eta_{I_2}}} \left( \frac{\left( \mathcal{Y}_{\chi_i \alpha}^{(s_2^0)} \right)^* \mathcal{Y}_{\chi_i \beta}^{(s_2^0)} }{u - M_{s_2^0}^2} \right) \right]. \quad (4.25)$$

#### 4.1.4 Higgs-portal contributions

In our scenario, the six heavy right-handed neutrinos  $N_{A_i}$  and  $N_{B_i}$  couple with the singlet scalar  $S$ , and after the spontaneous symmetry breaking with a nonzero VEV for  $S$ , the residual  $Z_2$  symmetry remains, and the quantum fluctuation of  $S$  ( $s'$ ) mixes with the physical Higgs field  $h'$  [refer to Eqs. (2.3), (2.4) and (2.5)]. Therefore,  $\chi\chi \rightarrow [\text{a pair of SM particles}]$  is also possible as a Higgs portal.

We introduce the following compact notation for clarity to the relevant part of our calculation:

$$-\mathcal{L}_{\text{Higgs Yukawa}} \supset \sum_{i=1}^3 \sum_{h^0=h,s} \left[ \mathcal{Y}_{A_i}^{(h^0)} \overline{(N_{A_i R})^c} N_{A_i R} h^0 + \mathcal{Y}_{B_i}^{(h^0)} \overline{(N_{B_i R})^c} N_{B_i R} h^0 \right. \\ \left. + \mathcal{Y}_{AB_i}^{(h^0)} \overline{(N_{B_i R})^c} N_{A_i R} h^0 + \mathcal{Y}_{AB_i}^{(h^0)} \overline{(N_{A_i R})^c} N_{B_i R} h^0 \right], \quad (4.26)$$

with

$$\begin{aligned} \mathcal{Y}_{A_i}^{(h)} &= \frac{y_{A_{ii}}}{2} c_{N_i}^2 s_\alpha + \frac{y_{B_{ii}}}{2} s_{N_i}^2 s_\alpha, & \mathcal{Y}_{B_i}^{(h)} &= \frac{y_{A_{ii}}}{2} s_{N_i}^2 s_\alpha + \frac{y_{B_{ii}}}{2} c_{N_i}^2 s_\alpha, \\ \mathcal{Y}_{A_i}^{(s)} &= \frac{y_{A_{ii}}}{2} c_{N_i}^2 c_\alpha + \frac{y_{B_{ii}}}{2} s_{N_i}^2 c_\alpha, & \mathcal{Y}_{B_i}^{(s)} &= \frac{y_{A_{ii}}}{2} s_{N_i}^2 c_\alpha + \frac{y_{B_{ii}}}{2} c_{N_i}^2 c_\alpha, \\ \mathcal{Y}_{AB_i}^{(h)} &= \frac{y_{A_{ii}}}{2} s_{N_i} c_{N_i} s_\alpha - \frac{y_{B_{ii}}}{2} s_{N_i} c_{N_i} s_\alpha, & \mathcal{Y}_{AB_i}^{(s)} &= \frac{y_{A_{ii}}}{2} s_{N_i} c_{N_i} c_\alpha + \frac{y_{B_{ii}}}{2} s_{N_i} c_{N_i} c_\alpha, \end{aligned} \quad (4.27)$$

where the six Yukawa couplings  $y_{A_{ii}}$  and  $y_{B_{ii}}$  ( $i = 1, 2, 3$ ) do not appear in the active-neutrino mass formula and the lepton flavour violation, as shown in Eqs. (2.43), (2.44) and (3.1). So, these couplings are not constrained through these phenomena and play an important role in the Higgs-portal freeze-out DM scenario. Note that, in our current parametrisation, the six effective couplings in Eq. (4.27) are real.

The following part of the SM Higgs couplings is relevant for our study,

$$\mathcal{L}_{\text{Higgs, SM}} = \sum_{h^0=h,s} h^0 \left[ \mathcal{C}_W^{(h^0)} W_\mu^+ W^{-\mu} + \mathcal{C}_Z^{(h^0)} \frac{1}{2} Z_\mu Z^\mu \right] - \mathcal{Y}_f^{(h^0)} h^0 \bar{f} f, \quad (4.28)$$

with

$$\begin{aligned} \mathcal{C}_W^{(h)} &= \frac{2M_W^2 c_\alpha}{v_H}, & \mathcal{C}_Z^{(h)} &= \frac{2M_Z^2 c_\alpha}{v_H}, & \mathcal{Y}_f^{(h)} &= \frac{M_f c_\alpha}{v_H}, \\ \mathcal{C}_W^{(s)} &= -\frac{2M_W^2 s_\alpha}{v_H}, & \mathcal{C}_Z^{(s)} &= -\frac{2M_Z^2 s_\alpha}{v_H}, & \mathcal{Y}_f^{(s)} &= -\frac{M_f s_\alpha}{v_H}, \end{aligned} \quad (4.29)$$

where  $M_f$  is the mass of a SM fermion  $f$ .<sup>5</sup>

Under the interaction in Eq. (4.26) and Eq. (4.28), we get the  $s$ -channel scattering amplitudes as follows,

$$4 \overline{\left| \mathcal{M}_s^{(\text{H})} \right|^2} = \sum_f 16 \left[ (s - 4M_\chi^2) (s - 4M_f^2) \right] \left| \sum_{h^0=h,s} \frac{\mathcal{Y}_\chi^{(h^0)} \mathcal{Y}_f^{(h^0)}}{s - M_{h^0}^2 + iM_{h^0}\Gamma_{h^0}} \right|^2 \\ + 8 \left[ (s - 4M_\chi^2) \left( 2 - \frac{(s - 2M_W^2)^2}{4M_W^4} \right) \right] \left| \sum_{h^0=h,s} \frac{\mathcal{Y}_\chi^{(h^0)} \mathcal{C}_W^{(h^0)}}{s - M_{h^0}^2 + iM_{h^0}\Gamma_{h^0}} \right|^2 \\ + 8 \left[ (s - 4M_\chi^2) \left( 2 - \frac{(s - 2M_Z^2)^2}{4M_Z^4} \right) \right] \left| \sum_{h^0=h,s} \frac{\mathcal{Y}_\chi^{(h^0)} \mathcal{C}_Z^{(h^0)}}{s - M_{h^0}^2 + iM_{h^0}\Gamma_{h^0}} \right|^2, \quad (4.30)$$

---

<sup>5</sup>In the following analysis in Chapter 5, we will consider the top, bottom quarks (if kinematically accepted) as the final state  $f$  in our numerical scans for the DM mass  $\gtrsim 10^2$  GeV.

where  $f$  is summed over all SM fermions (coupled with the Higgs boson) and  $\Gamma_{h^0}$  represents the decay width of  $h^0$ .<sup>6</sup> The first term represents dark-matter pair annihilations into SM fermions, and the second and third terms represent those to SM massive gauge bosons  $W$  and  $Z$ , respectively.

In addition to the  $s$ -channel diagrams, we include  $t$ -channel and  $u$ -channel diagrams for  $\chi\chi \rightarrow hh$ , mediated via the Majorana fermions; this can be the dark matter particles and heavier ones. The following forms will be used for our numerical calculations,

$$4\overline{|\mathcal{M}_t^{(H)}|^2}_{11} = 4 \sum_{l,m=1,2} \left[ \frac{1}{2} (M_{\chi_1}^2 + M_{\chi_1}M_{\chi_l} + M_{\chi_1}M_{\chi_m}) (s + u - t - 4M_{\chi_1}^2) + \frac{1}{2} M_{\chi_l}M_{\chi_m} (s - 4M_{\chi_1}^2) + \frac{1}{2} M_{\chi_1}^2 (u - t) - \frac{M_h^4}{2} + \frac{1}{2} (M_{\chi_1}^2 - t) (M_{\chi_1}^2 - u) \right] \left( \frac{\mathcal{Y}_{\chi_l\chi_1}^{(h)} \mathcal{Y}_{\chi_l\chi_1}^{(h)}}{t - M_{\chi_l}^2} \right) \left( \frac{\mathcal{Y}_{\chi_1\chi_m}^{(h)} \mathcal{Y}_{\chi_1\chi_m}^{(h)}}{t - M_{\chi_m}^2} \right), \quad (4.31)$$

$$4\overline{|\mathcal{M}_u^{(H)}|^2}_{11} = 4 \sum_{l,m=1,2} \left[ \frac{1}{2} (M_{\chi_1}^2 + M_{\chi_1}M_{\chi_l} + M_{\chi_1}M_{\chi_m}) (s + t - u - 4M_{\chi_1}^2) + \frac{1}{2} M_{\chi_l}M_{\chi_m} (s - 4M_{\chi_1}^2) + \frac{1}{2} M_{\chi_1}^2 (t - u) - \frac{M_h^4}{2} + \frac{1}{2} (M_{\chi_1}^2 - t) (M_{\chi_1}^2 - u) \right] \left( \frac{\mathcal{Y}_{\chi_l\chi_1}^{(h)} \mathcal{Y}_{\chi_l\chi_1}^{(h)}}{u - M_{\chi_l}^2} \right) \left( \frac{\mathcal{Y}_{\chi_1\chi_m}^{(h)} \mathcal{Y}_{\chi_1\chi_m}^{(h)}}{u - M_{\chi_m}^2} \right), \quad (4.32)$$

$$4 \left( \overline{(\mathcal{M}_t^{(H)})^\dagger \mathcal{M}_u^{(H)}} + \overline{(\mathcal{M}_u^{(H)})^\dagger \mathcal{M}_t^{(H)}} \right)_{11} = -4 \sum_{l,m=1,2} \left[ -M_h^4 + (M_{\chi_1}^2 - t) (M_{\chi_1}^2 - u) - M_{\chi_1} (M_{\chi_l} + M_{\chi_m}) (u - t) - (s - 4M_{\chi_1}^2) (M_{\chi_1}^2 - M_{\chi_1}M_{\chi_l} + M_{\chi_1}M_{\chi_m} - M_{\chi_l}M_{\chi_m}) \right. \\ \times \left. \left( \frac{\mathcal{Y}_{\chi_l\chi_1}^{(h)} \mathcal{Y}_{\chi_l\chi_1}^{(h)}}{t - M_{\chi_l}^2} \right) \left( \frac{\mathcal{Y}_{\chi_1\chi_m}^{(h)} \mathcal{Y}_{\chi_1\chi_m}^{(h)}}{u - M_{\chi_m}^2} \right) \right], \quad (4.33)$$

where we put the condition that only the second-lightest Majorana fermion  $\chi_{i=2}$  ( $= \chi_2$ ) and the lightest as a dark matter  $\chi_{i=1}$  ( $= \chi_1 = \chi$ ) are taken into account. Also, we introduced similar notations for the Yukawa couplings as for the lepton-portal channels in Eq. (4.22) [refer to Eqs. (4.27) and (4.29)],

$$\mathcal{Y}_{\chi_1}^{(h)} := \text{the corresponding one from } \mathcal{Y}_{A_1}^{(h)}, \mathcal{Y}_{A_2}^{(h)}, \mathcal{Y}_{A_3}^{(h)}, \mathcal{Y}_{B_1}^{(h)}, \mathcal{Y}_{B_2}^{(h)}, \mathcal{Y}_{B_3}^{(h)}. \quad (4.34)$$

$$\mathcal{Y}_{\chi_1\chi_2}^{(h)} = \mathcal{Y}_{\chi_2\chi_1}^{(h)} := \text{the corresponding one from } \mathcal{Y}_{AB_1}^{(h)}, \mathcal{Y}_{AB_2}^{(h)}, \mathcal{Y}_{AB_3}^{(h)}. \quad (4.35)$$

Similar to the Lepton portal, we ought to consider additional diagrams involved in the coannihilation processes in the Higgs-portal scenario, too;  $\chi_2\chi_2 \rightarrow f\bar{f}$ ,  $\chi_1\chi_2 \rightarrow f\bar{f}$  as well as  $\chi_2\chi_2 \rightarrow b\bar{b}$ ,  $\chi_1\chi_2 \rightarrow b\bar{b}$  contribute to the relic in the co-annihilation scenario. Here,  $f$  and  $b$  are the standard model Fermions and Bosons, respectively.

$$4\overline{|\mathcal{M}_s^{(H,\text{co})}|^2}_{22} = \sum_f 16 [(s - 4M_{\chi_2}^2) (s - 4m_f^2)] \left| \sum_{h^0=h,s} \frac{\mathcal{Y}_{\chi_2}^{(h^0)} \mathcal{Y}_f^{(h^0)}}{s - M_{h^0}^2 + iM_{h^0}\Gamma_{h^0}} \right|^2 \\ + 8 \left[ (s - 4M_{\chi_2}^2) \left( 2 - \frac{(s - 2M_W^2)^2}{4M_W^4} \right) \right] \left| \sum_{h^0=h,s} \frac{\mathcal{Y}_{\chi_2}^{(h^0)} \mathcal{C}_W^{(h^0)}}{s - M_{h^0}^2 + iM_{h^0}\Gamma_{h^0}} \right|^2$$

---

<sup>6</sup>We will provide the calculation of  $\Gamma_s$  in Appendix A.

$$+8 \left[ (s - 4M_{\chi_2}^2) \left( 2 - \frac{(s - 2M_Z^2)^2}{4M_Z^4} \right) \right] \left| \sum_{h^0=h,s} \frac{\mathcal{Y}_{\chi_2}^{(h^0)} \mathcal{C}_Z^{(h^0)}}{s - M_{h^0}^2 + iM_{h^0}\Gamma_{h^0}} \right|^2, \quad (4.36)$$

$$\begin{aligned} 4 \overline{\left| \mathcal{M}_s^{(\text{H,co})} \right|_{12}^2} &= \sum_f 16 \left[ (s - (M_{\chi_1} + M_{\chi_2})^2) (s - 4m_f^2) \right] \left| \sum_{h^0=h,s} \frac{\mathcal{Y}_{\chi_1\chi_2}^{(h^0)} \mathcal{Y}_f^{(h^0)}}{s - M_{h^0}^2 + iM_{h^0}\Gamma_{h^0}} \right|^2 \\ &+ 8 \left[ (s - (M_{\chi_1} + M_{\chi_2})^2) \left( 2 - \frac{(s - 2M_W^2)^2}{4M_W^4} \right) \right] \left| \sum_{h^0=h,s} \frac{\mathcal{Y}_{\chi_1\chi_2}^{(h^0)} \mathcal{C}_W^{(h^0)}}{s - M_{h^0}^2 + iM_{h^0}\Gamma_{h^0}} \right|^2 \\ &+ 8 \left[ (s - (M_{\chi_1} + M_{\chi_2})^2) \left( 2 - \frac{(s - 2M_Z^2)^2}{4M_Z^4} \right) \right] \left| \sum_{h^0=h,s} \frac{\mathcal{Y}_{\chi_1\chi_2}^{(h^0)} \mathcal{C}_Z^{(h^0)}}{s - M_{h^0}^2 + iM_{h^0}\Gamma_{h^0}} \right|^2, \end{aligned} \quad (4.37)$$

where  $\mathcal{Y}_{\chi_2}^{(h^0)}$  is defined as similar as  $\mathcal{Y}_{\chi_1}^{(h^0)}$  in Eq. (4.34).

In the co-annihilation scenario, we replace the mass difference between the two species with  $\delta M_{ij} = |M_{\chi_j} - M_{\chi_i}|$ , where  $i = 1, 2$  and  $j = 1, 2$ , and  $\delta M_{ii} = 0$ .

$$\begin{aligned} 4 \left| \mathcal{M}_t^{(\text{H,co})} \right|_{ij}^2 &= 2 \sum_{l=1,2} \sum_{m=1,2} \left[ -M_h^2 (s - \delta M_{ij}^2 - (2M_{\chi_i} + M_{\chi_l} + M_{\chi_m}) \delta M_{ij}) \right. \\ &+ (s - M_{\chi_i}^2 - M_{\chi_j}^2) (M_{\chi_i}^2 + M_{\chi_i}M_{\chi_l} + M_{\chi_i}M_{\chi_m} + M_{\chi_l}M_{\chi_m}) \\ &+ (2M_{\chi_i} + M_{\chi_l} + M_{\chi_m}) (M_{\chi_j} (M_{\chi_i}^2 - t) - M_{\chi_i} (M_{\chi_j}^2 - u)) \\ &\left. + \frac{1}{2} (M_h^2 + M_{\chi_i}^2 - t) (M_h^2 + M_{\chi_j}^2 - u) \right] \left( \frac{(\mathcal{Y}_{\chi_i\chi_i}^{(h)}) \mathcal{Y}_{\chi_l\chi_j}^{(h)}}{t - M_{\chi_l}^2} \right) \left( \frac{(\mathcal{Y}_{\chi_i\chi_m}^{(h)}) \mathcal{Y}_{\chi_j\chi_m}^{(h)}}{t - M_{\chi_m}^2} \right), \end{aligned} \quad (4.38)$$

$$\begin{aligned} 4 \overline{\left| \mathcal{M}_u^{(\text{H,co})} \right|_{22}^2} &= 4 \sum_{l=1,2} \sum_{m=1,2} \left[ \frac{1}{2} (M_{\chi_2}^2 + M_{\chi_2}M_{\chi_l} + M_{\chi_2}M_{\chi_m}) (s + t - u - 4M_{\chi_2}^2) \right. \\ &+ \frac{1}{2} M_{\chi_l}M_{\chi_m} (s - 4M_{\chi_2}^2) + \frac{1}{2} M_{\chi_2}^2 (t - u) - \frac{M_h^4}{2} \\ &\left. + \frac{1}{2} (M_{\chi_2}^2 - t) (M_{\chi_2}^2 - u) \right] \left( \frac{(\mathcal{Y}_{\chi_l\chi_2}^{(h)}) \mathcal{Y}_{\chi_l\chi_2}^{(h)}}{u - M_{\chi_l}^2} \right) \left( \frac{(\mathcal{Y}_{\chi_2\chi_m}^{(h)}) \mathcal{Y}_{\chi_2\chi_m}^{(h)}}{u - M_{\chi_m}^2} \right), \end{aligned} \quad (4.39)$$

$$\begin{aligned} 4 \left( \overline{\left( \mathcal{M}_t^{(\text{H,co})} \right)^\dagger \mathcal{M}_u^{(\text{H,co})}} + \overline{\left( \mathcal{M}_u^{(\text{H,co})} \right)^\dagger \mathcal{M}_t^{(\text{H,co})}} \right)_{22} &= -4 \sum_{l=1,2} \sum_{m=1,2} \left[ -M_h^4 + (M_{\chi_2}^2 - t) (M_{\chi_2}^2 - u) \right. \\ &- M_{\chi_2} (M_{\chi_l} + M_{\chi_m}) (u - t) - (s - 4M_{\chi_2}^2) (M_{\chi_2}^2 - M_{\chi_2}M_{\chi_l} + M_{\chi_2}M_{\chi_m} - M_{\chi_l}M_{\chi_m}) \\ &\times \left. \left( \frac{(\mathcal{Y}_{\chi_l\chi_2}^{(h)}) \mathcal{Y}_{\chi_l\chi_2}^{(h)}}{t - M_{\chi_l}^2} \right) \left( \frac{(\mathcal{Y}_{\chi_2\chi_m}^{(h)}) \mathcal{Y}_{\chi_2\chi_m}^{(h)}}{u - M_{\chi_m}^2} \right) \right]. \end{aligned} \quad (4.40)$$

Note that the other possible processes with  $s$  in the final state,  $\chi + \chi \rightarrow h + s$  and  $\chi + \chi \rightarrow s + s$ . As we

will discuss, we focus on the kinematic region in  $2M_\chi \lesssim M_s$ , where the two processes are kinematically suppressed and may not contribute significantly. Therefore, we ignore them.

## 4.2 Constraints via Direct Detection

### 4.2.1 Lepton-portal contributions

We define  $\mathcal{A}_S$  as the Anapole moment; it is the effective coupling between a photon and the dark matter candidate (Majorana fermion) [214] via a charged scalar - SM lepton loop.

$$\mathcal{A}_S = -\frac{e}{96\pi^2 M_\chi^2} \sum_{s^+ = \eta_1^+, \eta_2^+} \sum_{\alpha=\mu, \tau} \left| \mathcal{Y}_{\chi\alpha}^{(s^+)} \right|^2 \mathcal{F} \left( \frac{m_{l_\alpha}}{M_\chi}, \frac{M_{s^+}}{M_\chi} \right) \quad (4.41)$$

$$-\frac{e}{32\pi^2 M_\chi^2} \sum_{s^+ = \eta_1^+, \eta_2^+} \left| \mathcal{Y}_{\chi e}^{(s^+)} \right|^2 \mathcal{F}_e \left( \frac{\sqrt{|q|^2}}{M_\chi}, \frac{M_{s^+}}{M_\chi} \right). \quad (4.42)$$

This calculation assumes the mass of the electron to be negligible; hence  $\alpha$  is only summed over  $\mu$  and  $\tau$ , the second line in Eq. (4.42) is the electron loop contribution. The formula holds only when momentum transfer from dark matter to the target nucleus  $q^2$  is greater than the lepton mass squared ( $q^2 > m_l^2$ ), as in our case. We use shorthand notations,  $\mu := M_{s^+}/M_\chi$  and  $\epsilon := m_{l_\alpha}/M_\chi$  below,

$$\mathcal{F}(\mu, \epsilon) = \frac{3}{2} \log \left( \frac{\mu^2}{\epsilon^2} \right) - \frac{1 + 3\mu^2 - 3\epsilon^2}{\sqrt{(\mu^2 - 1 - \epsilon^2)^2 - 4\epsilon^2}} \operatorname{Arctanh} \left( \frac{\sqrt{(\mu^2 - 1 - \epsilon^2)^2 - 4\epsilon^2}}{\mu^2 - 1 + \epsilon^2} \right), \quad (4.43)$$

$$\mathcal{F}_e \left( \frac{\sqrt{|q|^2}}{M_\chi}, \mu \right) = \frac{-10 + 12 \log \left( \frac{\sqrt{|q|^2}}{M_\chi} \right) - (3 + 9\mu^2) \log(\mu^2 - 1) - (3 - 9\mu^2) \log(\mu^2)}{9(\mu^2 - 1)}, \quad (4.44)$$

We quote (the relevant part of) the spin-independent differential cross-section of dark matter scattering off a nucleus having atomic number  $Z$  formula from [214],<sup>7</sup>

$$\frac{d\sigma_\chi^L}{dE_R} = 4\mathcal{A}_S^2 \left[ \alpha_{\text{EM}} Z^2 \left( 2m_T - \left( 1 + \frac{m_T}{M_\chi} \right)^2 \frac{E_R}{v^2} \right) F_Z^2(q^2) \right], \quad (4.45)$$

where  $E_R$  is the recoil energy,  $\alpha_{\text{EM}}$  the fine-structure constant in Electromagnetism,  $Z$  is the nuclear charge of the detector atom,  $m_T$  is the detector nucleus mass, and  $v$  is the velocity of the dark matter particle relative to that of the nucleus.  $F_Z(q)$  is the nuclear charge form factor [214],

$$F_Z(q) = 3e^{-\frac{q^2 s^2}{2}} \frac{(\sin(qr) - qr \cos(qr))}{(qr)^3}, \quad (4.46)$$

---

<sup>7</sup>Note that the full form of Eq. (4.45) is as follows,

$$\frac{d\sigma_\chi^L}{dE_R} = 4\mathcal{A}_S^2 \left[ \alpha_{\text{EM}} Z^2 \left( 2m_T - \left( 1 + \frac{m_T}{M_\chi} \right)^2 \frac{E_R}{v^2} \right) F_Z^2(q^2) + d_A^2 \left( \frac{J+1}{3J} \right) \frac{2E_R m_T^2}{\pi v^2} F_S^2(q^2) \right],$$

where the second term in the cross section describes the scattering with the magnetic dipole moment of the nucleus. This is subdominant in the Xenon detectors, which is relevant to our paper. Hence, it is dropped going forward.  $d_A$ ,  $J$  and  $F_S(q^2)$  are the nuclear dipole moment, the spin form factor, and the spin of the target nucleus.

where  $s = 1 \text{ fm}$ ,  $r = \sqrt{R^2 - 5s^2}$ ,  $R = 1.2A^{1/3} \text{ fm}$  (with the nuclear mass number  $A$ ). The (squared) momentum transfer from dark matter to the target nucleus  $q^2$  takes

$$q^2 = 2m_T E_R. \quad (4.47)$$

To compare with the latest dark matter direct detection experiments [183], we must write down the total DM-nucleon spin-independent cross section. We can express the DM velocity relative to the nucleus in terms of nucleus recoil energy [215],

$$v = \left[ \frac{m_T E_R}{\mu_{\chi T}^2 (1 - \cos \theta)} \right]^{1/2}, \quad (4.48)$$

where  $\mu_{\chi T}$  is the reduced mass of the dark matter-nucleus system. As described in [215], we integrate Eq. (4.45) over the solid angle and the recoil energy the detector is sensitive to. In the case of the LZ detector, we integrate from 5.5 to 55 KeV recoil energies, in which region the detector efficiency is  $> 50\%$  [183]

We can now compare the latest results of the LZ cross section per nucleon [183] with our calculated cross section

$$\sigma_{\chi p}^L = \frac{\sigma_{\chi}^L}{A}, \quad (4.49)$$

where  $A = 129$  for Xenon. The detector uses a mixture of isotopes of which  $\text{Xe}^{129}$  has the largest contribution. In Eq. (4.49), we have used a conservative, simple way to convert our calculated total cross-section into cross-section per nucleon.

#### 4.2.2 Higgs-portal contributions

We quote the spin-independent cross-section of dark matter scattering off a nucleon, having formula from [216],

$$y_{\chi H} = \begin{cases} \frac{y_{A_{ii}}}{2} c_{N_i}^2 + \frac{y_{B_{ii}}}{2} s_{N_i}^2 & \text{if } \chi \text{ is } N_{A_i} (i = 1, 2, 3), \\ \frac{y_{A_{ii}}}{2} s_{N_i}^2 + \frac{y_{B_{ii}}}{2} c_{N_i}^2 & \text{if } \chi \text{ is } N_{B_i} (i = 1, 2, 3), \end{cases} \quad (4.50)$$

$$\sigma_{\chi p}^H = \frac{\mu_{\chi p}^2}{\pi} \frac{y_{\chi H}^2 s_{\alpha}^2 c_{\alpha}^2 m_p^2}{v_H^2} \mathcal{F}_H(M_{\chi}, M_h, M_s, v) f_p^2. \quad (4.51)$$

We define coupling coupling  $y_{\chi H}$  between the neutral singlet  $S$  (gauge basis) and DM candidate  $\chi$  (mass basis) as is described in [216],

$$\begin{aligned} \mathcal{F}_H(M_{\chi}, M_{H_1}, M_{H_2}, v) &= \frac{1}{4M_{\chi}^2 v^2} \left[ \sum_{i=1,2} \left( \frac{1}{M_{H_i}^2} - \frac{1}{4M_{\chi}^2 v^2 + M_{H_i}^2} \right) \right. \\ &\quad \left. - \frac{2}{(M_{H_2}^2 - M_{H_1}^2)} \sum_{i=1}^2 (-1)^{i-1} \log \left( 1 + \frac{4M_{\chi}^2 v^2}{M_{H_i}^2} \right) \right], \end{aligned} \quad (4.52)$$

$$\mu_{\chi p} = \frac{m_p M_{\chi}}{m_p + M_{\chi}}, \quad (4.53)$$

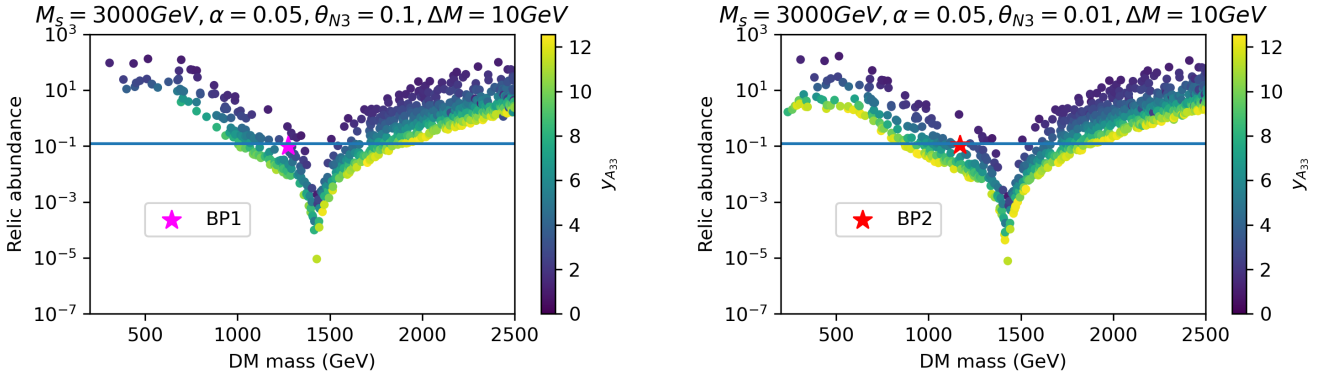


Figure 3: Results of the relic abundance calculations under  $M_s = 3 \text{ TeV}$ ,  $M_{\chi_2} - M_{\chi_1} (= \Delta M) = 10 \text{ GeV}$ ,  $\alpha = 0.05$ ;  $\theta_{N_3} = 0.1$  (Left panel) and  $\theta_{N_3} = 0.01$  (Right panel), taking account of coannihilation. The horizontal blue line depicts the experimental observation of the DM relic abundance ( $\Omega h^2 = 0.120 \pm 0.001$ ) [211]. Note that each point of the panels is consistent with the observed neutrino profiles, the constraints via the lepton flavour violation ( $l_\alpha \rightarrow l_\beta + \gamma$ ) and  $T$  parameter. The colours of the points indicate the magnitudes of  $y_{A_{33}}$ , while we take  $y_{B_{33}} = 0$ . The details of the two benchmark points are available in Table 3.

where we took  $M_{H_1} = M_h$  and  $M_{H_2} = M_s$ . Here, proton mass  $m_p$  is assumed to be nucleon mass,  $\mu_{xp}$  is dark matter-nucleon reduced mass.  $v$  is dark matter velocity in the laboratory frame and  $f_p \approx 0.326$  is nucleon form factor. To compare with the results of LZ [183], we input the dark matter velocity  $v$  in Eq. (4.51) for the spin-independent cross section per nucleon. The mean velocity of the dark matter halo is  $v = 220 \text{ km/s} = 73.5 \times 10^{-5} \approx 10^{-3}$  in natural units is used in our analysis.

## 5 Numerical Analysis

We will discuss the dark matter phenomenology of the current scenario, taking into account the observed active neutrino texture, and constraints via the lepton flavour violation ( $l_\alpha \rightarrow l_\beta + \gamma$ ),  $T$  parameter oblique constraint and the stability of the scalar potential. For simplicity, we focus on the normal ordering in the active neutrino mass matrix below.

A key parameter of our dark matter scenario is the mixing angle  $\alpha$  between the Higgs doublet and the singlet, which determines the magnitudes of the Higgs-portal channels in the relic abundance and constraints via the direct detection. Note that  $\alpha = 0$  corresponds to the pure lepton-portal scenario. We choose the Majorana fermion  $N_{B_3}$  ( $= \chi_1 = \chi$ ) as a dark matter candidate, where under the texture in Eqs. (2.37) and (4.26).  $N_{A_3}$  ( $= \chi_2$ ) is an efficient partner of coannihilation. As shown in Eqs. (4.27) and (4.50), the relevant Yukawa couplings to the gauge singlet among them, namely  $y_{A_{33}}$  and  $y_{B_{33}}$ , play a primary role in relic abundance and direct detection. We take the other  $y_{A_{ii}}$  and  $y_{B_{ii}}$  as zero ( $y_{A_{11}} = y_{A_{22}} = y_{B_{11}} = y_{B_{22}} = 0$ ). Another important parameter is the mixing angle for the ‘third’-generation Majorana fermions  $\theta_{N_3}$ , which modulates the interactions for relic abundance and direct detection. Finally, we should point out that the dark matter candidate can hit the pole of the (mostly-singlet) scalar  $s$  if the mass is around half of it. The resonance enhancement in the annihilation (without large couplings) helps dark matter phenomenology.

As a benchmark, we choose  $M_s = 3 \text{ TeV}$ ,  $\Delta M := M_{\chi_2} - M_{\chi_1} = 10 \text{ GeV}$ ,  $\alpha = 0.05$ , where the Higgs-portal channel is switched on and the coannihilation mechanism may work. Figure 3 provides the results of our numerical scans for  $\theta_{N_3} = 0.1$  (Left panel) and  $\theta_{N_3} = 0.01$  (Right panel), where other

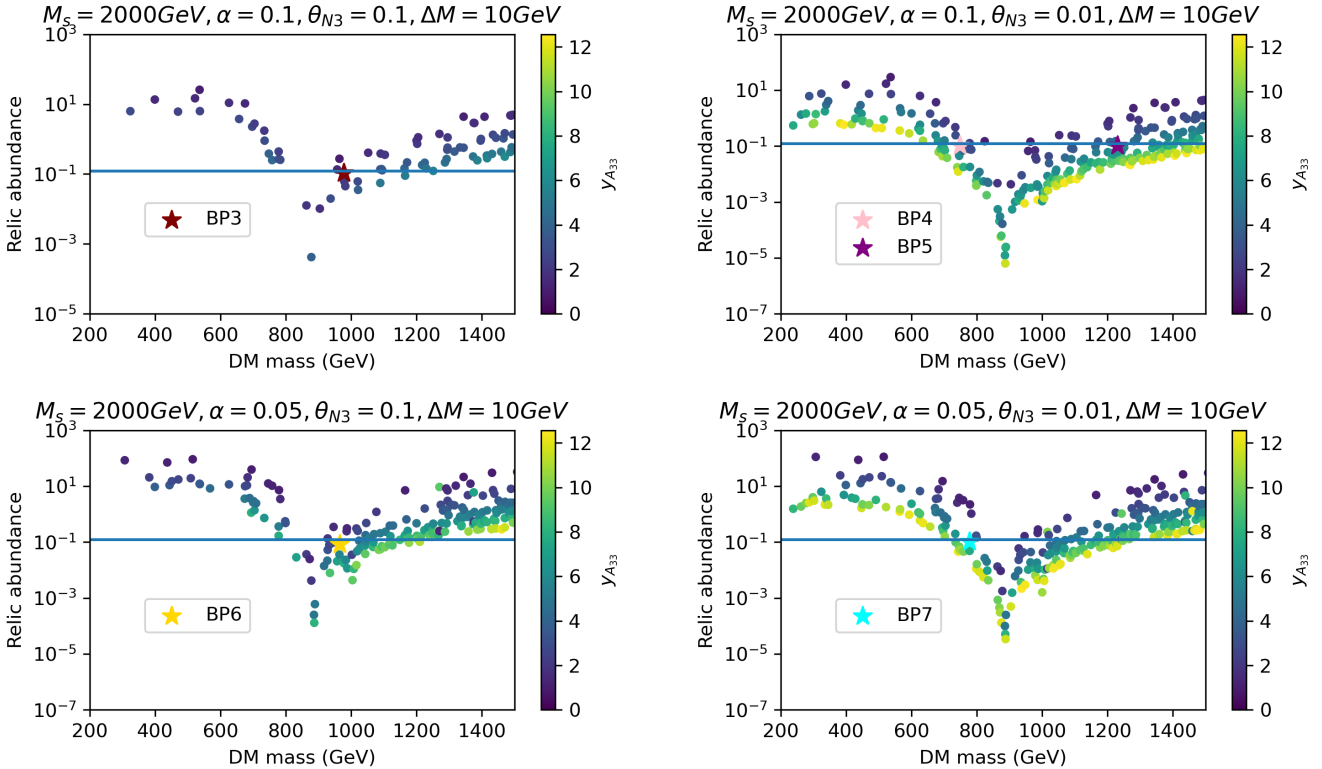


Figure 4: Results of the relic abundance calculations under  $M_s = 2 \text{ TeV}$ ,  $M_{\chi_2} - M_{\chi_1} (= \Delta M) = 10 \text{ GeV}$ ;  $(\alpha, \theta_{N_3}) = (0.1, 0.1)$  (Left upper),  $(0.1, 0.01)$  (Right upper),  $(0.05, 0.1)$  (Left lower),  $(0.05, 0.01)$  (Right lower), respectively, taking account of coannihilation. The other parameter choices and conventions are the same as those of Fig. 3. The details of the five benchmark points are available in Table 3.

relevant parameters are scanned.<sup>8</sup> Note that each point of the panels is consistent with the observed neutrino profiles, the constraints via the lepton flavour violation ( $l_\alpha \rightarrow l_\beta + \gamma$ ) and the  $T$  parameter. The colours of the points indicate the magnitudes of  $y_{A_{33}}$ , while we take  $y_{B_{33}} = 0$  to evade the direct-detection constraint. These results show that if we introduce an order-one Yukawa  $y_{A_{33}}$  (keeping  $y_{B_{33}} = 0$ ), our model can explain the TeV-scale dark matter remnant simultaneously with the preferred neutrino mass terms. The effective area extends over a wide range, not only in the vicinity of the resonance around 1.5 TeV. It can also be read that  $\theta_{N_3}$  affects the valid range of the parameters, as shown in Fig. 3, a smaller  $\theta_{N_3}$  is slightly more significant for a small value of  $\alpha$ . We provide the full sets of model parameters for the two benchmarks (BP1, BP2) in Table 3. Note that for a sizable choice of  $\alpha$ , the Higgs-portal interaction increases rapidly, and the direct detection discards such a point.

We provide our investigations for a lighter  $s$  of  $M_s = 2 \text{ TeV}$ , keeping  $\Delta M (= M_{\chi_2} - M_{\chi_1}) = 10 \text{ GeV}$ , taking into account coannihilation. The results are available in Fig. 4, where we focus on the four choices of  $(\alpha, \theta_{N_3}) = (0.1, 0.1)$  (Left upper),  $(0.1, 0.01)$  (Right upper),  $(0.05, 0.1)$  (Left lower), and  $(0.05, 0.01)$  (Right lower), respectively.

<sup>8</sup>For each scan, we randomly selected the parameters  $M_{\chi_1} (= M_{N_{B_3}})$ ,  $M_{N_{A_1}}$ ,  $M_{N_{B_1}}$ ,  $M_{N_{A_2}}$ ,  $M_{N_{B_2}}$ ,  $M_{\eta_1^+}$ ,  $M_{\eta_2^+}$ ,  $M_{R_1}$ ,  $M_{R_2}$ ,  $\theta_R$ ,  $\lambda_5$ ,  $y_{A_{33}}$ , while the following other independent relevant parameters are fixed;  $M_s$ ,  $M_{\chi_2} (= M_{N_{A_3}})$ ,  $\theta_{N_1}$ ,  $\theta_{N_2}$ ,  $\theta_{N_3}$ ,  $\theta_{cs}$ ,  $\alpha$ ,  $\lambda_6 (= 0)$ , and  $y_{B_{33}} (= 0)$ . Note that the values of  $M_{I_1}$  and  $M_{I_2}$  are determined by the parameters above, but we show the corresponding digits for convenience. Also, the two differences between  $M_{R_i}$  and  $M_{I_i}$  ( $i = 1, 2$ ) are not observed within the shown digits in Table 3, but they should be nonzero to produce the minuscule mass differences of the active neutrinos (see Section 2.2). Due to the same reason,  $\theta_I$  (not shown in Table 3) becomes extremely close to  $\theta_R$ . See Table 3 for concrete information.

Parameters	BP1	BP2	BP3	BP4	BP5	BP6	BP7
$\Omega h^2$	0.1019	0.1119	0.1075	0.1042	0.1039	0.0830	0.1041
$M_s$ (TeV)	3.0	3.0	2.0	2.0	2.0	2.0	2.0
$M_{\chi_1} (= M_{N_{B_3}})$ (GeV)	1274	1169	978	748	1230	965	778
$M_{\chi_2} (= M_{N_{A_3}})$ (GeV)	1284	1179	988	758	1240	975	788
$M_{\eta_1^+}$ (GeV)	2199.48	2795.66	2015.27	1299.27	2138.41	2157.74	1393.35
$M_{\eta_2^+}$ (GeV)	2006.75	2405.21	1173.00	897.00	1814.11	1706.14	933.00
$M_{R_1}$ (GeV)	2235.39	2808.58	2056.27	1305.33	2182.50	2206.11	1408.59
$M_{R_2}$ (GeV)	2019.67	2414.53	1190.37	857.16	1819.99	1716.45	962.39
$M_{N_{A_1}}$ (GeV)	1534	1408	1179	903	1482	1164	939
$M_{N_{A_2}}$ (GeV)	1533	1407	1178	902	1481	1163	938
$M_{N_{B_1}}$ (GeV)	1535	1409	1180	904	1483	1165	940
$M_{N_{B_2}}$ (GeV)	1532	1406	1177	901	1480	1162	937
$\theta_R$	0.5859	0.5484	0.6322	0.6864	0.5482	0.6958	0.7500
$\theta_{N_1} (= \theta_{N_2}), \theta_{N_3}$	0.7, 0.1	0.7, 0.01	0.7, 0.1	0.7, 0.01	0.7, 0.01	0.7, 0.1	0.7, 0.01
$\theta_{cs}$	0.6	0.6	0.6	0.6	0.6	0.6	0.6
$\alpha$	0.05	0.05	0.1	0.1	0.1	0.05	0.05
$\log_{10}(\lambda_5)$	-6.0307	-6.1558	-6.8970	-6.7433	-6.1206	-6.4266	-6.6757
$\lambda_6$	0	0	0	0	0	0	0
$y_{A_{33}}$	2.8509	3.8996	1.5849	3.8393	4.9502	3.7451	5.2354
$y_{B_{33}}$	0	0	0	0	0	0	0
$M_{I_1}$ (GeV)	2235.39	2808.58	2056.27	1305.33	2182.50	2206.11	1409.59
$M_{I_2}$ (GeV)	2019.67	2414.53	1190.37	857.16	1819.99	1716.45	962.39

Table 3: The values of the relevant parameters for the seven benchmark points in Figs. 3 and 4 and realised relic abundances ( $\Omega h^2$ ) are shown. Note that they are consistent with the observed neutrino profiles, the lepton flavour violation ( $l_\alpha \rightarrow l_\beta + \gamma$ ),  $T$  parameter, and DM direct detection.

Here, as a general trend, it becomes more difficult to avoid various restrictions because the masses of heavy particles tend to be smaller, compared with those in the scan for  $M_s = 3$  TeV (refer to Fig. 3), in effective parameter points. As seen in the previous scans for  $M_s = 3$  TeV (refer to Fig. 3), the smaller  $\theta_{N_3}$  tends to yield more effective configurations. Furthermore, even with the same  $\theta_{N_3}$ , a smaller nonzero  $\alpha$  tended to result in more effective configurations. We provide the full sets of model parameters for the five benchmarks (BP3, BP4, BP5, BP6, BP7) in Table 3.<sup>9</sup>

The scan results in Figs. 3 and 4 clearly show that this scenario can still correctly reproduce the coordination of active neutrinos and the relic abundance of thermal WIMP dark matter while avoiding the latest direct search limitations on dark matter and other theoretical limitations, where active-neutrino masses and mixings are induced at 1-loop level as shown in Fig. 1, and the Yukawa coupling  $y_{A_{33}}$  tends to be  $\mathcal{O}(1)$ . We provide a few comments:

- If we choose  $M_{\chi_2}$  sizably above  $M_{\chi_1}$ , coannihilation is deactivated and most of the relevant parameter points addressing the DM relic abundance are gone, see Appendix B for checking this point.
- If we switch off the Higgs portal coupling by  $\alpha = 0$ , only the lepton-portal coupling remains. As

<sup>9</sup>For the shift of the peak from the naive location  $M_s/2 = 1$  TeV, see Chapter 6 of [217] for details.

Parameter	BP1	BP2	BP3	BP4	BP5	BP6	BP7
$\lambda_{S\eta_A}$	0.7105	0.9196	0.5929	0.4385	0.6829	0.6594	0.4845
$\lambda_{S\eta_B}$	0.6551	0.8175	0.4982	0.3963	0.6030	0.6052	0.3879
$\lambda_{2a}$	2.8	3.7	4	3.5	4	3.5	3.5
$\lambda_{2b}$	3	4	4	3.5	4	3.8	3.6
$\lambda_{2c}$	1	1	3	0.1	4	4.8	2.5
$\lambda_{2d}$	1	1	3	0.1	4.4	5	2.5
$\lambda_{3A}$	-3.5287	-4.3015	-0.3693	4.0333	-5.7771	1.7173	-8.6457
$\lambda_{3B}$	-1.4539	2.4240	-4.5045	-0.2452	0.7748	-7.8595	7.3934
$\lambda_{4A}$	4.5287	5.3014	1.3693	-3.0333	6.7771	-0.7173	9.6456
$\lambda_{4B}$	2.4539	-1.4240	5.5045	1.2452	0.2252	8.8595	-6.3934
$m_{\eta_A}$ (GeV)	2048.17 <i>i</i>	2048.69 <i>i</i>	2048.30 <i>i</i>	2048.54 <i>i</i>	2048.72 <i>i</i>	2048.13 <i>i</i>	2048.18 <i>i</i>
$m_{\eta_B}$ (GeV)	1964.41 <i>i</i>	1964.48 <i>i</i>	1964.47 <i>i</i>	1964.56 <i>i</i>	1965.08 <i>i</i>	1964.62 <i>i</i>	1964.71 <i>i</i>
$\lambda_{HS}$	0.3646	0.36461	0.3218	0.3218	0.3218	0.1617	0.1617
$\lambda_H$	0.6290	0.629044	0.9144	0.9144	0.9144	0.4227	0.4227
$\lambda_S$	0.1796	0.179551	0.0792	0.0792	0.0792	0.0798	0.0798

Table 4: For each of the seven benchmark points (BP1 to BP7) of Figs. 3 and 4, we provide a set of valid parameters describing the potential (also not being relevant for the phenomena considered in the numerical scans). In any one of the sets, all of the conditions for the bounded from below [from Eq. (3.20) to Eq. (3.32)] and the inert condition [from Eqs. (3.37) and (3.38)] are satisfied.

far as we checked, no valid parameter point for addressing the neutrino masses/mixings and the DM relic abundance (even with coannihilation), also evading the latest bound on the DM direct detection [183] and other constraints.<sup>10</sup>

- Since, as shown in Table 3, also Figs. 3 and 4, the masses of the dark matter candidate and the other new fermions and scalars tend to be above (or around) 1 TeV, and thus to investigate the current scenario at the LHC by focusing on events with large missing  $E_T$  is uneasy. However, as we will debate in Section 6, we can investigate the current scenario with the help of the LHC by focusing on the measurement of the trilinear Higgs self-coupling.

In the previous numerical scans in Figs. 3 and 4, also in Table 4, we did not include the constraints on the shape of the scalar potential; the bounded from below [from Eq. (3.20) to Eq. (3.32)] and the inert condition [from Eqs. (3.37) and (3.38)]. To confirm this point, in Table 4, for each of the seven benchmark points (BP1 to BP7) of Figs. 3 and 4, we provide a set of valid parameters describing the potential (also not being relevant for the phenomena considered in the numerical scans), where, in any one of the sets, all of the conditions for the bounded from below [from Eq. (3.20) to Eq. (3.32)] and the inert condition [from Eqs. (3.37) and (3.38)] are satisfied. Here, at some benchmark points, some quartic couplings are quite large, but they still satisfy a naive perturbation limit of  $4\pi$ . From the above discussion, it can be said that our model tends to maintain the stability of the potential perturbatively while keeping the stability of dark matter by appropriately selecting the parameters of the potential.

<sup>10</sup>Note that we found parameter points with the correct amount of the DM relic abundance in the pure lepton-portal case ( $\alpha = 0$ ) with coannihilation, being consistent with the previous LZ constraint on the direct detection [182], and the others.

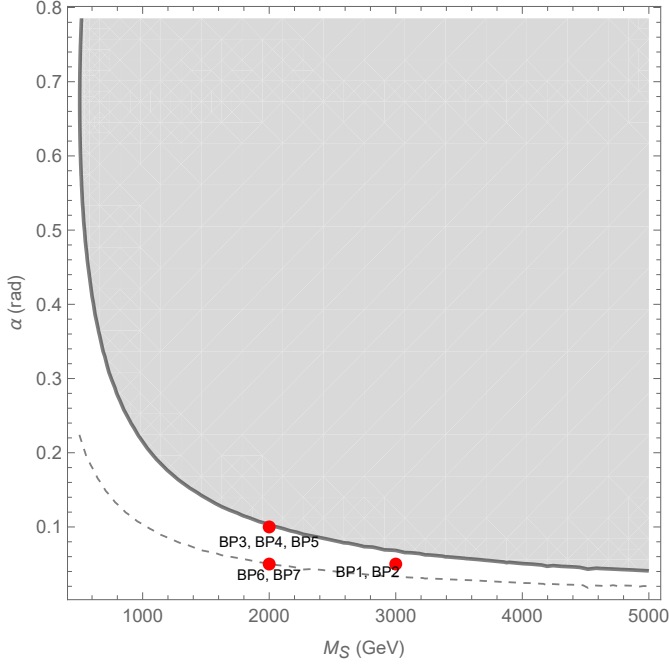


Figure 5: The grey-shaded region shows the 95%-CL disfavoured region on the  $(M_s, \alpha)$  plane (under the choice  $v_S = 5$  TeV) by the ATLAS constraints on the trilinear Higgs self-coupling [218]. The dashed curve represents the 95%-CL future prospect of the ATLAS and CMS HL-LHC projection under the SM hypothesis [219]. Red points represent the benchmark points discussed in Section 5 (see Figs. 3 and 4, and Table 3 for details).

## 6 Bounds on Higgs trilinear self-coupling

The ATLAS experiment places stringent constraints on the Higgs trilinear self-coupling [218, 220]. The parameter  $\kappa_3$  quantifies the deviation from the Standard Model prediction for the trilinear Higgs self-coupling, defined as

$$\kappa_3 = \frac{\lambda_{hhh}}{\lambda_{hhh}^{\text{SM}}}. \quad (6.1)$$

The current bound by ATLAS on  $\kappa_3$  [218] is

$$-0.4 \leq \kappa_3 \leq 6.3 \quad (\text{at 95\% Confidence Level}). \quad (6.2)$$

In the SM, the trilinear Higgs coupling arises from the scalar potential:

$$\begin{aligned} \mathcal{V}^{\text{SM}} &\supset \frac{\lambda_H}{2} (H^\dagger H)^2, \\ &\supset \frac{\lambda_H v_H}{2} h'^3 = \frac{1}{3!} 3 \lambda_H v_H h'^3 = \frac{1}{3!} \lambda_{hhh}^{\text{SM}} h'^3, \end{aligned}$$

where the Higgs doublet is expanded around its VEV as shown in Eq. (2.3) (see also Eq. (2.4)). Therefore, the SM trilinear coupling is fully determined by the electroweak symmetry breaking scale  $v_H = 246$  GeV and the Higgs mass  $M_h = 125$  GeV,

$$\lambda_{hhh}^{\text{SM}} = 3 \lambda_H v_H, \quad \lambda_H = \frac{M_h^2}{v_H^2} \simeq 0.26. \quad (6.3)$$

In our model, additional contributions to the trilinear coupling arise from the scalar singlet  $S$ , leading to the extended scalar potential:

$$\begin{aligned}\mathcal{V} &\supset \frac{\lambda_{HS}}{2} S^2 (H^\dagger H) + \frac{\lambda_H}{2} (H^\dagger H)^2 + \frac{\lambda_S}{4} S^4, \\ &\supset \frac{1}{2} \{v_H (\lambda_H c_\alpha^3 + \lambda_{HS} c_\alpha s_\alpha^3) + v_S (2\lambda_S s_\alpha^3 + \lambda_{HS} c_\alpha^2 s_\alpha)\} h^3, \\ &= \frac{1}{3!} \lambda_{hhh} h^3.\end{aligned}\tag{6.4}$$

After spontaneous symmetry breaking and mixing between the Higgs and singlet scalars, the physical trilinear coupling becomes:

$$\lambda_{hhh} = 3 \{v_H (\lambda_H c_\alpha^3 + \lambda_{HS} c_\alpha s_\alpha^3) + v_S (2\lambda_S s_\alpha^3 + \lambda_{HS} c_\alpha^2 s_\alpha)\}. \tag{6.5}$$

where we remind the mixing angle,  $s_\alpha = \sin(\alpha)$ ,  $c_\alpha = \cos(\alpha)$ , namely,  $s' = s_\alpha h + c_\alpha s$ ,  $h' = c_\alpha h - s_\alpha s$ . Here,  $\lambda_{hhh}$  can be completely determined if we specify the  $Z_4$  symmetry breaking  $v_S$ , mass of the new singlet  $M_s$  and Higgs mixing angle  $\alpha$  via,

$$\lambda_H = \frac{M_h^2 c_\alpha^2 + M_s^2 s_\alpha^2}{v_H^2}, \quad \lambda_S = \frac{M_s^2 c_\alpha^2 + M_h^2 s_\alpha^2}{2v_S^2}, \quad \lambda_{HS} = -\frac{(M_h^2 - M_s^2) \sin(2\alpha)}{2v_H v_S}. \tag{6.6}$$

We pin down the corresponding points of the seven benchmark points discussed in Section 5 as a function of  $\alpha$  and  $M_s$  under the choice  $v_S = 5$  TeV, and the result is summarised in Fig. 5.<sup>11</sup> Note that all of the benchmark points are consistent with the latest ATLAS result [218], and the five benchmark points (Nos. 1, 2, 3, 4, 5) are located near the current boundary. The 95% confidence-level combined ATLAS and CMS HL-LHC projection under the SM hypothesis was estimated as  $\kappa_3 \in [0.1, 2.3]$  [219], and the benchmark points will be indirectly investigated in the future.

## 7 Comments on the domain wall problem

The authors of [221] make the observation that when a discrete symmetry is spontaneously broken, multiple degenerate ground states become available. As there is no requirement for the universe to select a particular choice of ground state, we will have causally disconnected spatial regions having different ground states. The different ground state regions will be separated by stable domain walls (DWs). The energy density of these domain walls scales as  $\rho_{\text{DW}} \propto 1/R$ , where  $R$  is the radius of the universe,  $\rho_{\text{DW}}$  decreases more slowly than normal radiation or matter energy density dominating the energy density of the universe, which can lead to disagreement with observation.

In our model, the  $Z_4$  symmetry is spontaneously broken when the singlet field  $S$  acquires a VEV, to a  $Z_2$  subgroup. We consider two possible mechanisms to address this issue in our model.<sup>12</sup>

### 7.1 Domain wall production before Inflation

The simplest way is to consider the symmetry-breaking scale to be higher than the inflation scale. If the domain walls are produced before inflation, the resulting domain walls are inflated away. Low-scale inflation models with  $V^{1/4} \simeq 10 - 10^4$  TeV [222–224] offer a viable setting in which domain

---

<sup>11</sup>As recognised from Eq. (6.6), if  $v_S$  is notably greater than  $v_H$ , the disfavoured region is not sensitive to the value of  $v_S$ .

<sup>12</sup>We may mention that while some works [109, 111, 118] have proposed Scotogenic scenarios based on  $Z_4$  to a  $Z_2$ , no comments on the domain wall problem were found in them.

walls produced by discrete symmetry breaking can be inflated away. Though our model benchmark points have VEV  $\sim \mathcal{O}(10 \text{ TeV})$ , we can increase the VEV above the inflation scale without altering the particle physics phenomenology discussed in this article to dilute away domain walls produced by discrete symmetry breaking.

## 7.2 Domain wall decay in a $U(1)_X$ -embedded scenario

Another way to address this issue is the use of the gauged discrete symmetry prescription described in [225] and [226]. We embed our  $Z_4$  symmetry into a continuous gauge symmetry such as  $U(1)_X$ , in this new scenario the universe first breaks the continuous gauge symmetry at some high scale  $v_1$  to our  $Z_4$  discrete symmetry forming strings and then subsequently  $Z_4$  is broken to  $Z_2$  at scale  $v_S$  forming domain walls bounded by strings.

$$U(1)_X \xrightarrow{v_1} Z_4 \xrightarrow{v_S} Z_2.$$

Inflation must occur before the high symmetry breaking scale  $v_1$ , so that the strings produced are not diluted away. These domain walls are metastable and collapse in time  $t_c \sim \mu/\sigma \sim v_1^2/v_S^3$  (from dimension analysis in [227]), where  $\mu$  and  $\sigma$  respectively denote the string mass per unit length and wall mass per unit area. If we assume scales of symmetry breaking  $v_1 \sim 10^{16} \text{ GeV}$  and  $v_S \sim 10 \text{ TeV}$  or  $\sim 1 \text{ TeV}$ , the domain walls collapse in time  $t_c \sim 10^{-4} \text{ s}$  or  $t_c \sim 10^{-2} \text{ s}$ .<sup>13</sup> The homogeneity and isotropy of our universe require that the domain walls disappear quite early in the evolution of our universe. The most stringent bound is from big bang nucleosynthesis (BBN), the domain wall must disappear before BBN  $T \sim 1 \text{ MeV}$  [200] if we assume there is not domain wall dominated era in the universe evolution the temperature corresponds to  $t \sim 1 \text{ s}$ , therefore the bound on domain wall collapse is  $t_c \lesssim 1 \text{ s}$  [221]. This method was also used by the authors of [228] to analyse the gravitational signal resulting from the collapse of this metastable string-bounded domain wall system. While a detailed discussion of this process is not in the scope of our article, we show that we are able to overcome the domain wall issue within reasonable extensions of our model and its parameters while preserving our original result.<sup>14</sup>

## 7.3 Explicit soft $Z_2$ breaking

As a final mechanism to address the domain wall problem, we consider introducing a soft, explicit breaking of the discrete symmetry, which avoids the domain wall problem. The softly broken  $Z_4$  symmetry lifts the degeneracy of the VEV, triggering domain wall collapse. Most studies illustrating this mechanism typically use  $Z_2$  as a starting point [229–232]. For  $Z_N$  with  $N > 2$ , the breaking is typically considered in the context of complex scalar fields [233, 234], where the vacuum structure becomes elaborate. Nonetheless, heuristically, the arguments discussed may still be valid for our model. Let us begin with our potential for the  $S$  field,

$$V_0(S) = +\frac{m_S^2}{2}S^2 + \frac{\lambda_S}{4}S^4, \quad (7.1)$$

with parameterisation  $S = (v_S + s')$ . Though the  $Z_4$  symmetry seems to allow four degenerate solutions for the VEV,

$$v_S = v_0 e^{\frac{N\pi}{2}}, \quad N = 0, 1, 2, 3. \quad (7.2)$$

<sup>13</sup>Note that for a lower/higher  $v_1$ , we get a looser/tighter bound.

<sup>14</sup>While a description of the formulae for  $\mu$  and  $\sigma$  is given in the original paper [225], it contains a version of the formulae in Eqs. (12) and (13), which is a model-specific formula. A more general case is studied in [227], and the formulae can be found in Eqs. (4) and (11).

These are only consistent if  $S$  were complex, if not, the imaginary solutions of the VEV lead to a complex potential which is unphysical. For a real scalar field  $S$  with  $Z_4$  charge  $-1$ , only the two real minima are allowed. Therefore, in our setup,  $S$  is effectively charged under a  $Z_2$  symmetry and can only take VEV,

$$v_S = \pm v_0 \quad (7.3)$$

An explicit  $Z_4$  symmetry breaking term is added which introduces a bias in the vacuum structure and generates a pressure on the domain walls,

$$\delta V = \epsilon S^3 \rightarrow \epsilon v_0^3 e^{\frac{N\pi}{2}}, \quad (7.4)$$

Here  $\epsilon$  is a dimensionfull parameter controlling the strength of the explicit breaking and  $N = 0, 2$  corresponding to the real field configuration of our setup. The energy difference between the two vacua,

$$\Delta V = V(+v_S) - V(-v_S) = 2\epsilon v_S^3. \quad (7.5)$$

This energy difference between the two vacuum states provides a pressure leading to domain wall collapse. We require that the domain walls disappear before nucleosynthesis [229]; therefore, the pressure must satisfy,

$$\frac{\Delta V}{\sigma} > \frac{1}{10^{10} \text{cm}} \sim 10^{-24} \text{GeV}, \quad (7.6)$$

which leads to the lower bound on  $\epsilon$

$$\epsilon \gtrsim 5 \times 10^{-25} \text{GeV}. \quad (7.7)$$

Here  $\sigma$  is the domain wall tension  $\sigma \sim v_S^3$ .

On the other hand, the explicit soft-breaking term disables the absolute stability of the fermionic DM candidate, which becomes a very long-lived particle. A possible decay channel of  $\chi$  is  $\chi \rightarrow \nu_{\text{SM}} h h$  ( $\nu_{\text{SM}}$  is a SM neutrino), and the magnitude of the corresponding total decay width of a decaying  $\chi$  is very roughly estimated through naive dimensional analysis and the 3-body phase space factor (for massless final states) as

$$\Gamma_{\text{decaying-}\chi} \sim \frac{3}{192\pi^3} \times (\epsilon c_{\text{inert}})^2 \times \frac{M_\chi^3}{M_{\text{med}}^4}, \quad (7.8)$$

where the factor 3 comes from the three SM neutrinos, the violation of the inert condition in the terms  $(H^\dagger H) \left( \eta_A^\dagger \eta_A \right)$  and  $(H^\dagger H) \left( \eta_B^\dagger \eta_B \right)$  is parametrised as  $\epsilon c_{\text{inert}}$  with a dimensionless constant  $c_{\text{inert}}$ ,  $M_{\text{med}}$  represents a mass of the scalar mediator into a pair of the SM Higgs boson, and here we assumed that all of the dimensionless coupling constants are  $\mathcal{O}(1)$ . The corresponding mean lifetime is estimated as

$$\begin{aligned} \tau_{\text{decaying-}\chi} &= \Gamma_{\text{decaying-}\chi}^{-1} \\ &\sim (4 \times 10^{30} \text{s}) \times \left( \frac{5 \times 10^{-25} \text{GeV}}{\epsilon} \right)^2 \left( \frac{1}{c_{\text{inert}}} \right)^2 \left( \frac{M_{\text{med}}}{1 \text{TeV}} \right)^4 \left( \frac{1 \text{TeV}}{M_\chi} \right)^3, \end{aligned} \quad (7.9)$$

where, if this value is longer than the age of the universe  $\sim 10^{17}$  s, this decaying DM can explain the relic abundance correctly. Via Eq. (7.9), we can conclude that, for a very wide region of  $\{\epsilon, c_{\text{inert}}\}$ , the effect of the soft explicit breaking of the  $Z_2$  symmetry is harmless for the existence of a suitable DM candidate. This means that the simplest option for evading the domain-wall problem works fine in our setup.

## 8 Summary

We have constructed a new Scotogenic type model based on a global  $Z_4$  symmetry involving dark matter candidates. After the symmetry breaking of it as  $Z_4$  to  $Z_2$  via the singlet scalar VEV, the lightest Majorana fermion works as a viable WIMP DM candidate and the mass terms for active neutrinos are generated as a finite quantum correction. A key point of realising our Scotogenic structure is to introduce two types of Majorana fermions (heavy right-handed neutrinos) and inert Higgs doublets with opposite  $Z_4$  parities. Since a large VEV for the singlet scalar is not so harmful in an appropriate realisation of the Higgs mechanism for the SM gauge symmetry, we can naturally realise a TeV-scale fermionic DM candidate, where constraints via direct detection experiments are less than those for sub-TeV WIMPs. For the case that  $N_{B_3}$  is the DM candidate, we find a natural coannihilation partner  $N_{A_3}$ . By taking ‘asymmetric’ profiles in the Yukawa couplings to the singlet scalar  $S$  as  $y_{A_{33}} \sim \mathcal{O}(1)$  but  $y_{B_{33}} = 0$  and small but nonzero  $\alpha$  and  $\theta_{N_3}$ , a ‘well-tempered’ situation is realised, where the direct-detection cross section is relatively suppressed, and the decent-sized Higgs-portal interaction (with coannihilation) naturally leads to a correct amount of the relic abundance of the fermionic thermal WIMP DM. Our scenario has lots of parameter points where the observed DM relic abundance is explained under the correct realisation of the active neutrino masses and mixing angles (refer to Figs. 3 and 4).

The current scenario, above-TeV DM and its mediators, are favoured to evade the severe constraint via direct detection. At the LHC, such cases are hard to investigate via events with large missing transverse energy, but the development in the measurement of the Higgs trilinear self-coupling enables us to survey the validity of our scenario indirectly. As summarised in Table 4 and Fig. 5, in our scenario, valid parameter points for the active neutrino profiles and the correct amount of WIMP DM tend to be located near or a bit away from the current boundary provided by the ATLAS experiment. The future ATLAS-CMS investigation at high-luminosity LHC will survey such benchmark points.

Since our scenario predicts the transition of the global discrete symmetry  $Z_4 \rightarrow Z_2$ , the formation of domain walls at an early stage of the universe can lead to a mismatch with observations. We proposed three possible solutions, where the two require some extension of the model, while the last, simplest one, introducing an explicit soft  $Z_2$ -symmetry breaking term, can be addressed within the present scenario. We checked that the simplest prescription works fine, where the lifetime of the decaying DM easily becomes longer than the age of the universe.

We focus on a significant property of our scenario. As shown in Tables 3 and 4, the Yukawa coupling to the singlet scalar  $y_{A_{33}}$  and some of the scalar quartic couplings tend to be  $\mathcal{O}(1)$  at valid benchmarks. If they follow the running through the renormalisation group equations, the running couplings may blow up or blow down at an energy scale that is not so far from the TeV scale. Therefore, if we attempt to explain the properties of neutrinos and dark matter in this scenario, the scale of inflation must be quite low. It looks like an interesting future study to investigate which low-energy inflation scenarios are consistent with our scenario. Furthermore, our scenario includes numerous right-handed neutrinos and numerous new scalar fields, including  $SU(2)_L$  inert doublets. It is an interesting challenge to consider various TeV-scale leptogenesis scenarios under such circumstances. Also, the feature of  $Z_4$  to  $Z_2$  symmetry breaking with a real scalar field can also be studied in the future through gravitational wave production.

## Acknowledgements

We appreciate Igor Ivanov and Tetsuo Shindou for providing us with various fruitful comments during the workshop HPNP2025. We thank Shiv Nadar Institution of Eminence for providing us with workstations for numerical calculations. One of the authors (N. J. J.) is grateful to the Office of the Dean of Academics

and the Department of Physics of Shiv Nadar Institution of Eminence for the kind financial support for the business trip to Japan in June 2025.

## Appendix

### A Decay width of $s$

We begin with the scalar potential:

$$\mathcal{V} \supset \frac{\lambda_{HS}}{2} S^2 (H^\dagger H) + \frac{\lambda_H}{2} (H^\dagger H)^2 + \frac{\lambda_S}{4} S^4. \quad (\text{A.1})$$

After acquiring VEV, the SM Higgs and Singlet scalars are parametrised as follows,

$$\begin{aligned} H &= \begin{pmatrix} 0 \\ \frac{1}{\sqrt{2}}(v_H + h') \end{pmatrix}, & S &= (v_S + s'), \\ s' &= s_\alpha h + c_\alpha s, & h' &= c_\alpha h - s_\alpha s. \end{aligned}$$

To compute the decay width  $\Gamma_s$ , we first isolate the interaction term in the potential that contributes to the decay of the singlet scalar  $s$  into two Higgs bosons  $hh$ :

$$\mathcal{V} \supset \frac{1}{2} \lambda_{shh} s h h.$$

The effective trilinear coupling coefficient  $c_{shh}$  is

$$\lambda_{shh} = -3\lambda_H v_H c_\alpha^2 s_\alpha + \frac{\lambda_{HS}}{4} \{v_S(c_\alpha + 3c_{3\alpha}) + v_H(-s_\alpha + 3s_{3\alpha})\} + 6\lambda_S v_S c_\alpha s_\alpha^2. \quad (\text{A.2})$$

The square amplitude for this process is,

$$|M_{shh}|^2 = \lambda_{shh}^2. \quad (\text{A.3})$$

The decay width of a particle of mass  $M_s$  decaying into two identical Higgs particles is

$$\Gamma_{s \rightarrow hh} = \frac{1}{2!} \frac{p^*}{32\pi^2 M_s^2} \int |M_{shh}|^2 d\Omega, \quad (\text{A.4})$$

$$p^* = \frac{1}{2M_s} \sqrt{(M_s^2 - 4M_h^2) M_s^2}, \quad (\text{A.5})$$

$$p^* \simeq \frac{M_s}{2}, \quad (\text{A.6})$$

where we used the approximation  $M_h \ll M_s$  for our focused parameter region.

$$\Gamma_{s \rightarrow hh} = \frac{|M_{shh}|^2}{32\pi M_s}, \quad (\text{A.7})$$

where this the decay width of  $s$  is dominantly described by  $s \rightarrow hh$  as  $\Gamma_s \simeq \Gamma_{s \rightarrow hh}$ .

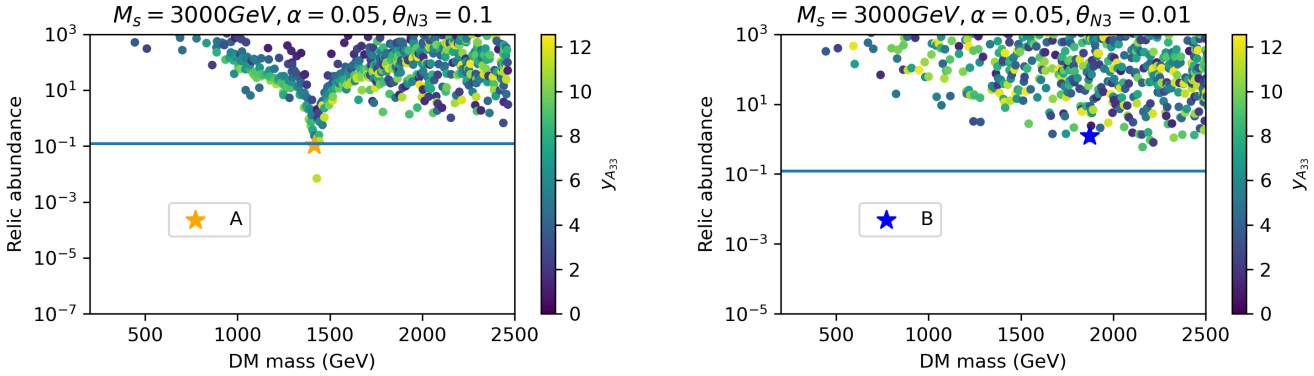


Figure 6: Results of the relic abundance calculations under  $M_s = 3$  TeV,  $\alpha = 0.05$ ;  $\theta_{N_3} = 0.1$  (Left panel) and  $\theta_{N_3} = 0.01$  (Right panel), without coannihilation. The horizontal blue line depicts the experimental observation of the DM relic abundance ( $\Omega h^2 = 0.120 \pm 0.001$ ) [211]. Note that each point of the panels is consistent with the observed neutrino profiles, the constraints via the lepton flavour violation ( $l_\alpha \rightarrow l_\beta + \gamma$ ) and  $T$  parameter. The colours of the points indicate the magnitudes of  $y_{A_{33}}$ , while we take  $y_{B_{33}} = 0$ . The details of the two benchmark points are available in Table 5.

## B DM results without coannihilation

Here, we provide the numerical scans similar to those in Section 5, but without coannihilation by taking the mass of the coannihilation partner  $M_{\chi_2} (= M_{N_{A_3}})$  as 20% larger than the DM mass  $M_{\chi_1} (= M_{N_{B_3}})$ , while the other schemes are the same. For each scan, as before, we randomly selected the parameters  $M_{\chi_1} (= M_{N_{B_3}})$ ,  $M_{N_{A_1}}$ ,  $M_{N_{B_1}}$ ,  $M_{N_{A_2}}$ ,  $M_{N_{B_2}}$ ,  $M_{\eta_1^+}$ ,  $M_{\eta_2^+}$ ,  $M_{R_1}$ ,  $M_{R_2}$ ,  $\theta_R$ ,  $\lambda_5$ ,  $y_{A_{33}}$ , while the following other independent relevant parameters are fixed;  $M_s$ ,  $M_{\chi_2} (= M_{N_{A_3}})$ ,  $\theta_{N_1}$ ,  $\theta_{N_2}$ ,  $\theta_{N_3}$ ,  $\theta_{cs}$ ,  $\alpha$ ,  $\lambda_6 (= 0)$ , and  $y_{B_{33}} (= 0)$ . We chose the three significant parameters  $M_s$ ,  $\alpha$  and  $\theta_{N_3}$  as 3 TeV, 0.05, and 0.1 or 0.01, respectively. The results of the scans are available in Fig. 6, where Left and Right panels correspond to  $\theta_{N_3} = 0.1$  and  $\theta_{N_3} = 0.01$ . It is apparent from the results, no valid points for addressing the DM relic and the active neutrino profiles are found, except for very near the narrow resonance of  $s$ .<sup>15</sup> The details of the two focused points A and B are available in Table 5.<sup>16</sup> While the choice of asymmetric Yukawa couplings is not optimal in the non-coannihilation regime, the inferences remain unchanged, i.e. only the narrow resonance region can produce the correct relic abundance.

## References

- [1] Super-Kamiokande Collaboration, Y. Fukuda et al., ‘‘Evidence for oscillation of atmospheric neutrinos,’’ *Phys. Rev. Lett.* **81** (1998) 1562–1567, [arXiv:hep-ex/9807003](https://arxiv.org/abs/hep-ex/9807003).
- [2] SNO Collaboration, Q. R. Ahmad et al., ‘‘Direct evidence for neutrino flavor transformation from neutral current interactions in the Sudbury Neutrino Observatory,’’ *Phys. Rev. Lett.* **89** (2002) 011301, [arXiv:nucl-ex/0204008](https://arxiv.org/abs/nucl-ex/0204008).

<sup>15</sup>In our scan for  $\theta_{N_3} = 0.01$ , due to a suppressed DM interaction owing to the smaller value of  $\theta_{N_3}$ , we were not able to find a point near the resonance of  $s$ .

<sup>16</sup>Note that the values of  $M_{I_1}$  and  $M_{I_2}$  are determined by the parameters above, but we show the corresponding digits for convenience. Also, the two differences between  $M_{R_i}$  and  $M_{I_i}$  ( $i = 1, 2$ ) are not observed within the shown digits in Table 3, but they should be nonzero to produce the minuscule mass differences of the active neutrinos (see Section 2.2). Due to the same reason,  $\theta_I$  (not shown in Table 5) becomes extremely close to  $\theta_R$ .

Parameters	A	B
$\Omega h^2$	0.1107	1.2359
$M_s$ (TeV)	3.0	3.0
$M_{X_1} (= M_{N_{B_3}})$ (GeV)	1415	1873
$M_{X_2} (= M_{N_{A_3}})$ (GeV)	1698	1883
$M_{\eta_1^+}$ (GeV)	3135.74	3645.31
$M_{\eta_2^+}$ (GeV)	3131.73	3478.74
$M_{R_1}$ (GeV)	3171.44	3611.76
$M_{R_2}$ (GeV)	3084.18	3469.54
$M_{N_{A_1}}$ (GeV)	1704	2253
$M_{N_{A_2}}$ (GeV)	1703	2252
$M_{N_{B_1}}$ (GeV)	1705	2254
$M_{N_{B_2}}$ (GeV)	1702	2251
$\theta_R$	0.3529	0.3270
$\theta_{N_1} (= \theta_{N_2}), \theta_{N_3}$	0.7, 0.1	0.7, 0.01
$\theta_{cs}$	0.6	0.6
$\alpha$	0.05	0.05
$\log_{10}(\lambda_5)$	-6.7201	-7.2654
$\lambda_6$	0	0
$y_{A_{33}}$	8.0394	5.5746
$y_{B_{33}}$	0	0
$M_{I_1}$ (GeV)	3171.44	3611.76
$M_{I_2}$ (GeV)	3084.18	3469.54

Parameter	A	B
$\lambda_{S\eta A}$	1.1854	1.1480
$\lambda_{S\eta B}$	1.3617	1.1564
$\lambda_{2_a}$	5	5
$\lambda_{2_b}$	7	5
$\lambda_{2_c}$	7	5
$\lambda_{2_d}$	8	8.5
$\lambda_{3A}$	-4.5508	-0.0226
$\lambda_{3B}$	8.8775	12.1819
$\lambda_{4A}$	5.5508	1.0226
$\lambda_{4B}$	-7.8775	-11.1819
$m_{\eta A}$ (GeV)	$2203.44 i$	$1199.68 i$
$m_{\eta B}$ (GeV)	$2733.92 i$	$1530.95 i$
$\lambda_{HS}$	0.36461	0.36461
$\lambda_H$	0.629044	0.629044
$\lambda_S$	0.179551	0.179551

Table 5: [Left Table] The values of the relevant parameters for the two benchmark points without coannihilation in Fig. 6, and realised relic abundances ( $\Omega h^2$ ) are shown. Note that they are consistent with the observed neutrino profiles, the lepton flavour violation ( $l_\alpha \rightarrow l_\beta + \gamma$ ),  $T$  parameter, and DM direct detection. [Right Table] For each of the two benchmark points (A and B) of Fig. 6, we provide a set of valid parameters describing the potential (also not being relevant for the phenomena considered in the numerical scans). In any one of the sets, all of the conditions for the bounded from below [from Eq. (3.20) to Eq. (3.32)] and the inert condition [from Eqs. (3.37) and (3.38)] are satisfied.

- [3] C. Giganti, S. Lavignac, and M. Zito, ‘‘Neutrino oscillations: The rise of the PMNS paradigm,’’ [Prog. Part. Nucl. Phys. \*\*98\*\* \(2018\) 1–54, arXiv:1710.00715 \[hep-ex\]](#).
- [4] B. Pontecorvo, ‘‘Mesonium and anti-mesonium,’’ [Sov. Phys. JETP \*\*6\*\* \(1957\) 429](#).
- [5] B. Pontecorvo, ‘‘Inverse beta processes and nonconservation of lepton charge,’’ [Zh. Eksp. Teor. Fiz. \*\*34\*\* \(1957\) 247](#).
- [6] Z. Maki, M. Nakagawa, and S. Sakata, ‘‘Remarks on the unified model of elementary particles,’’ [Prog. Theor. Phys. \*\*28\*\* \(1962\) 870–880](#).
- [7] DUNE Collaboration, B. Abi et al., ‘‘Long-baseline neutrino oscillation physics potential of the DUNE experiment,’’ [Eur. Phys. J. C \*\*80\*\* no. 10, \(2020\) 978, arXiv:2006.16043 \[hep-ex\]](#).
- [8] Hyper-Kamiokande Collaboration, K. Abe et al., ‘‘Physics potentials with the second Hyper-Kamiokande detector in Korea,’’ [PTEP \*\*2018\*\* no. 6, \(2018\) 063C01, arXiv:1611.06118 \[hep-ex\]](#).
- [9] Z.-z. Xing, ‘‘Flavor structures of charged fermions and massive neutrinos,’’ [Phys. Rept. \*\*854\*\* \(2020\) 1–147, arXiv:1909.09610 \[hep-ph\]](#).

- [10] P. Minkowski, “ $\mu \rightarrow e\gamma$  at a Rate of One Out of  $10^9$  Muon Decays?,” *Phys. Lett. B* **67** (1977) 421–428.
- [11] T. Yanagida, “Horizontal gauge symmetry and masses of neutrinos,” *Conf. Proc. C* **7902131** (1979) 95–99.
- [12] M. Gell-Mann, P. Ramond, and R. Slansky, “Complex Spinors and Unified Theories,” *Conf. Proc. C* **790927** (1979) 315–321, [arXiv:1306.4669 \[hep-th\]](https://arxiv.org/abs/1306.4669).
- [13] S. L. Glashow, “The Future of Elementary Particle Physics,” *NATO Sci. Ser. B* **61** (1980) 687.
- [14] R. N. Mohapatra and G. Senjanovic, “Neutrino Mass and Spontaneous Parity Nonconservation,” *Phys. Rev. Lett.* **44** (1980) 912.
- [15] P. Ramond, “The Family Group in Grand Unified Theories,” in *International Symposium on Fundamentals of Quantum Theory and Quantum Field Theory*. 2, 1979. [arXiv:hep-ph/9809459](https://arxiv.org/abs/hep-ph/9809459).
- [16] J. Schechter and J. W. F. Valle, “Neutrino Masses in  $SU(2) \times U(1)$  Theories,” *Phys. Rev. D* **22** (1980) 2227.
- [17] G. Lazarides, Q. Shafi, and C. Wetterich, “Proton Lifetime and Fermion Masses in an  $SO(10)$  Model,” *Nucl. Phys. B* **181** (1981) 287–300.
- [18] R. N. Mohapatra and G. Senjanovic, “Neutrino Masses and Mixings in Gauge Models with Spontaneous Parity Violation,” *Phys. Rev. D* **23** (1981) 165.
- [19] C. Wetterich, “Neutrino Masses and the Scale of B-L Violation,” *Nucl. Phys. B* **187** (1981) 343–375.
- [20] J. Schechter and J. W. F. Valle, “Neutrino Decay and Spontaneous Violation of Lepton Number,” *Phys. Rev. D* **25** (1982) 774.
- [21] R. Foot, H. Lew, X. G. He, and G. C. Joshi, “Seesaw Neutrino Masses Induced by a Triplet of Leptons,” *Z. Phys. C* **44** (1989) 441.
- [22] R. N. Mohapatra and J. W. F. Valle, “Neutrino Mass and Baryon Number Nonconservation in Superstring Models,” *Phys. Rev. D* **34** (1986) 1642.
- [23] D. Wyler and L. Wolfenstein, “Massless Neutrinos in Left-Right Symmetric Models,” *Nucl. Phys. B* **218** (1983) 205–214.
- [24] E. K. Akhmedov, M. Lindner, E. Schnapka, and J. W. F. Valle, “Left-right symmetry breaking in NJL approach,” *Phys. Lett. B* **368** (1996) 270–280, [arXiv:hep-ph/9507275](https://arxiv.org/abs/hep-ph/9507275).
- [25] E. K. Akhmedov, M. Lindner, E. Schnapka, and J. W. F. Valle, “Dynamical left-right symmetry breaking,” *Phys. Rev. D* **53** (1996) 2752–2780, [arXiv:hep-ph/9509255](https://arxiv.org/abs/hep-ph/9509255).
- [26] M. Fukugita and T. Yanagida, “Baryogenesis Without Grand Unification,” *Phys. Lett. B* **174** (1986) 45–47.
- [27] S. Weinberg, “Baryon and Lepton Nonconserving Processes,” *Phys. Rev. Lett.* **43** (1979) 1566–1570.
- [28] F. Bonnet, M. Hirsch, T. Ota, and W. Winter, “Systematic study of the  $d=5$  Weinberg operator at one-loop order,” *JHEP* **07** (2012) 153, [arXiv:1204.5862 \[hep-ph\]](https://arxiv.org/abs/1204.5862).
- [29] A. Zee, “A Theory of Lepton Number Violation, Neutrino Majorana Mass, and Oscillation,” *Phys. Lett. B* **93** (1980) 389. [Erratum: *Phys. Lett. B* 95, 461 (1980)].
- [30] T. P. Cheng and L.-F. Li, “Neutrino Masses, Mixings and Oscillations in  $SU(2) \times U(1)$  Models of Electroweak Interactions,” *Phys. Rev. D* **22** (1980) 2860.
- [31] A. Zee, “Quantum Numbers of Majorana Neutrino Masses,” *Nucl. Phys. B* **264** (1986) 99–110.
- [32] K. S. Babu, “Model of ‘Calculable’ Majorana Neutrino Masses,” *Phys. Lett. B* **203** (1988) 132–136.
- [33] E. Ma, “Pathways to naturally small neutrino masses,” *Phys. Rev. Lett.* **81** (1998) 1171–1174, [arXiv:hep-ph/9805219](https://arxiv.org/abs/hep-ph/9805219).
- [34] L. M. Krauss, S. Nasri, and M. Trodden, “A Model for neutrino masses and dark matter,” *Phys. Rev. D* **67** (2003) 085002, [arXiv:hep-ph/0210389](https://arxiv.org/abs/hep-ph/0210389).
- [35] Y. Cai, J. Herrero-García, M. A. Schmidt, A. Vicente, and R. R. Volkas, “From the trees to the forest: a review of radiative neutrino mass models,” *Front. in Phys.* **5** (2017) 63, [arXiv:1706.08524 \[hep-ph\]](https://arxiv.org/abs/1706.08524).
- [36] E. Ma, “Verifiable radiative seesaw mechanism of neutrino mass and dark matter,” *Phys. Rev. D* **73** (2006) 077301, [arXiv:hep-ph/0601225](https://arxiv.org/abs/hep-ph/0601225).
- [37] E. Ma and D. Suematsu, “Fermion Triplet Dark Matter and Radiative Neutrino Mass,” *Mod. Phys. Lett. A* **24** (2009) 583–589, [arXiv:0809.0942 \[hep-ph\]](https://arxiv.org/abs/0809.0942).

- [38] Y. Farzan, “A Minimal model linking two great mysteries: neutrino mass and dark matter,” [Phys. Rev. D](#) **80** (2009) 073009, [arXiv:0908.3729 \[hep-ph\]](#).
- [39] C.-H. Chen, C.-Q. Geng, and D. V. Zhuridov, “Neutrino Masses, Leptogenesis and Decaying Dark Matter,” [JCAP](#) **10** (2009) 001, [arXiv:0906.1646 \[hep-ph\]](#).
- [40] Y. Farzan, S. Pascoli, and M. A. Schmidt, “AMEND: A model explaining neutrino masses and dark matter testable at the LHC and MEG,” [JHEP](#) **10** (2010) 111, [arXiv:1005.5323 \[hep-ph\]](#).
- [41] M. Aoki, S. Kanemura, and K. Yagyu, “Doubly-charged scalar bosons from the doublet,” [Phys. Lett. B](#) **702** (2011) 355–358, [arXiv:1105.2075 \[hep-ph\]](#). [Erratum: [Phys.Lett.B](#) 706, 495–495 (2012)].
- [42] M. K. Parida, “Radiative Seesaw in SO(10) with Dark Matter,” [Phys. Lett. B](#) **704** (2011) 206–210, [arXiv:1106.4137 \[hep-ph\]](#).
- [43] Y. Cai, X.-G. He, M. Ramsey-Musolf, and L.-H. Tsai, “R $\nu$ MDM and Lepton Flavor Violation,” [JHEP](#) **12** (2011) 054, [arXiv:1108.0969 \[hep-ph\]](#).
- [44] W. Chao, “Dark matter, LFV and neutrino magnetic moment in the radiative seesaw model with fermion triplet,” [Int. J. Mod. Phys. A](#) **30** no. 01, (2015) 1550007, [arXiv:1202.6394 \[hep-ph\]](#).
- [45] Y. Farzan and E. Ma, “Dirac neutrino mass generation from dark matter,” [Phys. Rev. D](#) **86** (2012) 033007, [arXiv:1204.4890 \[hep-ph\]](#).
- [46] H. Okada and T. Toma, “Fermionic Dark Matter in Radiative Inverse Seesaw Model with  $U(1)_{B-L}$ ,” [Phys. Rev. D](#) **86** (2012) 033011, [arXiv:1207.0864 \[hep-ph\]](#).
- [47] D. Hehn and A. Ibarra, “A radiative model with a naturally mild neutrino mass hierarchy,” [Phys. Lett. B](#) **718** (2013) 988–991, [arXiv:1208.3162 \[hep-ph\]](#).
- [48] Y. Kajiyama, H. Okada, and K. Yagyu, “Two Loop Radiative Seesaw Model with Inert Triplet Scalar Field,” [Nucl. Phys. B](#) **874** (2013) 198–216, [arXiv:1303.3463 \[hep-ph\]](#).
- [49] M. Hirsch, R. A. Lineros, S. Morisi, J. Palacio, N. Rojas, and J. W. F. Valle, “WIMP dark matter as radiative neutrino mass messenger,” [JHEP](#) **10** (2013) 149, [arXiv:1307.8134 \[hep-ph\]](#).
- [50] E. Ma, “Unified Framework for Matter, Dark Matter, and Radiative Neutrino Mass,” [Phys. Rev. D](#) **88** no. 11, (2013) 117702, [arXiv:1307.7064 \[hep-ph\]](#).
- [51] V. Brdar, I. Picek, and B. Radovcic, “Radiative Neutrino Mass with Scotogenic Scalar Triplet,” [Phys. Lett. B](#) **728** (2014) 198–201, [arXiv:1310.3183 \[hep-ph\]](#).
- [52] S. S. C. Law and K. L. McDonald, “A Class of Inert N-tuplet Models with Radiative Neutrino Mass and Dark Matter,” [JHEP](#) **09** (2013) 092, [arXiv:1305.6467 \[hep-ph\]](#).
- [53] H. Okada, T. Toma, and K. Yagyu, “Inert Extension of the Zee-Babu Model,” [Phys. Rev. D](#) **90** (2014) 095005, [arXiv:1408.0961 \[hep-ph\]](#).
- [54] S. Patra, N. Sahoo, and N. Sahu, “Dipolar dark matter in light of the 3.5 keV x-ray line, neutrino mass, and LUX data,” [Phys. Rev. D](#) **91** no. 11, (2015) 115013, [arXiv:1412.4253 \[hep-ph\]](#).
- [55] S. Fraser, E. Ma, and O. Popov, “Scotogenic Inverse Seesaw Model of Neutrino Mass,” [Phys. Lett. B](#) **737** (2014) 280–282, [arXiv:1408.4785 \[hep-ph\]](#).
- [56] H. Okada and Y. Orikasa, “Classically conformal radiative neutrino model with gauged B – L symmetry,” [Phys. Lett. B](#) **760** (2016) 558–564, [arXiv:1412.3616 \[hep-ph\]](#).
- [57] S. Baek, H. Okada, and K. Yagyu, “Flavour Dependent Gauged Radiative Neutrino Mass Model,” [JHEP](#) **04** (2015) 049, [arXiv:1501.01530 \[hep-ph\]](#).
- [58] T. A. Chowdhury and S. Nasri, “Lepton Flavor Violation in the Inert Scalar Model with Higher Representations,” [JHEP](#) **12** (2015) 040, [arXiv:1506.00261 \[hep-ph\]](#).
- [59] M. A. Díaz, N. Rojas, S. Urrutia-Quiroga, and J. W. F. Valle, “Heavy Higgs Boson Production at Colliders in the Singlet-Triplet Scotogenic Dark Matter Model,” [JHEP](#) **08** (2017) 017, [arXiv:1612.06569 \[hep-ph\]](#).
- [60] P. M. Ferreira, W. Grimus, D. Jurciukonis, and L. Lavoura, “Scotogenic model for co-bimaximal mixing,” [JHEP](#) **07** (2016) 010, [arXiv:1604.07777 \[hep-ph\]](#).
- [61] A. Ahriche, K. L. McDonald, and S. Nasri, “The Scale-Invariant Scotogenic Model,” [JHEP](#) **06** (2016) 182, [arXiv:1604.05569 \[hep-ph\]](#).

- [62] F. von der Pahlen, G. Palacio, D. Restrepo, and O. Zapata, “Radiative Type III Seesaw Model and its collider phenomenology,” [Phys. Rev. D](#) **94** no. 3, (2016) 033005, [arXiv:1605.01129 \[hep-ph\]](#).
- [63] W.-B. Lu and P.-H. Gu, “Mixed Inert Scalar Triplet Dark Matter, Radiative Neutrino Masses and Leptogenesis,” [Nucl. Phys. B](#) **924** (2017) 279–311, [arXiv:1611.02106 \[hep-ph\]](#).
- [64] A. Merle, M. Platscher, N. Rojas, J. W. F. Valle, and A. Vicente, “Consistency of WIMP Dark Matter as radiative neutrino mass messenger,” [JHEP](#) **07** (2016) 013, [arXiv:1603.05685 \[hep-ph\]](#).
- [65] P. Rocha-Moran and A. Vicente, “Lepton Flavor Violation in the singlet-triplet scotogenic model,” [JHEP](#) **07** (2016) 078, [arXiv:1605.01915 \[hep-ph\]](#).
- [66] T. Nomura, H. Okada, and Y. Orikasa, “Radiative neutrino model with  $SU(2)_L$  triplet fields,” [Phys. Rev. D](#) **94** no. 11, (2016) 115018, [arXiv:1610.04729 \[hep-ph\]](#).
- [67] K. Cheung, T. Nomura, and H. Okada, “Three-loop neutrino mass model with a colored triplet scalar,” [Phys. Rev. D](#) **95** no. 1, (2017) 015026, [arXiv:1610.04986 \[hep-ph\]](#).
- [68] T. A. Chowdhury and S. Nasri, “The Sommerfeld Enhancement in the Scotogenic Model with Large Electroweak Scalar Multiplets,” [JCAP](#) **01** (2017) 041, [arXiv:1611.06590 \[hep-ph\]](#).
- [69] K. Cheung, T. Nomura, and H. Okada, “A Three-loop Neutrino Model with Leptoquark Triplet Scalars,” [Phys. Lett. B](#) **768** (2017) 359–364, [arXiv:1701.01080 \[hep-ph\]](#).
- [70] S. Lee, T. Nomura, and H. Okada, “Radiatively Induced Neutrino Mass Model with Flavor Dependent Gauge Symmetry,” [Nucl. Phys. B](#) **931** (2018) 179–191, [arXiv:1702.03733 \[hep-ph\]](#).
- [71] E. C. F. S. Fortes, A. C. B. Machado, J. Montaño, and V. Pleitez, “Lepton masses and mixing in a scotogenic model,” [Phys. Lett. B](#) **803** (2020) 135289, [arXiv:1705.09414 \[hep-ph\]](#).
- [72] Y.-L. Tang, “Some Phenomenologies of a Simple Scotogenic Inverse Seesaw Model,” [Phys. Rev. D](#) **97** no. 3, (2018) 035020, [arXiv:1709.07735 \[hep-ph\]](#).
- [73] C. Guo, S.-Y. Guo, and Y. Liao, “Dark matter and LHC phenomenology of a scale invariant scotogenic model,” [Chin. Phys. C](#) **43** no. 10, (2019) 103102, [arXiv:1811.01180 \[hep-ph\]](#).
- [74] N. Rojas, R. Srivastava, and J. W. F. Valle, “Simplest Scoto-Seesaw Mechanism,” [Phys. Lett. B](#) **789** (2019) 132–136, [arXiv:1807.11447 \[hep-ph\]](#).
- [75] A. Aranda, C. Bonilla, and E. Peinado, “Dynamical generation of neutrino mass scales,” [Phys. Lett. B](#) **792** (2019) 40–42, [arXiv:1808.07727 \[hep-ph\]](#).
- [76] Z.-L. Han and W. Wang, “Predictive Scotogenic Model with Flavor Dependent Symmetry,” [Eur. Phys. J. C](#) **79** no. 6, (2019) 522, [arXiv:1901.07798 \[hep-ph\]](#).
- [77] D. Suematsu, “Low scale leptogenesis in a hybrid model of the scotogenic type I and III seesaw models,” [Phys. Rev. D](#) **100** no. 5, (2019) 055008, [arXiv:1906.12008 \[hep-ph\]](#).
- [78] S. Pramanick, “Scotogenic S3 symmetric generation of realistic neutrino mixing,” [Phys. Rev. D](#) **100** no. 3, (2019) 035009, [arXiv:1904.07558 \[hep-ph\]](#).
- [79] D. Restrepo and A. Rivera, “Phenomenological consistency of the singlet-triplet scotogenic model,” [JHEP](#) **04** (2020) 134, [arXiv:1907.11938 \[hep-ph\]](#).
- [80] S. Mandal, N. Rojas, R. Srivastava, and J. W. F. Valle, “Dark matter as the origin of neutrino mass in the inverse seesaw mechanism,” [Phys. Lett. B](#) **821** (2021) 136609, [arXiv:1907.07728 \[hep-ph\]](#).
- [81] I. M. Ávila, V. De Romeri, L. Duarte, and J. W. F. Valle, “Phenomenology of scotogenic scalar dark matter,” [Eur. Phys. J. C](#) **80** no. 10, (2020) 908, [arXiv:1910.08422 \[hep-ph\]](#).
- [82] P. Escribano, M. Reig, and A. Vicente, “Generalizing the Scotogenic model,” [JHEP](#) **07** (2020) 097, [arXiv:2004.05172 \[hep-ph\]](#).
- [83] T. Nomura, H. Okada, and Y. Uesaka, “A two-loop induced neutrino mass model, dark matter, and LFV processes  $\ell_i \rightarrow \ell_j \gamma$ , and  $\mu e \rightarrow ee$  in a hidden local  $U(1)$  symmetry,” [Nucl. Phys. B](#) **962** (2021) 115236, [arXiv:2008.02673 \[hep-ph\]](#).
- [84] A. Beniwal, J. Herrero-García, N. Leerdam, M. White, and A. G. Williams, “The ScotoSinglet Model: a scalar singlet extension of the Scotogenic Model,” [JHEP](#) **21** (2020) 136, [arXiv:2010.05937 \[hep-ph\]](#).
- [85] V. De Romeri, M. Puerta, and A. Vicente, “Dark matter in a charged variant of the Scotogenic model,” [Eur.](#)

- [Phys. J. C](#) **82** no. 7, (2022) 623, [arXiv:2106.00481 \[hep-ph\]](#).
- [86] B. De, D. Das, M. Mitra, and N. Sahoo, “Magnetic moments of leptons, charged lepton flavor violations and dark matter phenomenology of a minimal radiative Dirac neutrino mass model,” [JHEP](#) **08** (2022) 202, [arXiv:2106.00979 \[hep-ph\]](#).
- [87] D. W. Kang, J. Kim, and H. Okada, “Muon  $g - 2$  in  $U(1)_{\mu-\tau}$  symmetric gauged radiative neutrino mass model,” [Phys. Lett. B](#) **822** (2021) 136666, [arXiv:2107.09960 \[hep-ph\]](#).
- [88] M. Sarazin, J. Bernigaud, and B. Herrmann, “Dark matter and lepton flavour phenomenology in a singlet-doublet scotogenic model,” [JHEP](#) **12** (2021) 116, [arXiv:2107.04613 \[hep-ph\]](#).
- [89] K. I. Nagao, T. Nomura, and H. Okada, “A model explaining the new CDF II W boson mass linking to muon  $g - 2$  and dark matter,” [Eur. Phys. J. Plus](#) **138** no. 4, (2023) 365, [arXiv:2204.07411 \[hep-ph\]](#).
- [90] A. Ahriche, “A scotogenic model with two inert doublets,” [JHEP](#) **02** (2023) 028, [arXiv:2208.00500 \[hep-ph\]](#).
- [91] R. Cepedello, P. Escribano, and A. Vicente, “Neutrino masses, flavor anomalies, and muon g-2 from dark loops,” [Phys. Rev. D](#) **107** no. 3, (2023) 035034, [arXiv:2209.02730 \[hep-ph\]](#).
- [92] E. J. Chun, A. Roy, S. Mandal, and M. Mitra, “Fermionic dark matter in Dynamical Scotogenic Model,” [JHEP](#) **08** (2023) 130, [arXiv:2303.02681 \[hep-ph\]](#).
- [93] P. Escribano, V. M. Lozano, and A. Vicente, “Scotogenic explanation for the 95 GeV excesses,” [Phys. Rev. D](#) **108** no. 11, (2023) 115001, [arXiv:2306.03735 \[hep-ph\]](#).
- [94] D. Borah, S. Mahapatra, P. K. Paul, and N. Sahu, “Scotogenic  $U(1)L\mu-L\tau$  origin of  $(g-2)\mu$ , W-mass anomaly and 95 GeV excess,” [Phys. Rev. D](#) **109** no. 5, (2024) 055021, [arXiv:2310.11953 \[hep-ph\]](#).
- [95] B. Garbrecht and E. Wang, “A Scotogenic Model as a Prototype for Leptogenesis with One Single Gauge Singlet,” [arXiv:2404.02207 \[hep-ph\]](#).
- [96] T. Nomura and O. Popov, “Extended scotogenic model of neutrino mass and proton decay,” [Phys. Rev. D](#) **110** no. 7, (2024) 075035, [arXiv:2406.00651 \[hep-ph\]](#).
- [97] K. M. Cárdenas, G. Mohlabeng, and A. C. Vincent, “Global fit to loopy dark matter and neutrino masses,” [Phys. Rev. D](#) **111** no. 5, (2025) 055024, [arXiv:2411.03470 \[hep-ph\]](#).
- [98] L. Singh, R. Srivastava, S. Verma, and S. Yadav, “Type-III Scotogenic Model: Inflation, Dark Matter and Collider Phenomenology,” [arXiv:2501.13171 \[hep-ph\]](#).
- [99] P. Escribano, V. M. Lozano, S. Norero, and A. Vicente, “Exploring Dimuon Higgs Decay in an Extended Scotogenic Model,” [arXiv:2501.17244 \[hep-ph\]](#).
- [100] E. Ma, “Dark Scalar Doublets and Neutrino Tribimaximal Mixing from  $A(4)$  Symmetry,” [Phys. Lett. B](#) **671** (2009) 366–368, [arXiv:0808.1729 \[hep-ph\]](#).
- [101] A. Adulpravitchai, M. Lindner, A. Merle, and R. N. Mohapatra, “Radiative Transmission of Lepton Flavor Hierarchies,” [Phys. Lett. B](#) **680** (2009) 476–479, [arXiv:0908.0470 \[hep-ph\]](#).
- [102] E. Ma, A. Natale, and A. Rashed, “Scotogenic  $A_4$  Neutrino Model for Nonzero  $\theta_{13}$  and Large  $\delta_{CP}$ ,” [Int. J. Mod. Phys. A](#) **27** (2012) 1250134, [arXiv:1206.1570 \[hep-ph\]](#).
- [103] S. Bhattacharya, E. Ma, A. Natale, and A. Rashed, “Radiative Scaling Neutrino Mass with  $A_4$  Symmetry,” [Phys. Rev. D](#) **87** (2013) 097301, [arXiv:1302.6266 \[hep-ph\]](#).
- [104] Y. Kajiyama, H. Okada, and T. Toma, “Multicomponent dark matter particles in a two-loop neutrino model,” [Phys. Rev. D](#) **88** no. 1, (2013) 015029, [arXiv:1303.7356 \[hep-ph\]](#).
- [105] E. Ma, “Neutrino Mixing and Geometric CP Violation with Delta(27) Symmetry,” [Phys. Lett. B](#) **723** (2013) 161–163, [arXiv:1304.1603 \[hep-ph\]](#).
- [106] E. Ma and A. Natale, “Scotogenic  $Z_2$  or  $U(1)_D$  Model of Neutrino Mass with  $\Delta(27)$  Symmetry,” [Phys. Lett. B](#) **734** (2014) 403–405, [arXiv:1403.6772 \[hep-ph\]](#).
- [107] H. Okada, N. Okada, and Y. Orikasa, “Radiative seesaw mechanism in a minimal 3-3-1 model,” [Phys. Rev. D](#) **93** no. 7, (2016) 073006, [arXiv:1504.01204 \[hep-ph\]](#).
- [108] S. Baek, H. Okada, and Y. Orikasa, “A Two Loop Radiative Neutrino Model,” [Nucl. Phys. B](#) **941** (2019) 744–754, [arXiv:1703.00685 \[hep-ph\]](#).

- [109] A. Ahriche, A. Jueid, and S. Nasri, “A natural scotogenic model for neutrino mass & dark matter,” [Phys. Lett. B](#) **814** (2021) 136077, [arXiv:2007.05845 \[hep-ph\]](#).
- [110] S.-L. Chen, A. Dutta Banik, and Z.-K. Liu, “Common origin of radiative neutrino mass, dark matter and leptogenesis in scotogenic Georgi-Machacek model,” [Nucl. Phys. B](#) **966** (2021) 115394, [arXiv:2011.13551 \[hep-ph\]](#).
- [111] F. J. de Anda, O. Medina, J. W. F. Valle, and C. A. Vaquera-Araujo, “Scotogenic Majorana neutrino masses in a predictive orbifold theory of flavor,” [Phys. Rev. D](#) **105** no. 5, (2022) 055030, [arXiv:2110.06810 \[hep-ph\]](#).
- [112] S. Chuliá Centelles, R. Cepedello, and O. Medina, “Absolute neutrino mass scale and dark matter stability from flavour symmetry,” [JHEP](#) **10** (2022) 080, [arXiv:2204.12517 \[hep-ph\]](#).
- [113] D. M. Barreiros, H. B. Camara, and F. R. Joaquim, “Flavour and dark matter in a scoto/type-II seesaw model,” [JHEP](#) **08** (2022) 030, [arXiv:2204.13605 \[hep-ph\]](#).
- [114] C. Bonilla, J. Herms, O. Medina, and E. Peinado, “Discrete dark matter mechanism as the source of neutrino mass scales,” [JHEP](#) **06** (2023) 078, [arXiv:2301.10811 \[hep-ph\]](#).
- [115] J. Ganguly, J. Gluza, B. Karmakar, and S. Mahapatra, “Phenomenology of the flavor symmetric scoto-seesaw model with dark matter and TM1 mixing,” [Phys. Rev. D](#) **110** no. 3, (2024) 035012, [arXiv:2311.15997 \[hep-ph\]](#).
- [116] S. Arora and B. C. Chauhan, “Dark Matter and Muon ( $g - 2$ ) from a Discrete  $Z_4$  Symmetric Model,” [LHEP](#) **2024** (2024) 512.
- [117] J. Kim, S.-S. Kim, H. M. Lee, and R. Padhan, “Small neutrino masses from a decoupled singlet scalar field,” [Phys. Lett. B](#) **861** (2025) 139243, [arXiv:2407.13595 \[hep-ph\]](#).
- [118] L. M. G. de la Vega, P. J. Fitzpatrick, R. Martinez-Ramirez, and E. Peinado, “Dark matter for Majorana neutrinos in a  $Z_4$  symmetry,” [Phys. Rev. D](#) **110** no. 11, (2024) 115024, [arXiv:2407.14447 \[hep-ph\]](#).
- [119] A. E. Cárcamo Hernández, D. Salinas-Arizmendi, J. Vignatti, and A. Zerwekh, “Phenomenology of an Extended  $1 + 2$  Higgs Doublet Model with  $S_3$  Family Symmetry,” [Eur. Phys. J. C](#) **84** (2024) 1135, [arXiv:2408.01497 \[hep-ph\]](#).
- [120] R. Kumar, N. Nath, R. Srivastava, and S. Yadav, “Dirac Scoto Inverse-Seesaw from  $A_4$  Flavor Symmetry,” [arXiv:2505.01407 \[hep-ph\]](#).
- [121] J. Kubo and D. Suematsu, “Neutrino masses and CDM in a non-supersymmetric model,” [Phys. Lett. B](#) **643** (2006) 336–341, [arXiv:hep-ph/0610006](#).
- [122] W.-F. Chang and C.-F. Wong, “A Model for Neutrino Masses and Dark Matter with the Discrete Gauge Symmetry,” [Phys. Rev. D](#) **85** (2012) 013018, [arXiv:1104.3934 \[hep-ph\]](#).
- [123] Y. Kajiyama, H. Okada, and K. Yagyu, “ $T_7$  Flavor Model in Three Loop Seesaw and Higgs Phenomenology,” [JHEP](#) **10** (2013) 196, [arXiv:1307.0480 \[hep-ph\]](#).
- [124] E. Ma, I. Picek, and B. Radovčić, “New Scotogenic Model of Neutrino Mass with  $U(1)_D$  Gauge Interaction,” [Phys. Lett. B](#) **726** (2013) 744–746, [arXiv:1308.5313 \[hep-ph\]](#).
- [125] D. Aristizabal Sierra, M. Dhen, C. S. Fong, and A. Vicente, “Dynamical flavor origin of  $\mathbb{Z}_N$  symmetries,” [Phys. Rev. D](#) **91** no. 9, (2015) 096004, [arXiv:1412.5600 \[hep-ph\]](#).
- [126] H. Hatanaka, K. Nishiwaki, H. Okada, and Y. Oriksa, “A Three-Loop Neutrino Model with Global  $U(1)$  Symmetry,” [Nucl. Phys. B](#) **894** (2015) 268–283, [arXiv:1412.8664 \[hep-ph\]](#).
- [127] K. Nishiwaki, H. Okada, and Y. Oriksa, “Three loop neutrino model with isolated  $k^{\pm\pm}$ ,” [Phys. Rev. D](#) **92** no. 9, (2015) 093013, [arXiv:1507.02412 \[hep-ph\]](#).
- [128] H. Okada and Y. Oriksa, “Radiative neutrino model with an inert triplet scalar,” [Phys. Rev. D](#) **94** no. 5, (2016) 055002, [arXiv:1512.06687 \[hep-ph\]](#).
- [129] S. Kanemura, K. Nishiwaki, H. Okada, Y. Oriksa, S. C. Park, and R. Watanabe, “LHC 750 GeV diphoton excess in a radiative seesaw model,” [PTEP](#) **2016** no. 12, (2016) 123B04, [arXiv:1512.09048 \[hep-ph\]](#).
- [130] J.-H. Yu, “Hidden Gauged  $U(1)$  Model: Unifying Scotogenic Neutrino and Flavor Dark Matter,” [Phys. Rev. D](#) **93** no. 11, (2016) 113007, [arXiv:1601.02609 \[hep-ph\]](#).

- [131] T. Nomura and H. Okada, “A four-loop Radiative Seesaw Model,” *Phys. Lett. B* **770** (2017) 307–313, [arXiv:1601.04516 \[hep-ph\]](#).
- [132] W. Wang, R. Wang, Z.-L. Han, and J.-Z. Han, “The  $B - L$  Scotogenic Models for Dirac Neutrino Masses,” *Eur. Phys. J. C* **77** no. 12, (2017) 889, [arXiv:1705.00414 \[hep-ph\]](#).
- [133] T. Nomura and H. Okada, “Radiative neutrino mass in an alternative  $U(1)_{B-L}$  gauge symmetry,” *Nucl. Phys. B* **941** (2019) 586–599, [arXiv:1705.08309 \[hep-ph\]](#).
- [134] T. Nomura and H. Okada, “A model with isospin doublet  $U(1)_D$  gauge symmetry,” *Int. J. Mod. Phys. A* **33** no. 14n15, (2018) 1850089, [arXiv:1706.05268 \[hep-ph\]](#).
- [135] E. Ma, D. Restrepo, and O. Zapata, “Anomalous leptonic  $U(1)$  symmetry: Syndetic origin of the QCD axion, weak-scale dark matter, and radiative neutrino mass,” *Mod. Phys. Lett. A* **33** (2018) 1850024, [arXiv:1706.08240 \[hep-ph\]](#).
- [136] T. Nomura and H. Okada, “Neutrino mass in flavor dependent gauged lepton model,” *Phys. Rev. D* **97** no. 5, (2018) 055044, [arXiv:1707.06083 \[hep-ph\]](#).
- [137] C. Hagedorn, J. Herrero-García, E. Molinaro, and M. A. Schmidt, “Phenomenology of the Generalised Scotogenic Model with Fermionic Dark Matter,” *JHEP* **11** (2018) 103, [arXiv:1804.04117 \[hep-ph\]](#).
- [138] Z.-L. Han and W. Wang, “ $Z'$  Portal Dark Matter in  $B - L$  Scotogenic Dirac Model,” *Eur. Phys. J. C* **78** no. 10, (2018) 839, [arXiv:1805.02025 \[hep-ph\]](#).
- [139] J. Calle, D. Restrepo, C. E. Yaguna, and O. Zapata, “Minimal radiative Dirac neutrino mass models,” *Phys. Rev. D* **99** no. 7, (2019) 075008, [arXiv:1812.05523 \[hep-ph\]](#).
- [140] C. D. R. Carvajal and O. Zapata, “One-loop Dirac neutrino mass and mixed axion-WIMP dark matter,” *Phys. Rev. D* **99** no. 7, (2019) 075009, [arXiv:1812.06364 \[hep-ph\]](#).
- [141] S. Centelles Chuliá, R. Cepedello, E. Peinado, and R. Srivastava, “Scotogenic dark symmetry as a residual subgroup of Standard Model symmetries,” *Chin. Phys. C* **44** no. 8, (2020) 083110, [arXiv:1901.06402 \[hep-ph\]](#).
- [142] E. Ma, “Scotogenic  $U(1)_\chi$  Dirac neutrinos,” *Phys. Lett. B* **793** (2019) 411–414, [arXiv:1901.09091 \[hep-ph\]](#).
- [143] S. K. Kang, O. Popov, R. Srivastava, J. W. F. Valle, and C. A. Vaquera-Araujo, “Scotogenic dark matter stability from gauged matter parity,” *Phys. Lett. B* **798** (2019) 135013, [arXiv:1902.05966 \[hep-ph\]](#).
- [144] T. Nomura and H. Okada, “A modular  $A_4$  symmetric model of dark matter and neutrino,” *Phys. Lett. B* **797** (2019) 134799, [arXiv:1904.03937 \[hep-ph\]](#).
- [145] S. Jana, P. K. Vishnu, and S. Saad, “Minimal dirac neutrino mass models from  $U(1)_R$  gauge symmetry and left-right asymmetry at colliders,” *Eur. Phys. J. C* **79** no. 11, (2019) 916, [arXiv:1904.07407 \[hep-ph\]](#).
- [146] E. Ma, “Scotogenic cobimaximal Dirac neutrino mixing from  $\Delta(27)$  and  $U(1)_\chi$ ,” *Eur. Phys. J. C* **79** no. 11, (2019) 903, [arXiv:1905.01535 \[hep-ph\]](#).
- [147] T. Nomura and H. Okada, “A two loop induced neutrino mass model with modular  $A_4$  symmetry,” *Nucl. Phys. B* **966** (2021) 115372, [arXiv:1906.03927 \[hep-ph\]](#).
- [148] J. Fuentes-Martín, M. Reig, and A. Vicente, “Strong  $CP$  problem with low-energy emergent QCD: The 4321 case,” *Phys. Rev. D* **100** no. 11, (2019) 115028, [arXiv:1907.02550 \[hep-ph\]](#).
- [149] H. Okada and Y. Orikasa, “Modular  $S_3$  symmetric radiative seesaw model,” *Phys. Rev. D* **100** no. 11, (2019) 115037, [arXiv:1907.04716 \[hep-ph\]](#).
- [150] C. Bonilla, L. M. G. de la Vega, J. M. Lamprea, R. A. Lineros, and E. Peinado, “Fermion Dark Matter and Radiative Neutrino Masses from Spontaneous Lepton Number Breaking,” *New J. Phys.* **22** no. 3, (2020) 033009, [arXiv:1908.04276 \[hep-ph\]](#).
- [151] Z.-L. Han, R. Ding, S.-J. Lin, and B. Zhu, “Gauged  $U(1)_{L_\mu - L_\tau}$  scotogenic model in light of  $R_{K^{(*)}}$  anomaly and AMS-02 positron excess,” *Eur. Phys. J. C* **79** no. 12, (2019) 1007, [arXiv:1908.07192 \[hep-ph\]](#).
- [152] T. Nomura, H. Okada, and O. Popov, “A modular  $A_4$  symmetric scotogenic model,” *Phys. Lett. B* **803** (2020) 135294, [arXiv:1908.07457 \[hep-ph\]](#).
- [153] J. Leite, O. Popov, R. Srivastava, and J. W. F. Valle, “A theory for scotogenic dark matter stabilised by

- residual gauge symmetry,” [Phys. Lett. B](#) **802** (2020) 135254, [arXiv:1909.06386 \[hep-ph\]](#).
- [154] S. Jana, P. K. Vishnu, and S. Saad, “Minimal realizations of Dirac neutrino mass from generic one-loop and two-loop topologies at  $d = 5$ ,” [JCAP](#) **04** (2020) 018, [arXiv:1910.09537 \[hep-ph\]](#).
- [155] W. Wang and Z.-L. Han, “ $U(1)_{B-3L_\alpha}$  extended scotogenic models and single-zero textures of neutrino mass matrices,” [Phys. Rev. D](#) **101** no. 11, (2020) 115040, [arXiv:1911.00819 \[hep-ph\]](#).
- [156] L. M. G. de la Vega, N. Nath, and E. Peinado, “Dirac neutrinos from Peccei-Quinn symmetry: two examples,” [Nucl. Phys. B](#) **957** (2020) 115099, [arXiv:2001.01846 \[hep-ph\]](#).
- [157] H. Okada and Y. Shoji, “A radiative seesaw model with three Higgs doublets in modular  $A_4$  symmetry,” [Nucl. Phys. B](#) **961** (2020) 115216, [arXiv:2003.13219 \[hep-ph\]](#).
- [158] J. Kim, T. Nomura, and H. Okada, “A radiative seesaw model linking to XENON1T anomaly,” [Phys. Lett. B](#) **811** (2020) 135862, [arXiv:2007.09894 \[hep-ph\]](#).
- [159] C.-F. Wong, “Anomaly-free chiral  $U(1)_D$  and its scotogenic implication,” [Phys. Dark Univ.](#) **32** (2021) 100818, [arXiv:2008.08573 \[hep-ph\]](#).
- [160] M. K. Behera, S. Singirala, S. Mishra, and R. Mohanta, “A modular  $A_4$  symmetric scotogenic model for neutrino mass and dark matter,” [J. Phys. G](#) **49** no. 3, (2022) 035002, [arXiv:2009.01806 \[hep-ph\]](#).
- [161] N. Bernal, J. Calle, and D. Restrepo, “Anomaly-free Abelian gauge symmetries with Dirac scotogenic models,” [Phys. Rev. D](#) **103** no. 9, (2021) 095032, [arXiv:2102.06211 \[hep-ph\]](#).
- [162] H. Okada, Y. Orikasa, and Y. Shoji, “Radiative dark matter and neutrino masses from an alternative  $U(1)$  B-L gauge symmetry,” [JCAP](#) **07** (2021) 006, [arXiv:2102.10944 \[hep-ph\]](#).
- [163] T. Nomura and H. Okada, “Radiative neutrino mass model in dark non-Abelian gauge symmetry,” [Phys. Rev. D](#) **105** no. 7, (2022) 075010, [arXiv:2106.10451 \[hep-ph\]](#).
- [164] P. Escribano and A. Vicente, “An ultraviolet completion for the Scotogenic model,” [Phys. Lett. B](#) **823** (2021) 136717, [arXiv:2107.10265 \[hep-ph\]](#).
- [165] A. Dasgupta, T. Nomura, H. Okada, O. Popov, and M. Tanimoto, “Dirac Radiative Neutrino Mass with Modular Symmetry and Leptogenesis,” [arXiv:2111.06898 \[hep-ph\]](#).
- [166] M. Berbig, “Freeze-In of radiative keV-scale neutrino dark matter from a new  $U(1)_{B-L}$ ,” [JHEP](#) **09** (2022) 101, [arXiv:2203.04276 \[hep-ph\]](#).
- [167] D. Portillo-Sánchez, P. Escribano, and A. Vicente, “Ultraviolet extensions of the Scotogenic model,” [JHEP](#) **08** (2023) 023, [arXiv:2301.05249 \[hep-ph\]](#).
- [168] T. de Boer, M. Klasen, and S. Zeinstra, “Anomaly-free dark matter models with one-loop neutrino masses and a gauged  $U(1)$  symmetry,” [JHEP](#) **01** (2024) 013, [arXiv:2309.06920 \[hep-ph\]](#).
- [169] T. Nomura and H. Okada, “Scotogenic models with a general lepton flavor dependent  $U(1)$  gauge symmetry,” [Phys. Lett. B](#) **848** (2024) 138393, [arXiv:2304.03905 \[hep-ph\]](#).
- [170] T. Nomura and H. Okada, “Radiative inverse seesaw model with hidden  $U(1)$  gauge symmetry enhancing lepton  $g - 2$ ,” [arXiv:2403.14193 \[hep-ph\]](#).
- [171] T. Nomura, H. Okada, and O. Popov, “Non-holomorphic modular  $A_4$  symmetric scotogenic model,” [Phys. Lett. B](#) **860** (2025) 139171, [arXiv:2409.12547 \[hep-ph\]](#).
- [172] K. Agudelo, D. Restrepo, A. Rivera, and D. Suarez, “Multicomponent secluded WIMP dark matter and Dirac neutrino masses with an extra Abelian gauge symmetry,” [Phys. Rev. D](#) **111** no. 9, (2025) 095018, [arXiv:2412.02027 \[hep-ph\]](#).
- [173] K. S. Babu and S. Saad, “Ultraviolet completion of a two-loop neutrino mass model,” [JHEP](#) **03** (2025) 132, [arXiv:2412.14562 \[hep-ph\]](#).
- [174] Z. A. Borboruah, L. Malhotra, U. Patel, S. Patra, and S. U. Sankar, “Left-Right Symmetric Neutrino Mass Model without Scalar Bi-doublet,” [arXiv:2504.08267 \[hep-ph\]](#).
- [175] I. Doršner, M. Matković, and S. Saad, “Nonrenormalizable  $SU(5)$  GUTs: Leptoquark-induced neutrino masses,” [Phys. Rev. D](#) **111** no. 11, (2025) 115039, [arXiv:2504.16022 \[hep-ph\]](#).
- [176] J. Leite, J. Perez-Soler, and A. Vicente, “Scotogenic mechanism from an extended  $SU(2)_1 \times SU(2)_2 \times U(1)_Y$  electroweak symmetry,” [arXiv:2507.21223 \[hep-ph\]](#).

- [177] M. Reig, D. Restrepo, J. W. F. Valle, and O. Zapata, “Bound-state dark matter and Dirac neutrino masses,” *Phys. Rev. D* **97** no. 11, (2018) 115032, [arXiv:1803.08528 \[hep-ph\]](#).
- [178] M. Reig, D. Restrepo, J. W. F. Valle, and O. Zapata, “Bound-state dark matter with Majorana neutrinos,” *Phys. Lett. B* **790** (2019) 303–307, [arXiv:1806.09977 \[hep-ph\]](#).
- [179] D. Aristizabal Sierra, M. Hirsch, and S. G. Kovalenko, “Leptoquarks: Neutrino masses and accelerator phenomenology,” *Phys. Rev. D* **77** (2008) 055011, [arXiv:0710.5699 \[hep-ph\]](#).
- [180] P. Fileviez Perez and M. B. Wise, “On the Origin of Neutrino Masses,” *Phys. Rev. D* **80** (2009) 053006, [arXiv:0906.2950 \[hep-ph\]](#).
- [181] M. Kohda, H. Sugiyama, and K. Tsumura, “Lepton number violation at the LHC with leptoquark and diquark,” *Phys. Lett. B* **718** (2013) 1436–1440, [arXiv:1210.5622 \[hep-ph\]](#).
- [182] LZ Collaboration, J. Aalbers et al., “First Dark Matter Search Results from the LUX-ZEPLIN (LZ) Experiment,” *Phys. Rev. Lett.* **131** no. 4, (2023) 041002, [arXiv:2207.03764 \[hep-ex\]](#).
- [183] LZ Collaboration, J. Aalbers et al., “Dark Matter Search Results from 4.2 Tonne-Years of Exposure of the LUX-ZEPLIN (LZ) Experiment,” [arXiv:2410.17036 \[hep-ex\]](#).
- [184] M. Freytsis and Z. Ligeti, “On dark matter models with uniquely spin-dependent detection possibilities,” *Phys. Rev. D* **83** (2011) 115009, [arXiv:1012.5317 \[hep-ph\]](#).
- [185] S. Ipek, D. McKeen, and A. E. Nelson, “A Renormalizable Model for the Galactic Center Gamma Ray Excess from Dark Matter Annihilation,” *Phys. Rev. D* **90** no. 5, (2014) 055021, [arXiv:1404.3716 \[hep-ph\]](#).
- [186] G. Arcadi, M. Lindner, F. S. Queiroz, W. Rodejohann, and S. Vogl, “Pseudoscalar Mediators: A WIMP model at the Neutrino Floor,” *JCAP* **03** (2018) 042, [arXiv:1711.02110 \[hep-ph\]](#).
- [187] N. F. Bell, G. Busoni, and I. W. Sanderson, “Loop Effects in Direct Detection,” *JCAP* **08** (2018) 017, [arXiv:1803.01574 \[hep-ph\]](#). [Erratum: *JCAP* 01, E01 (2019)].
- [188] T. Abe, M. Fujiwara, and J. Hisano, “Loop corrections to dark matter direct detection in a pseudoscalar mediator dark matter model,” *JHEP* **02** (2019) 028, [arXiv:1810.01039 \[hep-ph\]](#).
- [189] T. Abe, M. Fujiwara, J. Hisano, and Y. Shoji, “Maximum value of the spin-independent cross section in the 2HDM+a,” *JHEP* **01** (2020) 114, [arXiv:1910.09771 \[hep-ph\]](#).
- [190] V. Barger, M. McCaskey, and G. Shaughnessy, “Complex Scalar Dark Matter vis-‐a-vis CoGeNT, DAMA/LIBRA and XENON100,” *Phys. Rev. D* **82** (2010) 035019, [arXiv:1005.3328 \[hep-ph\]](#).
- [191] D. Barducci, A. Bharucha, N. Desai, M. Frigerio, B. Fuks, A. Goudelis, S. Kulkarni, G. Polesello, and D. Sengupta, “Monojet searches for momentum-dependent dark matter interactions,” *JHEP* **01** (2017) 078, [arXiv:1609.07490 \[hep-ph\]](#).
- [192] C. Gross, O. Lebedev, and T. Toma, “Cancellation Mechanism for Dark-Matter–Nucleon Interaction,” *Phys. Rev. Lett.* **119** no. 19, (2017) 191801, [arXiv:1708.02253 \[hep-ph\]](#).
- [193] R. Balkin, M. Ruhdorfer, E. Salvioni, and A. Weiler, “Charged Composite Scalar Dark Matter,” *JHEP* **11** (2017) 094, [arXiv:1707.07685 \[hep-ph\]](#).
- [194] K. Ishiwata and T. Toma, “Probing pseudo Nambu-Goldstone boson dark matter at loop level,” *JHEP* **12** (2018) 089, [arXiv:1810.08139 \[hep-ph\]](#).
- [195] Y. Abe, T. Toma, K. Tsumura, and N. Yamatsu, “Pseudo-Nambu-Goldstone dark matter model inspired by grand unification,” *Phys. Rev. D* **104** no. 3, (2021) 035011, [arXiv:2104.13523 \[hep-ph\]](#).
- [196] N. Okada, D. Raut, Q. Shafi, and A. Thapa, “Pseudo-Goldstone dark matter in SO(10),” *Phys. Rev. D* **104** no. 9, (2021) 095002, [arXiv:2105.03419 \[hep-ph\]](#).
- [197] C.-W. Chiang, K. Tsumura, Y. Uchida, and N. Yamatsu, “Pseudo-Nambu-Goldstone dark matter in SU(7) grand unification,” *Phys. Rev. D* **109** no. 5, (2024) 055040, [arXiv:2311.13753 \[hep-ph\]](#).
- [198] J. A. Casas and A. Ibarra, “Oscillating neutrinos and  $\mu \rightarrow e, \gamma$ ,” *Nucl. Phys. B* **618** (2001) 171–204, [arXiv:hep-ph/0103065](#).
- [199] I. Cordero-Carrión, M. Hirsch, and A. Vicente, “General parametrization of Majorana neutrino mass models,” *Phys. Rev. D* **101** no. 7, (2020) 075032, [arXiv:1912.08858 \[hep-ph\]](#).

- [200] **Particle Data Group** Collaboration, S. Navas *et al.*, “Review of particle physics,” [Phys. Rev. D](#) **110** no. 3, (2024) 030001.
- [201] I. Esteban, M. C. Gonzalez-Garcia, M. Maltoni, I. Martinez-Soler, J. P. Pinheiro, and T. Schwetz, “NuFit-6.0: updated global analysis of three-flavor neutrino oscillations,” [JHEP](#) **12** (2024) 216, [arXiv:2410.05380 \[hep-ph\]](#).
- [202] M. Thomson, [Modern particle physics](#). Cambridge University Press, New York, 10, 2013.
- [203] **MEG II** Collaboration, K. Afanaciev *et al.*, “A search for  $\mu^+ \rightarrow e^+ \gamma$  with the first dataset of the MEG II experiment,” [Eur. Phys. J. C](#) **84** no. 3, (2024) 216, [arXiv:2310.12614 \[hep-ex\]](#). [Erratum: [Eur.Phys.J.C](#) 84, 1042 (2024)].
- [204] **BaBar** Collaboration, B. Aubert *et al.*, “Searches for Lepton Flavor Violation in the Decays  $\tau^\pm \rightarrow e^\pm \gamma$  and  $\tau^\pm \rightarrow \mu^\pm \gamma$ ,” [Phys. Rev. Lett.](#) **104** (2010) 021802, [arXiv:0908.2381 \[hep-ex\]](#).
- [205] W. Grimus, L. Lavoura, O. M. Ogreid, and P. Osland, “A Precision constraint on multi-Higgs-doublet models,” [J. Phys. G](#) **35** (2008) 075001, [arXiv:0711.4022 \[hep-ph\]](#).
- [206] P. D. Group, R. Workman, V. Burkert, V. Crede, E. Klempert, U. Thoma, L. Tiator, K. Agashe, G. Aielli, B. Allanach, *et al.*, “Review of particle physics,” [Progress of theoretical and experimental physics](#) **2022** no. 8, (2022) 083C01.
- [207] K. Kannike, “Vacuum Stability of a General Scalar Potential of a Few Fields,” [Eur. Phys. J. C](#) **76** no. 6, (2016) 324, [arXiv:1603.02680 \[hep-ph\]](#). [Erratum: [Eur.Phys.J.C](#) 78, 355 (2018)].
- [208] V. Keus, S. F. King, and S. Moretti, “Three-Higgs-doublet models: symmetries, potentials and Higgs boson masses,” [JHEP](#) **01** (2014) 052, [arXiv:1310.8253 \[hep-ph\]](#).
- [209] J. Edsjo and P. Gondolo, “Neutralino relic density including coannihilations,” [Phys. Rev. D](#) **56** (1997) 1879–1894, [arXiv:hep-ph/9704361](#).
- [210] M. Srednicki, R. Watkins, and K. A. Olive, “Calculations of Relic Densities in the Early Universe,” [Nucl. Phys. B](#) **310** (1988) 693.
- [211] **Planck** Collaboration, N. Aghanim *et al.*, “Planck 2018 results. VI. Cosmological parameters,” [Astron. Astrophys.](#) **641** (2020) A6, [arXiv:1807.06209 \[astro-ph.CO\]](#). [Erratum: [Astron.Astrophys.](#) 652, C4 (2021)].
- [212] F. Tanedo, “Defense against the dark arts,” [Notes on dark matter and particle physics](#) (2011).
- [213] L. Husdal, “On Effective Degrees of Freedom in the Early Universe,” [Galaxies](#) **4** no. 4, (2016) 78, [arXiv:1609.04979 \[astro-ph.CO\]](#).
- [214] J. Kopp, L. Michaels, and J. Smirnov, “Loopy Constraints on Leptophilic Dark Matter and Internal Bremsstrahlung,” [JCAP](#) **04** (2014) 022, [arXiv:1401.6457 \[hep-ph\]](#).
- [215] Y. Bai and J. Berger, “Lepton Portal Dark Matter,” [JHEP](#) **08** (2014) 153, [arXiv:1402.6696 \[hep-ph\]](#).
- [216] G. Arcadi, A. Djouadi, and M. Kado, “The Higgs-portal for dark matter: effective field theories versus concrete realizations,” [Eur. Phys. J. C](#) **81** no. 7, (2021) 653, [arXiv:2101.02507 \[hep-ph\]](#).
- [217] P. Gondolo and G. Gelmini, “Cosmic abundances of stable particles: Improved analysis,” [Nucl. Phys. B](#) **360** (1991) 145–179.
- [218] **ATLAS** Collaboration, G. Aad *et al.*, “Constraints on the Higgs boson self-coupling from single- and double-Higgs production with the ATLAS detector using pp collisions at s=13 TeV,” [Phys. Lett. B](#) **843** (2023) 137745, [arXiv:2211.01216 \[hep-ex\]](#).
- [219] M. Cepeda *et al.*, “Report from Working Group 2: Higgs Physics at the HL-LHC and HE-LHC,” [CERN Yellow Rep. Monogr.](#) **7** (2019) 221–584, [arXiv:1902.00134 \[hep-ph\]](#).
- [220] P. Stylianou and G. Weiglein, “Constraints on the trilinear and quartic Higgs couplings from triple Higgs production at the LHC and beyond,” [Eur. Phys. J. C](#) **84** no. 4, (2024) 366, [arXiv:2312.04646 \[hep-ph\]](#).
- [221] Y. B. Zeldovich, I. Y. Kobzarev, and L. B. Okun, “Cosmological Consequences of the Spontaneous Breakdown of Discrete Symmetry,” [Zh. Eksp. Teor. Fiz.](#) **67** (1974) 3–11.
- [222] A. Ghoshal, N. Okada, and A. Paul, “eV Hubble scale inflation with a radiative plateau: Very light inflaton, reheating, and dark matter in B-L extensions,” [Phys. Rev. D](#) **106** no. 9, (2022) 095021, [arXiv:2203.03670](#)

[hep-ph].

- [223] A. Caputo, M. Geller, and G. Rossi, “New source for light dark matter isocurvature in low scale inflation,” *Phys. Rev. D* **110** no. 5, (2024) 055027, [arXiv:2306.00056 \[hep-ph\]](https://arxiv.org/abs/2306.00056).
- [224] M. Czerny, T. Higaki, and F. Takahashi, “Multi-Natural Inflation in Supergravity,” *JHEP* **05** (2014) 144, [arXiv:1403.0410 \[hep-ph\]](https://arxiv.org/abs/1403.0410).
- [225] A. Vilenkin and A. E. Everett, “Cosmic Strings and Domain Walls in Models with Goldstone and PseudoGoldstone Bosons,” *Phys. Rev. Lett.* **48** (1982) 1867–1870.
- [226] J. Preskill, S. P. Trivedi, F. Wilczek, and M. B. Wise, “Cosmology and broken discrete symmetry,” *Nucl. Phys. B* **363** (1991) 207–220.
- [227] D. I. Dunsky, A. Ghoshal, H. Murayama, Y. Sakakihara, and G. White, “GUTs, hybrid topological defects, and gravitational waves,” *Phys. Rev. D* **106** no. 7, (2022) 075030, [arXiv:2111.08750 \[hep-ph\]](https://arxiv.org/abs/2111.08750).
- [228] R. Maji, Q. Shafi, and A. Tiwari, “Topological structures, dark matter and gravitational waves in  $E_6$ ,” *JHEP* **08** (2024) 060, [arXiv:2406.06308 \[hep-ph\]](https://arxiv.org/abs/2406.06308).
- [229] S. E. Larsson, S. Sarkar, and P. L. White, “Evading the cosmological domain wall problem,” *Phys. Rev. D* **55** (1997) 5129–5135, [arXiv:hep-ph/9608319](https://arxiv.org/abs/hep-ph/9608319).
- [230] K. Saikawa, “A review of gravitational waves from cosmic domain walls,” *Universe* **3** no. 2, (2017) 40, [arXiv:1703.02576 \[hep-ph\]](https://arxiv.org/abs/1703.02576).
- [231] T. Hiramatsu, M. Kawasaki, and K. Saikawa, “Gravitational Waves from Collapsing Domain Walls,” *JCAP* **05** (2010) 032, [arXiv:1002.1555 \[astro-ph.CO\]](https://arxiv.org/abs/1002.1555).
- [232] G. B. Gelmini, M. Gleiser, and E. W. Kolb, “Cosmology of Biased Discrete Symmetry Breaking,” *Phys. Rev. D* **39** (1989) 1558.
- [233] Y. Wu, K.-P. Xie, and Y.-L. Zhou, “Collapsing domain walls beyond Z2,” *Phys. Rev. D* **105** no. 9, (2022) 095013, [arXiv:2204.04374 \[hep-ph\]](https://arxiv.org/abs/2204.04374).
- [234] Y. Wu, K.-P. Xie, and Y.-L. Zhou, “Classification of Abelian domain walls,” *Phys. Rev. D* **106** no. 7, (2022) 075019, [arXiv:2205.11529 \[hep-ph\]](https://arxiv.org/abs/2205.11529).